NORTHWESTERN UNIVERSITY

Geodetic and Seismic Studies of the New Madrid Seismic Zone and Implications for Earthquake Recurrence and Seismic Hazard

A DISSERTATION

SUBMITTED TO THE GRADUATE SCHOOL
IN PARTIAL FULFILLMENT OF THE REQUIREMENTS

for the degree

DOCTOR OF PHILOSOPHY

Field of Geological Sciences

By

Andrew Vern Newman

EVANSTON, ILLINOIS

December 2000

ABSTRACT

Geodetic and Seismic Studies of the New Madrid Seismic Zone and Implications for Earthquake Recurrence and Seismic Hazard

Andrew Vern Newman

The New Madrid Seismic Zone (NMSZ), in the central United States, was the site of large magnitude (**M**) earthquakes in 1811-12. Paleoseismic studies find events of similar size recurring about once every 500 years. Assessing the causes of deformation and estimating the recurrence of these events are necessary for determining earthquake hazard in the region. Global Positioning System (GPS) measurements made in 1991, 1993 and 1997 at 23 sites within 300 km of the NMSZ show minimal motion across the fault zone. Using a locked fault model, I find -0.2 ± 2.4 mm/yr (2 σ) of right-lateral fault parallel (NE-SW) motion across the network. This result is consistent with continuous GPS results away from the NMSZ which indicate less than 1 mm/yr of differential plate motion. Assuming horizontal slip accumulates at less than 2 mm/yr, the recurrence interval (T_r) for "New Madrid style" **M** 8 earthquakes, with 5-10 m slip, would exceed 2,500-5,000 years, significantly greater than the 500-1,000 years previously estimated. However, these GPS results are consistent with my re-evaluation of the frequency-magnitude relationship, paleoseismic recurrence estimates, and lack of fault-associated topography if the 1811-12 earthquakes and the

paleoearthquakes if the events were smaller, low **M** 7, and recurring every 500-1000 years. Also, smaller **M** 7 events are consistent with a new earthquake intensity study for the 1811-12 series. Reducing the size of the maximum magnitude events (M_{max}) has considerable effect on the predicted seismic hazard in New Madrid.

Currently, the U.S.G.S. seismic hazard maps show large accelerations for the central U.S. due to the NMSZ. These maps reflect crucial parameter assumptions, having large uncertainties because little data exists for large events. Since my GPS and seismic recurrence studies, along with other recent results, show that the M_{max} may be 7 with T_r of 500 years, rather than M_{max} 8 and T_r of 1000 years used by the U.S.G.S., I explore the effects that these parameters, along with several predicted ground shaking models, have on predicted 1 Hz and peak ground accelerations from the NMSZ. I find that changing these parameters significantly affects the predicted accelerations thus demonstrating the considerable uncertainties in seismic hazard from the NMSZ.

ACKNOWLEDGMENTS

I would like to thank Seth Stein, my thesis advisor, for his leadership and cooperativeness in the thesis and other projects that have contributed to my growth as a scientist. Thanks to Ray Russo and Donna Jurdy who have been a considerable help in reviewing my thesis in various stages.

Tim and Jackie Dixon (University of Miami) have shown me many things that have aided in my scientific growth; one of which is how to be very productive while working in warm and beautiful places–I will keep this in mind! Also, BIG THANKS for giving me the space and help needed to reduce the GPS data (no small task). I am also appreciative of the help that Fred Farina, Ailin Mao, and Edmundo Norabuena gave here. Thank you John Schneider, Andres Mendez and Sithipat Palanandana for much help in all things related to earthquake hazard. Without the knowledge that I have gained here, I may still be naive about real-world applications of my science. Emile Okal has taught me much and has guided me though my first scientific conferences–Thanks for all of your help. Thank you Peter Malin and Eylon Shalev for teaching me so much. It was because of you two that I got started in volcano geophysics. It is impossible for me to thank all who have helped in the GPS campaigns since so many have helped in monumentation, campaigns, data reduction software and techniques, and funding. I have followed the thesis work of John Weber and have used data that he, along with many others, have collected in two of the three GPS campaigns used here. He is also responsible for helping to build many of the geodetic monuments. Thanks John for starting me off and for your cooperation in the papers

that followed. Also thanks Joe Englen for coordinating the 1997 campaign and for your previous campaigns efforts. I would also like to thank the others who have built monuments, and those who granted permission for building monuments and NOT covering them with baseball fields a few years later. I much appreciated the help of the geology undergraduate students from Grand Valley State University, R. Graves, K. Wellington, C. Bunker, K. Nolan, and C. Griffen for their assistance during the 1997 field GPS campaign. I would also like to thank Dave Jefferson and the others at JPL, for precise orbit and timing of GPS satellites and for making these data freely available. The GPS campaigns were supported by NASA grants NAGW-2522 and NAG5-6685.

I would like to thank all of my friends that I have met through the geology program. We have all gone though some pretty great (e.g., night after qualifiers) and tough times (e.g., night before qualifiers) together. I will always remember each of you, and will be looking forward to revisiting old times over beer at meetings! Thanks Joe Werne for teaching me how to make beer, for the Tomah experience and for helping me get through those first two years! Ruth and Jaxen thanks for including me in your life. I look forward to seeing y'all again and seeing Jaxen grow up. Don't leave Holland before I come to visit! Ivy Chen, thank you for SO much. You know how happy you have made me in this past year. Thanks for putting up with so much through my Ph.D. preparation. We will see the world! Erin Beutel, You have always made it a priority to help me and others out when we needed it. Thanks for it all. Thank you Mike "40" Fortwangler, for aiding in my enlightenment. Many, many thanks to Ben Horner-Johnson, Johnathan Rich and Brandon Gomer

for all your help in all things GMT and Linux/UNIX. You have made much of my time here more productive. Adam Kanouse, thanks for the nicknames, basketball, and fun. Thanks Steve (Oblivi-) Meyers, for becoming human this last year... I was starting to worry. Thank you Phil Richardson and Wei-Chuang Huang, as fellow grad students and friends, you two have helped start me off in both seismology and buffets (Wei-Chuang). Adam and Lora Murphy, thank you for your friendship and B-movies. Also I would like to thank you (and many others) for being vegetarian hence leaving more meat for me. Thanks Po-Fei Chen, for being a great listener, and good meeting pal. Thanks Eryn Klosko, Sarah Wilkinson, and Shana Pimley, not only for being vegetarians, but for also the many laughs that we have shared. Han Li, I am impressed by your cheerfulness even when things are tough. I will try and follow this attitude. Michael Smith, a true philosopher, thank you for your unique view on things. I will try to remember that "sometimes the cup is just too damn big."

I would most like to thank my parents, Vern and Lynda Newman, who have made many sacrifices in their lives so that my brothers, sisters and myself could have all that we need to make it in this world. Thanks! I love you Mom and Dad! I would also like to thank each of my siblings, Teresa, Kaye, Chris, Dee, Keith, Matt, Tammy, Nicki and Zack (did I miss anyone?), for helping me to grow up and learn how to play well with others.

Oh wait I cannot forget some of the smaller things that have helped me over the last few years: coffee, beer, the Gnu project, and Linux. I also thank the creators of Generic Mapping Tools (GMT), Paul Wessel and Walter Smith, for making such a

great program that you have kept free for all [*Wessel and Smith*, 1995, 1998]. Lastly, thanks goes to *McNoleg* [1996], who has worked wonders for my soul by reminding me not to believe all that is published in science journals.

Contents

List of Tables

List of Figures

Chapter 1

Introduction

I have driven through the Mississippi Valley many times through my life, traveling from Texas to visit family in Chicago and Detroit. Though these drives are long and relatively unscenic, they are usually quite easy, partly because the ground is SO flat. With this in mind, it is somewhat difficult to understand why is it that the New Madrid seismic zone (NMSZ), an area of significantly increased seismicity with possibly the largest earthquakes in the continental United States, exists here. I have spent some time in many more active earthquake regions (California, Alaska, Greece, and Central America), and in each there is considerable topographic relief. Charles Darwin even noted there may be some correlation between mountains and earthquakes when visiting the magnificent Andes Mountains of South America on one of his famous trips on the *Beagle* saying, "We may confidently come to the conclusion that the forces which slowly and by little starts uplift continents, and those which at successive periods pour forth volcanic matter are identical. I believe that the frequent quakings of the earth are caused by the rending of the strata, necessarily consequent on the tension of the land when upraised.." [*Darwin*, 1845].

If Darwin had been aware of what had occurred during the winter of 1811-12 (when he was 2 years old), in the flat central United States, he might have never made such a statement. Though there are no volcanoes nor significant topography, the New Madrid region has been the source of several large magnitude earthquakes in the last 1200 years. In order to understand why large earthquakes occur more frequently in the NMSZ than in other eastern North American regions, one must take a look at the underlying geology.

1.1 Regional Geology

The New Madrid seismic zone lies within the largely inactive eastern United States, well within the stable North American plate [e.g., *Gripp and Gordon*, 1990; *Dixon et al.*, 1996]. However, this was not always the case. A combination of gravity, magnetic, seismic refraction, seismic reflection and stratigraphic studies have revealed higher density, Precambrian to early Cambrian complex failed rift structures beneath the seismic zone and continuing northeast, along with mafic plutonism, through New Brunswick, Canada [*Ervin and McGinnis*, 1975; *Braile et al.*, 1986; *Sexton et al.*, 1986; *Wheeler*, 1995, 1997] (see Figure 1.1). The extensive rift system was created during a period of continental extension that formed the Iapetus Ocean. Because the platform and craton surrounding the failed rift system have been mostly stable since the Late Proterozoic, the surrounding crust is considered to be relatively laterally homogeneous and with few faults [e.g., *Sloss*, 1988].

The Reelfoot Rift lies about 30 km below the surface expression of the NMSZ, having the same approximate northeastern trend as the recent seismicity [e.g., *Wheeler*,

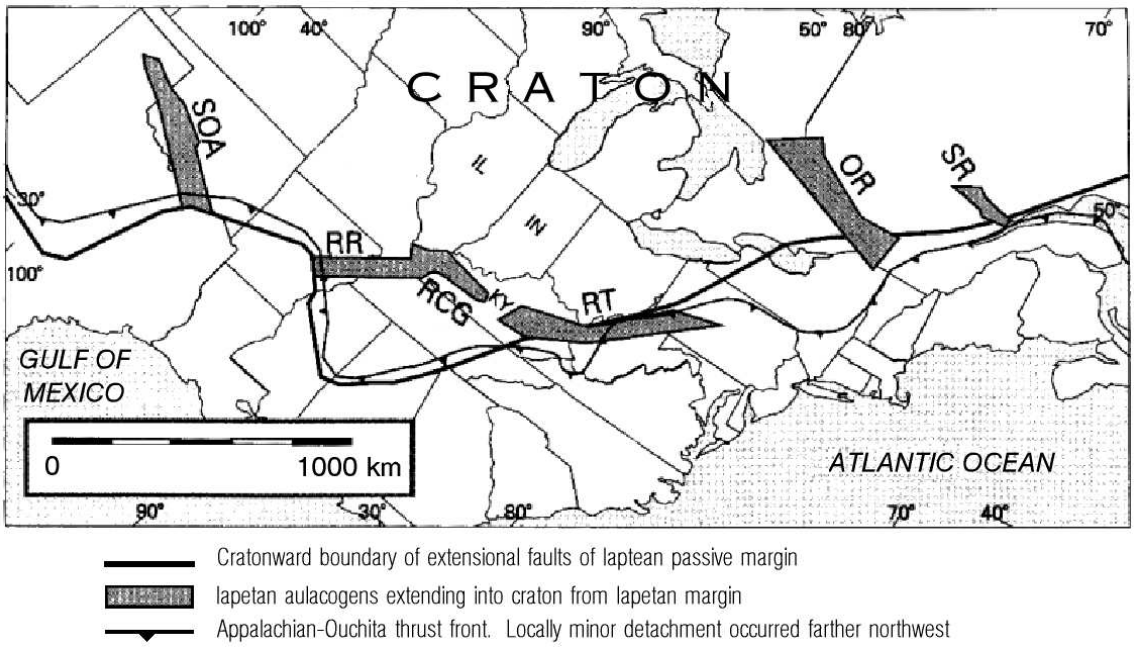

Figure 1.1: Known Late Proterozoic-Cambrian rifts and grabens in eastern North America [modified from *Wheeler*, 1997]. These are remnants from a continental extension period that formed the Iapetus ocean. The graben and rifting features are Southern Oklahoma Aulacogen (SOA), Reelfoot Rift (RR), Rough Creek Graben (RCG), Rome Trough (RT), Ottawa Rift (OR) and Saguenay Rift (SR).

1997]. The rift is believed to be responsible for slow, regional subsidence, due to increased gravity, which continued throughout much of the remainder of the Phanerozoic [*Braile et al.*, 1986], and was some Mesozoic plutonism. The subsidence, forming the Reelfoot, Rough Creek and other grabens, acts to thin the upper crust above the rift. The thinner and more fractured section in the otherwise thick upper crust in the mid-continent may allow far-field strain to localize over the rift system, thus forming large earthquakes. The cartoon cross section, Figure 1.2, illustrates the approximate current seismicity along the Blytheville fault zone segment (northeastern part of the southwestern inferred strike-slip fault), within the Reelfoot Graben and directly above the Reelfoot "Rift Pillow" (as assumed by *Stuart et al.* [1997]). Although the Reelfoot Rift is the most seismically active eastern North American failed rift segment, the Rough Creek graben (just north and running east-west) is the least active of the known Iapetan rifting structures, illustrating variability, possible due to rift orientation to major stress axes, in the seismicity with respect to the rift *Wheeler* [1997]. Also, just 40 km northwest of the Reelfoot rift is another NE trending basement geologic feature called the Commerce Geophysical Lineament [*Langenheim and Hildenbrand*, 1997]. Although, not much is known about its age or method of implacement, it is an intriguing feature that may aid in weakening the crust, thus making it more susceptible to earthquakes from far-field driving stresses.

The NMSZ lies under a thick sequence ($\sim$ 600 m) of sediments called the Mississippi Embayment (Figure 1.3). The embayment is composed of a succession of Tertiary and Cretaceous marine and terrestrial semi-consolidated strata that are blanketed by unconsolidated Quaternary alluvium from the Mississippi river (as much

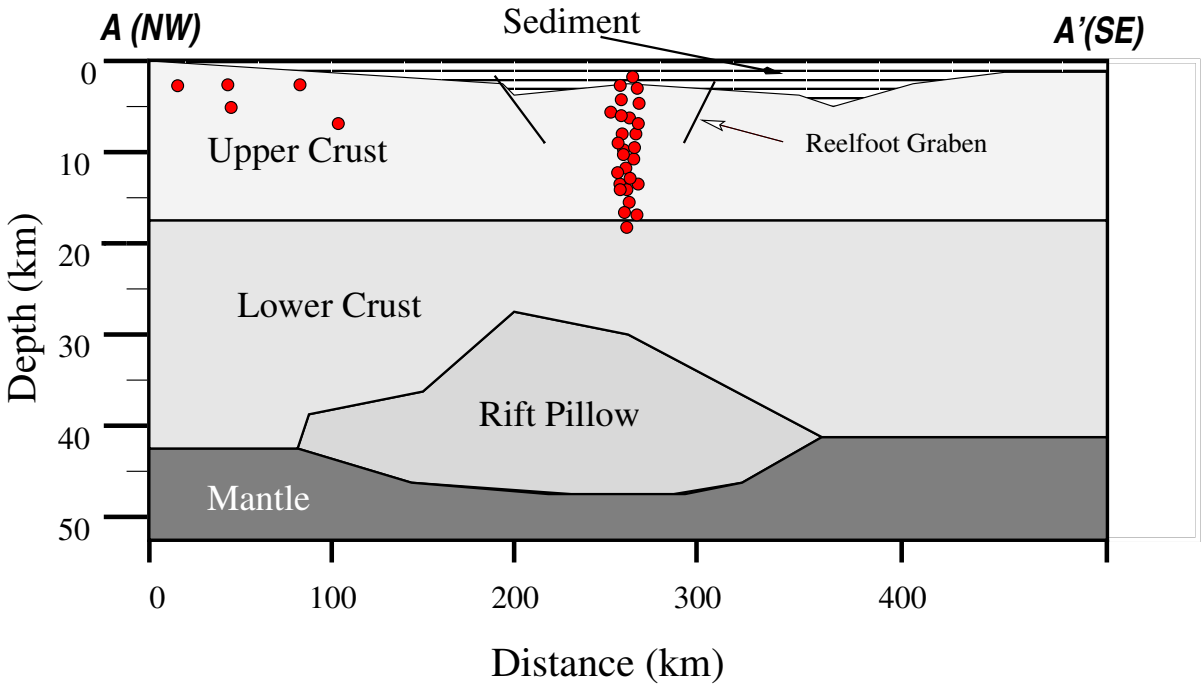

Figure 1.2: Shown is a representative NW-SE cartoon cross section, along line *AA'* in Figure 1.3, of the upper lithosphere across a segment just SW of the thrust segment of the NMSZ [after *Stuart et al.*, 1997; *Braile et al.*, 1997]. The region directly above the "rift pillow", an anomalously thick portion of the lower crust as inferred from Bouguer gravity measurements [*Stuart et al.*, 1997], is the approximate location of the seismically-defined southeastern strike-slip segment of the fault complex (shown as small circles in the upper crust, ●).

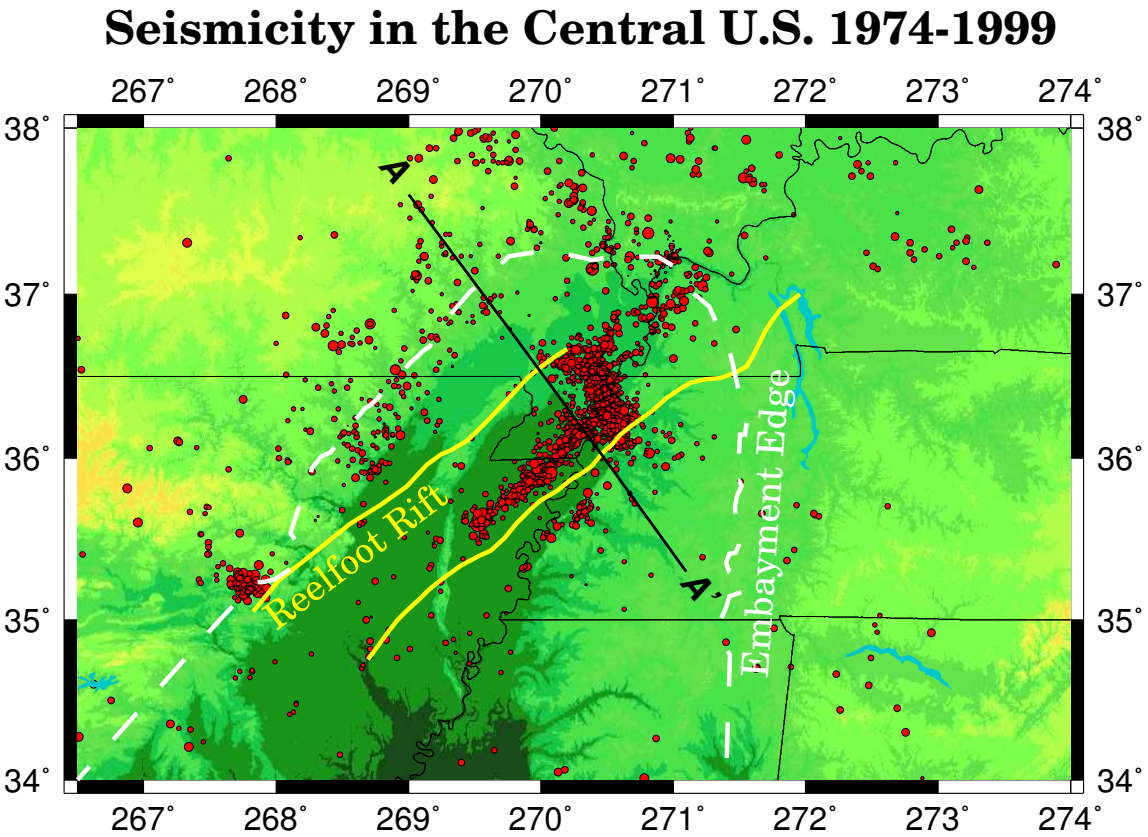

Figure 1.3: New Madrid seismicity recorded between 1974 and 1999. Earthquakes were identified and located by local networks across the region and reported to the Center for Earthquake Research and Information and/or Saint Louis University (CERI's Web site: *http://folkworm.ceri.memphis.edu/cat_nm.html*). Also shown are the approximate boundaries of the Reelfoot Rift and the Mississippi Embayment. The line *AA'* is the location for the cross section in Figure 1.2.

as 40 m thick) [*Crone*, 1981]. These sedimentary deposits, which extend southward to the Gulf of Mexico, conceal most fault scarps in the NMSZ [e.g., *Johnston and Schweig*, 1996]. Thus, no clear surface expressions of faulting are visible, making it difficult to determine much information directly from large historic earthquakes. Therefore, important information about such events must be obtained from human records and structural effects on landscapes and edifices.

1.2 Seismicity of New Madrid Seismic Zone

1.2.1 1811-12 Earthquake Series

In the winter of 1811-12, a significant sequence of large earthquakes occurred near the small town of New Madrid, Missouri [e.g., *Fuller*, 1912; *Johnston and Schweig*, 1996]. Three of these events are reported to have had extreme ground shaking: December 16 (∼2:15 am local); January 23 (∼9 am local); and February 7 (∼3:45 am local) [e.g., *Fuller*, 1912; *Nuttli*, 1973; *Street*, 1980, 1982; *Street and Nuttli*, 1984]. The earthquakes caused extensive ground shaking across the eastern portion of the United States, large enough that it is said to have rung the bell in the State House in Milledgeville, Georgia, some 800 kilometers away [*Fuller*, 1912]. On the basis of records such as this, the New Madrid 1811-12 main shocks have been considered to be "great" earthquakes [*Davison*, 1936; *Richter*, 1958]. Thus, they were placed in the same class of destructive earthquakes as the 1755 Lisbon and 1906 San Francisco earthquakes [*Johnston and Schweig*, 1996].

However, the earthquakes occurred before the invention of the seismometer in

a region that was sparsely populated (then the frontier region of the western United States). Hence, the actual size of the events is very hard to determine precisely [e.g., *Johnston*, 1996; *Hough et al.*, 2000], and reliable and adequately descriptive accounts of near-source ground effects from the large earthquakes are few. This is especially problematic since the size of the large earthquakes is a fundamental input parameter into seismic hazard analyses used for building codes and insurance policies (see Chapter 4).

By using the distribution of felt reports of ground shaking or other effects of the three main events, the earthquakes' magnitudes have been estimated. *Nuttli* [1973], *Street* [1982, 1984], *Street and Nuttli* [1984], *Johnston* [1996], and *Hough et al.* [2000] have compiled the reported near-source earthquake effects from many eyewitness accounts. On land, the behavior reported consisted of: roaring and explosive sounds; lakes filling or drying; ground fissuring; sand/coal/water fountains; uplift and subsidence; trees being uprooted, split or swaying; explosive cratering; vapor/cloudy atmosphere; sulphurous odor; rapid waves through land; and earthquake lights. On the Mississippi River, the behavior reported was: banks caving; water/sand/air spouts; islands sinking; water level rising; increased or retrograde current; large waves and turbulence; waterfalls or rapids; and submerged trees ejected. Many of the reported effects have occurred elsewhere or can be explained scientifically [*Fuller*, 1912; *Guccione et al.*, 1993; *Jibson and Keefer*, 1988; *Obermeier*, 1989; *Odum et al.*, 1998; *Stahle et al.*, 1992; *VanArsdale et al.*, 1995]. Using these reports, scientists have attributed Modified Mercalli intensities (MMI) to the felt areas and generated isoseismal maps (e.g., Figure 1.4 [*Nuttli*, 1973]), to estimate magnitudes for the three main events. A

wide range of magnitudes have been attributed to these events. As an example, the Dec. 16, 1811 mainshock has had a number of estimates of moment magnitude (**M**): 7.7, 7.0, 8.1, 7.3 [*Herrmann et al.*, 1978; *Nuttli*, 1983; *Johnston*, 1996; *Hough et al.*, 2000]. *Johnston* [1996] gives magnitudes for each of the three events as **M** 8.1 ± 0.31, 7.8 ± 0.33 and 8.0 ± 0.33, chronologically, and interprets these as equivalent to a total magnitude of **M** 8.3 for the 3 events.

A **M** 8.3 event ($M_0 = 3 \times 10^{28}$ dyne cm) seems large for New Madrid since it has been shown empirically that a strike-slip rupture (inferred from current seismicity and overell state of regional stress; see Section 1.2.2) of such magnitude should fail over a subsurface fault length of about 370 km and have a slip over 10 m, where the subsurface rupture length, RLD, is related to **M** by

$$\log_{10}(RLD) = 0.62\mathbf{M} - 2.57 \tag{1.1}$$

with uncertainties, $\sigma_{\mathbf{M}_{RLD}} = 0.15$, and the displacement, D, for a global average of strike-slip earthquakes is

$$\log_{10}(D) = 0.90\mathbf{M} - 6.32 \tag{1.2}$$

with uncertainties, $\sigma_{\mathbf{M}_D} = 0.28$ [*Wells and Coppersmith*, 1994] (see Figure 1.5). Since the total length of the faults believed to have ruptured in the sequence is ∼225 km, as defined by the locations of current seismicity, the coseismic slip would have to have exceeded 10 m. *Mueller et al.* [1999] use sediment offsets to infer that the total horizontal slip over the region is ∼4.5 meters over the past 2300 years, considerably

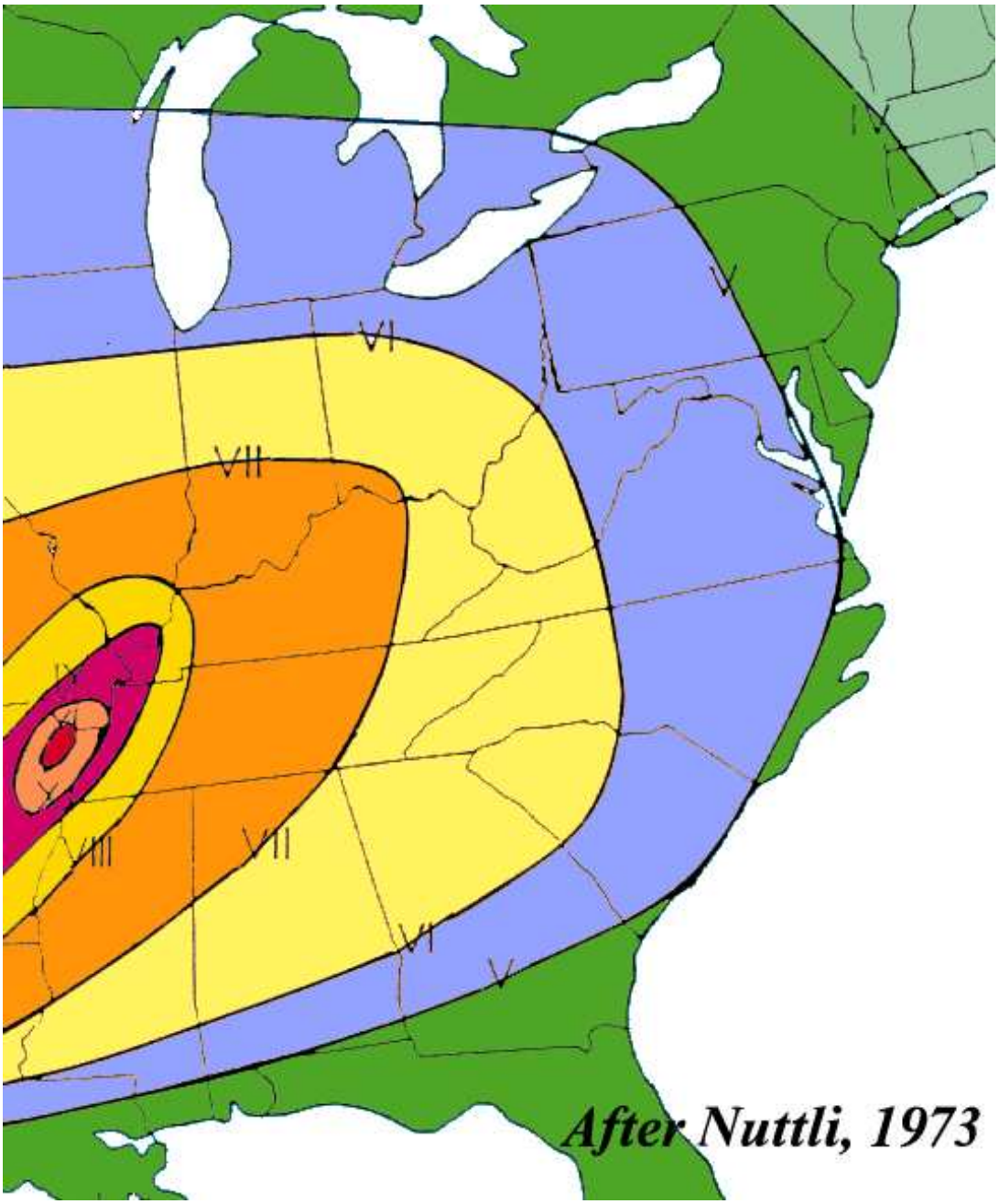

Figure 1.4: Modified Mercalli Isoseismicity Map of Dec. 16th, 1811 New Madrid Seismic Zone mainshock [*Nuttli*, 1973]. The extent of strong ground shaking was great, with many distant felt reports, including the ringing bells on a State building in Midgeville, Georgia [*Fuller*, 1912].

less than what would be inferred given the *Wells and Coppersmith* [1994] relationship for an **M** 8.3 event, even if only one such earthquake occurred in that time period.

1.2.2 Current Seismicity

The region remains active, with small to moderate earthquakes (Figure 1.6) concentrated along planar segments (Figure 1.3) which presumably reflect subsurface faults [*Himes et al.*, 1988; *Chiu et al.*, 1992; *Pujol et al.*, 1997]. Though the region is still considered the most seismically active zone in eastern North America, its activity is still rather modest. On average, one **M** 4 or greater occurs every year, and only one **M** 5 every ten years (Figure 1.6). In fact, the last earthquake with **M** greater than or equal to 6 was in 1895 (over 100 years ago) in southern Illinois. The frequency of the smaller events can give some insight into the recurrence of larger events and hence could be useful in seismic hazard (see Chapters 3 and 4).

The few available earthquake focal mechanisms from the fault zone suggest that right-lateral strike-slip occurs on two NE-SW striking, sub-vertical faults, with thrusting occurring on a shallowly SW-dipping fault, forming (and extending south of) the left step between the strike-slip faults [*Herrmann and Canas*, 1978; *Herrmann*, 1979; *Liu*, 1997]. The current seismicity may be localized in this region because of weaknesses in the crust due to Paleozoic failed rifting [*Braile et al.*, 1986; *Sexton et al.*, 1986], with stresses occurring either locally or acting upon the entire eastern portion of the continental North American plate [*Zoback and Zoback*, 1981; *Grana and Richardson*, 1996] (see Section 1.1).

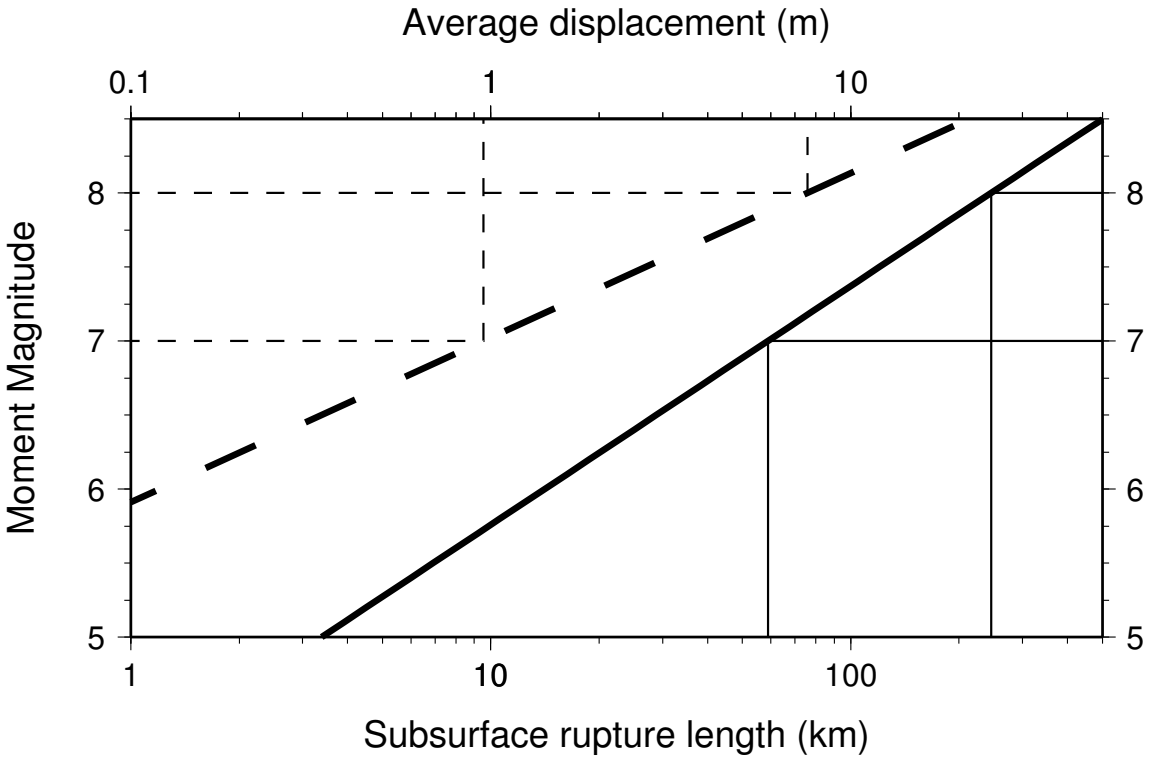

Figure 1.5: Shown here is an empirical relationship between moment magnitude, **M**, subsurface rupture length, RLD, and displacement, D for a global average of strike-slip earthquakes [*Wells and Coppersmith*, 1994]. The relationship found between **M** and RLD (Equation 1.1) is shown as the solid line and corresponds to the bottom horizontal axis (km), whereas that for D (Equation 1.2) is shown as the dashed line and corresponds to the top horizontal axis (m). The largest strike-slip event used in the regression by *Wells and Coppersmith* [1994] was **M** 8.1.

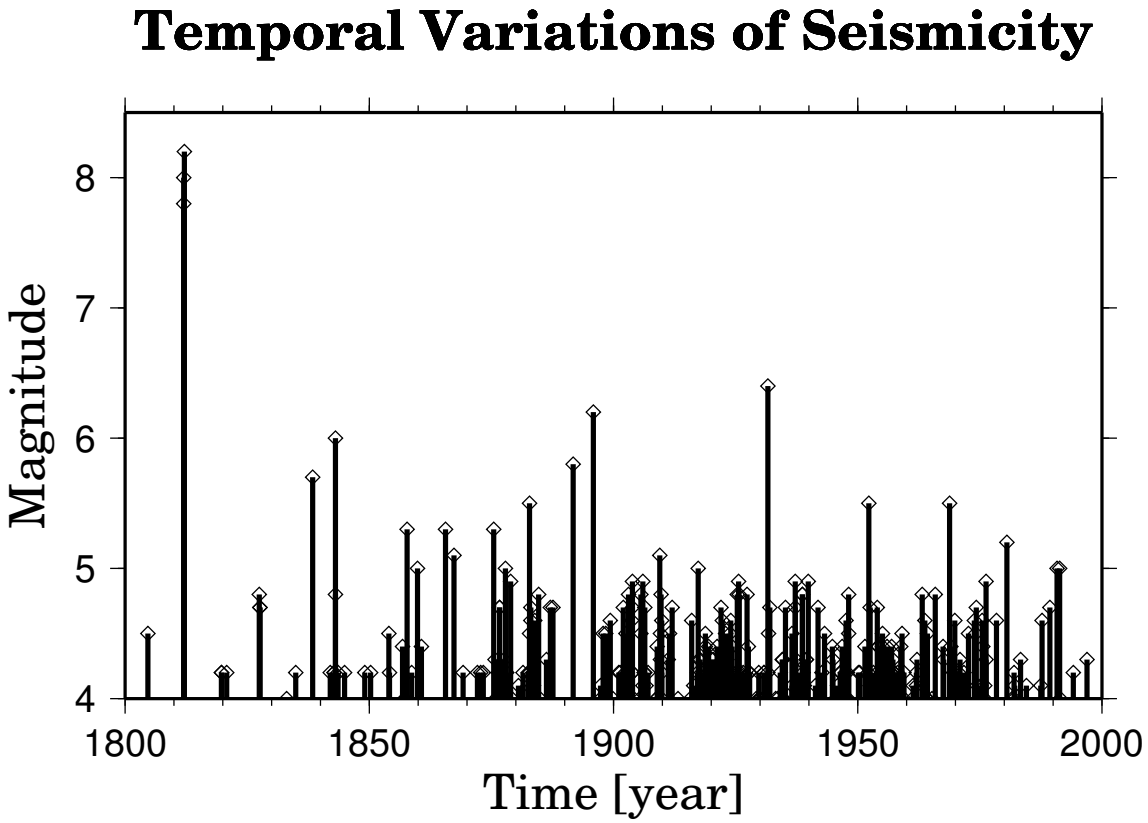

Figure 1.6: Earthquake history for the NMSZ. Since 1816, there have been 16 earthquakes with magnitude greater than 5 (about a 10-yr recurrence), and two with magnitude greater than 6 (about an 100-yr recurrence). Thus Magnitude 7 and 8 earthquakes can be expected to have about 1,000 and 10,000 yr recurrence times, respectively. The fewer smaller earthquakes before 1900 does not represent a lack of activity but rather a lack of earthquake reports for smaller events.

1.2.3 Paleoseismology

No earthquakes even close to the size of the New Madrid 1811-12 event have been instrumentally recorded in the study region. Thus, evidence for the location, timing and size of earlier events have been inferred from the geologic record. Such paleoseismic studies examine exposed fault scarps for evidence of prior activity, and trench sediment layers for evidence of prior liquefaction features, or sediment folding and faulting. Since the region is covered by an extensive sediment layer, there are few fault scarps available for paleoseismic studies. Hence it is necessary to rely on trenching to uncover information about prior events. Many sand blows and sand dikes, which result from rapidly increasing pore-water pressure in already saturated sand deposits [*Tuttle et al.*, 1999], have been found in the region. Many of these are associated with events that have occurred between 800 and 1970 A.D. [*Tuttle et al.*, 1996, 1998; *Li et al.*, 1998; *Tuttle*, 1999]. *Tuttle et al.* [1999] argue that there were at least two events during this period (∼900 A.D. and ∼1450 A.D.), and that the size and extent of liquefaction from these earthquakes implies that they were similar to those of the 1811-12 series. If this is true, then the recurrence interval for large earthquakes in the region is about every 500 years. It has also been shown by *Wesnousky and Leffler* [1992] that there is no evidence of large earthquakes in the past 5 to 10 thousand years, which can be used to argue that activity in the region is not temporally regular.

Although paleoseismic studies of liquefaction features have been shown to be valuable for determining the general location and timing of larger events [e.g., *Pond and Martin*, 1997], it is unclear how well they indicate earthquake size. Empirical

studies of the maximum extent of sediment susceptibility to earthquake ground shaking indicate that a large New Madrid earthquake should create an area of liquefaction features for earthquakes approximately one half a magnitude unit larger than would occur elsewhere [*Ambraseys*, 1988; *Obermeier et al.*, 1993; *Metzger*, 1996; *Pond*, 1996; *Pond and Martin*, 1997; *Obermeier and Pond*, 1999] (Figure 1.7). In other words, if paleoearthquakes were found to generate liquefaction features as far as 200 km from the assumed earthquake epicenter, it would be interpreted as a **M** 8.1 in the central U.S., but only around **M** 7.6 elsewhere.

Figure 1.7 shows that the estimated maximum distance of liquefaction expected for central U.S. events, constrained using only historic earthquakes, is considerably lower than the global average [*Pond and Martin*, 1997]. Whether this relationship is real is unclear. The discrepancy between the New Madrid liquefaction and the global average may be due to the paucity of data in the the region, forcing distance calibrations to be made from much fewer earthquakes, with no instrumentally recorded earthquakes greater than **M** 6. This suggests there is a possible problem, because this curve is commonly used to estimate the magnitude of paleoearthquakes [e.g., *Tuttle*, 1999]. Therefore, if new evidence reveals that magnitudes of the New Madrid 1811-12 earthquakes were considerably lower than assumed, the same should be true for all the previous earthquakes in the region with similar maximum extent of liquefaction features. Finally, the largest magnitude earthquake in the New Madrid region used to control the magnitude-distance relation was not a single event but three smaller events with epicenters distributed over an approximately 100 km northeast trending line [e.g., *Johnston and Schweig*, 1996]. If the three smaller events were considered,

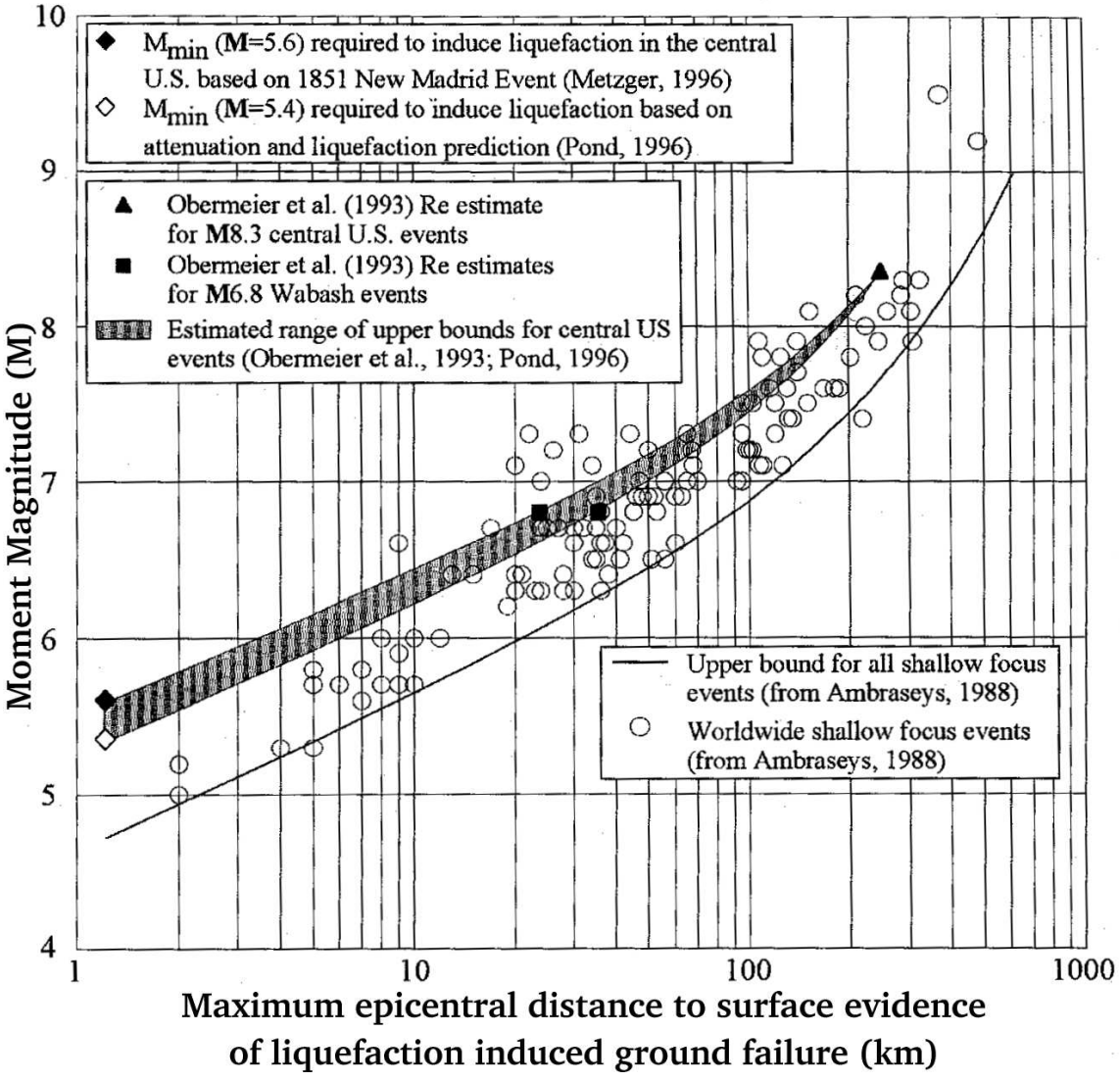

Figure 1.7: Relationship between moment magnitude, **M**, and distance to surface evidence of liquefaction effects [after *Pond and Martin*, 1997]. The estimated range of upper bounds (maximum distances of liquefaction) for central U.S. events, constrained using only historic earthquakes, is considerably lower than that of the global average.

the upper bound for central U.S. in this relation could be significantly changed for large earthquakes. In particular, the central U.S. data might then be much closer to or match the global average.

Obermeier and Pond [1999] explain that liquefaction effects are heavily controlled by the level of the water table; raising the table from 10 m depth to the surface could raise the liquefaction effects from near nothing to high levels. Thus, it is not clear that liquefaction studies alone can be used to determine the magnitude of a paleoearthquake with much accuracy, because water tables can fluctuate greatly in non-coastal regions. It is difficult to understand why large central U.S. earthquake should create smaller liquefaction areas than elsewhere, considering that the region has very little high-frequency attenuation [e.g., *Atkinson and Boore*, 1995; *Johnston*, 1996; *Atkinson and Boore*, 1997; *Abrahamson and Shedlock*, 1997; *Toro et al.*, 1997](see below and Chapter 4). Since liquefaction is a high-frequency phenomenon, the New Madrid region should have an increased areal extent of liquefaction.

The efficiency at which seismic waves are transmitted in the eastern United States is exemplified by a report of the November 9th, 1968 **M** 5.6 earthquake in southern Illinois. David Boore, a respected U.S. ground motion expert, reported feeling the earthquake in his Boston apartment, stating that "... a slight dizziness resulted from the swaying and by looking out a window the relative movement of the building was quite obvious." [*Lander*, 1969].

1.3 Mechanism for Large Earthquakes

Since the NMSZ is not at a plate boundary, much speculation has centered on the mechanism that drives large earthquakes in the region. The force could come from large scale, or plate-wide, compressive stress that can be inferred from the lithosphere being bounded by an area of extension to the east at the Mid-Atlantic Ridge and extension in the west in the the Basin and Range region west of the Rocky Mountains. *Zoback and Zoback* [1981] have shown from seismicity, well breakouts and hydro-fractures data, that the overall state of stress for the central eastern United States is in a generally trends east-west. An east-west stress orientation was also inferred locally from fault orientation and moment tensor solutions for small earthquakes in the NMSZ [*Street et al.*, 1974; *Liu*, 1997].

It is likely that the seismicity localized in the the Mississippi Valley because of lithospheric heterogeneities created by a Proterozoic to Paleozoic failed rift (see Section 1.1). The seismic zone is probably very young since there is little topographic relief and no evidence had been presented for extensive subsurface faulting in the region. *Stuart et al.* [1997] consider a detachment fault over the "rift pillow" as a possible mechanism for the seismicity. Though this model is shown to generate significant horizontal strain rates ($\sim 10^{-7}$ per year), the model depends greatly on the shape of the "rift pillow", which is poorly known. It has also been argued that the seismicity reflects stress induced by bending the lithospheric plate due to glacial loading and unloading during the Wisconsinon extent of the Laurentide ice sheet, which reached its maximum ∼250 km north of the NMSZ approximately 20,000 years ago [*Grollimund and Zoback*, 2000]. In contrast, *Wu and Johnston* [2000] argue that

the NMSZ is too far south for glacial unloading to generate stresses sufficient to cause great earthquakes.

1.4 Overview of Thesis

Assessing the causes of deformation and estimating the recurrence of large earthquakes from the New Madrid seismic zone are necessary for determining earthquake hazards in the central-eastern United States (CEUS). Therefore, I used high-precision Global Positioning System (GPS) measurements made in 1991, 1993, and a new campaign in 1997 at 23 sites within 300 km of the NMSZ, along with 8 platewide continuous GPS sites, to determine the state of far-field motions, and thus infer a minimum recurrence rate for large earthquakes (see Chapter 2).

Velocities measured from the campaign sites show minimal motion across the fault zone. Using a simple locked fault model, I find -0.2 $\pm$ 2.4 mm/yr (2 σ) of right-lateral fault parallel (NE-SW) motion across the entire network, which extends to bedrock far from the seismic zone. I further examine data from the stations nearer to the fault zone and find a slightly higher rate, 0.6 $\pm$ 3.2 mm/yr of right-lateral motion (see Section 2.4). It is not clear, though, whether the increased velocity is from a local tectonic signal, or from increased noise since all of these sites are in unconsolidated Quaternerary alluvium of the Mississippi embayment. The slow (or no) motion result from the campaign GPS study is consistent with results from the continuous GPS data away from the NMSZ which indicate less than 1 mm/yr of differential plate motion (see Section 2.5). Assuming horizontal slip accumulates at less than 2 mm/yr, the recurrence interval (T_r) for "New Madrid style" **M** 8 earthquakes, with 5-10 m slip,

would exceed 2,500-5,000 years. This results is inconsistent with *Johnston and Nava* [1985], who calculate a rapid earthquake recurrence, M_s 8.3 every 500-1100 years, from the observed Gutenberg-Richter frequency-magnitude relationship of smaller recent, and larger post-1816 historic earthquakes. Thus, I re-analyze this work, and determine a contrary result, based on a better understanding of the unity within the frequency-magnitude relationship [*Okal and Romanowicz*, 1994], with a **M** 8 recurring only every 14,000±7,000 years and a **M** 7 every 1,400±600 years (see Chapter 3).

These new results from GPS and my re-evaluation of the frequency-magnitude relationship recurrence are jointly consistent with paleoseismic recurrence estimates, and lack of fault-associated topography if the 1811-12 earthquakes and the paleoearthquakes were considerably smaller, low **M** 7, and recurring every 500-1000 years. Smaller **M** 7 events are also consistent with a new earthquake intensity study by *Hough et al.* [2000] for the 1811-12 series Reducing the size of the maximum magnitude events (M_{max}) has considerable effect on the predicted seismic hazard in New Madrid.

Currently, the U.S.G.S. seismic hazard maps predict considerable hazard for the central United States due to the expected recurrence of **M** 8 earthquakes every 1000 years on the New Madrid seismic zone [*Frankel et al.*, 1996]. Alternatively, my GPS and seismic recurrence results, along with other recent studies, show that the M_{max} may be as lows as 7 with T_r of 500 years. These maps also include predicted ground acceleration relationships, developed specifically for the mapping project, that are considerably higher than alternative published models for the eastern U.S., at distances greater than 100 km. The U.S.G.S. maps, thus, reflect crucial parameter

assumptions, which have large uncertainties which can have a considerable affect on the resulting predicted hazard in the CEUS. I explore the effects that these parameters (M_{max}, T_r, and predicted ground shaking) have on predicted 1 Hz and peak ground accelerations (PGA) in the CEUS (see Chapter 4). I find that considering an M_{max} of 7 rather than 8, lowering T_r from 1000 to 500 or using an alternative ground shaking model, each significantly change the predicted accelerations thus demonstrating the considerable uncertainties in seismic hazard from the NMSZ.

Chapter 2

GPS Study of the New Madrid Seismic Zone

2.1 Introduction

At rapidly moving plate boundaries one can measure relative plate motions from numerous geological or geophysical techniques, and then use these velocities to help estimate the minimum recurrence time for great earthquakes. Unlike interplate seismogenic zones, the New Madrid seismic zone, the most active region east of the Rocky Mountains, resides in a rigid continental interior previously shown to be stable to about 2 mm/yr or better [*Dixon et al.*, 1996]. With such low expected motion it is difficult to assess the forces that drive large and damaging earthquakes in the region. Without the use of geodetic data, we would be limited to inferring strain rates from seismic and paleoseismic data which have shown varying results [e.g., *Johnston and Nava*, 1985; *Anderson*, 1986; *Saucier*, 1991; *Wesnousky and Leffler*, 1992; *Hanks and Johnston*, 1992].

With the development of Global Positioning System (GPS) technologies for measuring crustal deformation, geodesists can measure absolute ground positions with great accuracy [*Dixon*, 1991; *Hager et al.*, 1991; *Stein*, 1993]. Using these positions measured over time, we can estimate site velocities with a precision of a few mm per year or better of horizontal motion. In seismogenic zones, such as the New Madrid, we can use this information along with estimates of the slip on large earthquakes to improve estimates of seismic hazards from the minimum recurrence times of the earthquakes with an inferred slip.

Along with Seth Stein, Tim Dixon, Joe Engeln and John Weber, I use local and far-field campaign as well as platewide continuous GPS data, to assess the current velocities of crustal motions and therefore draw inferences about the recurrence of large earthquakes in the New Madrid seismic zone (NMSZ). These results as well as those of the seismic recurrence study detailed in this and the following chapter have been published [*Newman et al.*, 1999a].

2.2 Campaign GPS at New Madrid

2.2.1 Previous Work

Prior to this study three previous geodetic studies were performed to estimate the current near-field strain across the New Madrid seismic zone. *Liu et al.* [1992] combined measurements from a 1991 GPS field campaign with data from an old triangulation network, measured in the 1950s, in the western portion of the southern New Madrid region (Figure 2.1). Although they found no resolvable strain in the eastern portion,

and no strain over the entire network, *Liu et al.* [1992] found considerable strain (-0.247 ± 0.047 μrad year^{-1}) in the western portion of their network. From this they interpreted a slip rate of 5-7 mm/yr, nearly 1/3 the estimated slip rate across the San Andreas fault in California, and concluded that the fault can accumulate the necessary strain energy for 1811-12 magnitude events once every 1000 years.

Snay et al. [1994] combined another 1991 GPS campaign north of the *Liu et al.* [1992] study (Figure 2.1), with previously collected GPS and triangulation-trilateration data. From this, they attempted to determine the strain rate across several sub-regions as well as the entire network, and were unable to demonstrate any resolvable strain rate. Their best resolved strain rate was in the northern region where they found 0.030 ± 0.019 μrad year^{-1}, which they note is not statistically different from zero at 95% confidence.

This study builds on the third prior near-field geodetic study [*Weber*, 1995; *Weber et al.*, 1998], who carried out two GPS campaigns across the NMSZ in November 1991 and October 1993. The *Weber et al.* [1998] study, extending considerably further away from the fault than the above mentioned campaigns, used 24 monuments (9 preexisting National Geodetic Survey (NGS), one Federal Aviation Administration (FAA), and 14 newly built monuments) in six states surrounding the NMSZ. These sites consist of small steel pins built directly into bedrock in regions outside the Mississippi Embayment, or stainless steel rods driven to refusal and protected from the non-tectonic soil effects using isolation collars in regions of unconsolidated alluvium and semi-consolidated bedrock in the Mississippi Embayment(Figure 2.2).

Due to the very short time (2 years) between occupations, the expected small

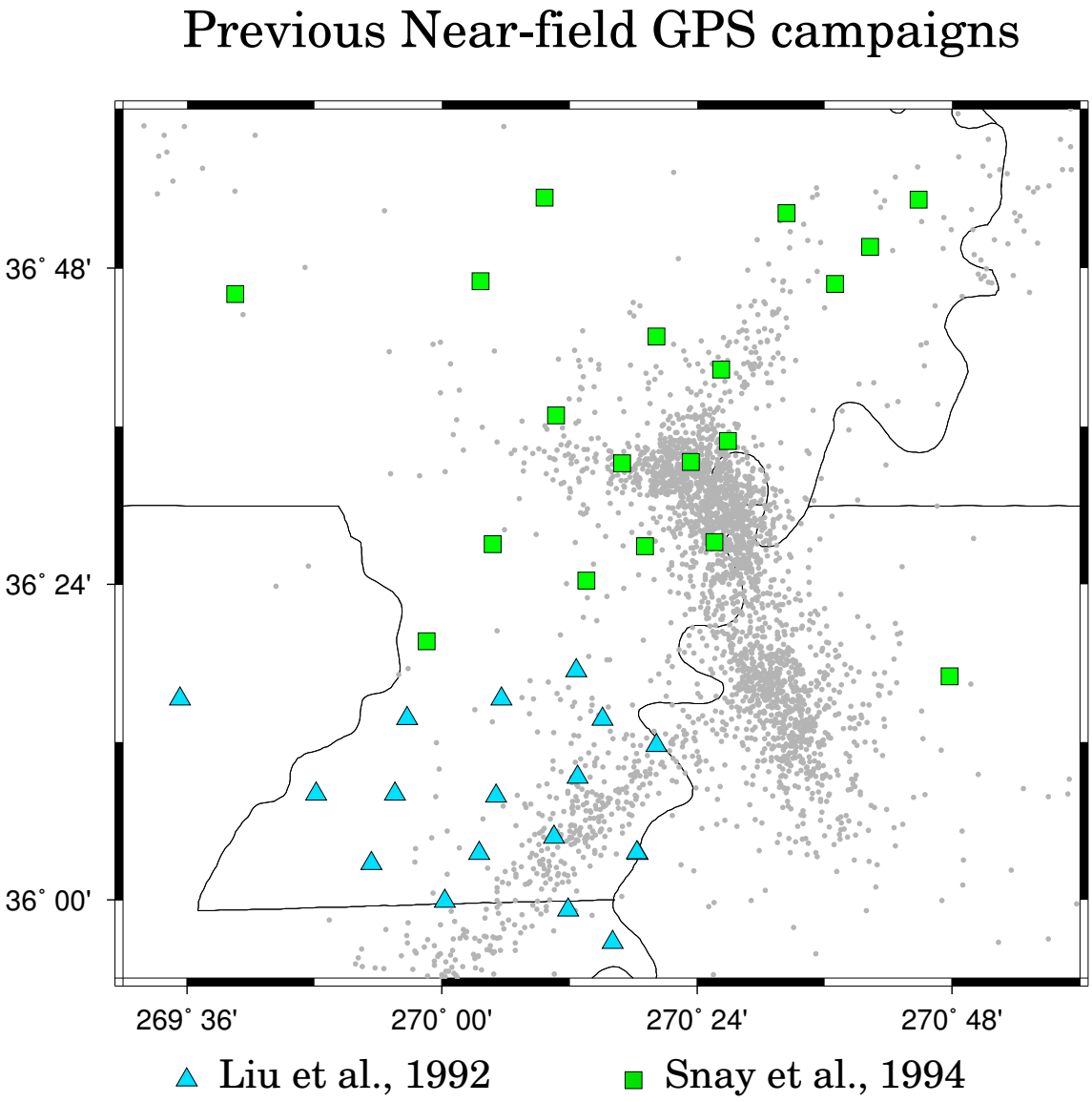

Figure 2.1: The location of GPS monuments that were used in the *Liu et al.* [1992] and *Snay et al.* [1994] studies are shown as upright triangles (▲) and squares (■), respectively. Sites used in these studies are within the less stable Mississippi Embayment with the exception of one site, close to MKND (used in my GPSstudy; see Figure 2.2), is not plotted since it is considerably north of the plot's range.

strain rate in the region, and the then available precision in the orbital estimates for the GPS satellites, the results from *Weber et al.* [1998] suggested, but did not require, 3 to 5 millimeters of right lateral fault-parallel motion across the southern portion of the network. The Northern section had shown no resolvable motion, consistent with the previous work by *Snay et al.* [1994]. GPS results from *Weber et al.* [1998] were not consistent, however, with *Liu et al.* [1992], which excluded the possibility of zero shear at 95% confidence and found high strain rates across the western part of the central network. Since the time span of *Weber et al.* [1998] was only two years and errors were high, it was necessary to re-occupy the sites to better resolve the motions across the region better.

2.2.2 1997 Campaign

In October 1997, we re-surveyed the network used by *Weber et al.* [1998]. One site (CRVL), the Caruthersville, MO soil site, had been destroyed by the installation of a baseball field earlier that year *. For six days, from October 5^{th} through 10^{th}, we recorded GPS signals for 8 hour periods over 2 days at each of the 23 remaining sites. The sites were each measured using Dorne-Margolin Trimble choke-ring antennas on tripods that were centered using optical plumbs between 1.1 and 1.7 meter above the monument pins. The weather was cooperative, with only brief showers, so the two 8-hour periods were sufficient for determining accurate positions.

*The loss of such monuments, though frustrating, is not uncommon in geodesy.
Much as the Caruthersville, Missouri monument now lies under several feet of dirt and turf, the earlier small town of Little Prairie (same location) is reported to have been covered by several feet of water after the Dec. 16, 1811 mainshock forcing residents to abandon the town [*Fuller*, 1912; *Penick Jr.*, 1981].

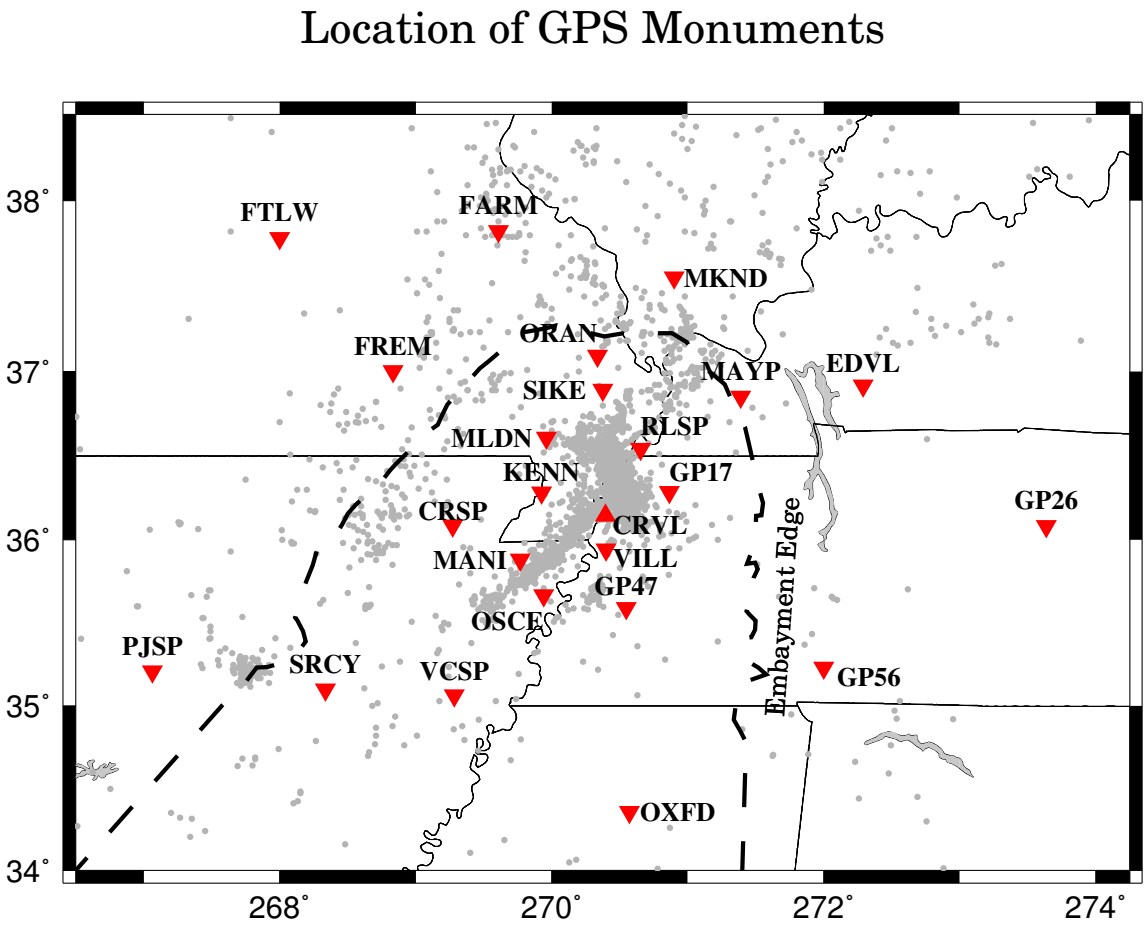

Figure 2.2: The location of GPS monuments that were used in this study are shown as inverted triangles (▼). Station CRVL, denoted by an upright triangle (▲), was destroyed during the installation of a new baseball field before our last survey in 1997 and was therefore not used in this analysis.

2.3 GPS Data Processing

I analyzed the 1991, 1993 and 1997 GPS data at the Geodesy lab in the University of Miami following the methodology of *Dixon et al.* [1997]. It was necessary to re-analyze the two previous campaigns because improved data reduction techniques and computational power allowed for higher precision results than possible at the time of *Weber et al.* [1998], it was also important to keep keep all the positions in the same ITRF reference frame. Since reduction of GPS for high precision ground motion has become relatively routine over the past 15 years, I will only detail the information and techniques that are unique to the reduction of data for this study (including the re-analysis of 1991 and 1993).

2.3.1 Data Reduction

Uncertainties in the location of the GPS satellites can be a significant error source for precision GPS [e.g., *Blewitt*, 1993]. Although the current GPS satellites broadcast their locations (satellite ephemerides) the data are not accurate enough for crustal studies. The Jet Propulsion Laboratory (JPL) makes available, high precision no-fiducial [†] satellite orbit and clock information. These data are distributed by JPL over the Internet for all times starting in 1995, and for most periods back to 1992, upon request[*personal communication David Jefferson, JPL*]. Global sitese werhere positions and velocities are defined in ITRF are then used to transform the site positions into ITRF 96 coordinates.

[†]The term *no-fiducial* is used for satillite path descriptions that are only loosly constrained for a specific reference frame.

Unfortunately for the 1991 GPS campaign data, the precise orbit information was unavailable. In order to do a rigorous comparison with the later data, also in ITRF-96 but done using JPL orbits, it was necessary to estimate fiducial orbits using data from the then-existing sparce continuous GPS network [e.g., *DeMets et al.*, 2000]. The orbits were referenced to three permanent sites that were running during the 1991 campaign and exhibited good global geometry (Tromsö, Norway (TROM), Hartford, South Africa (HART), and Fairbanks, Alaska (FAIR) fixed to their ITRF-96 positions and velocities). This orbital information was used as input into the GIPSY-OASIS II (GPS Inferred Positioning SYstem-Orbit Analysis and SImulation Software) GPS software [*Lichten and Border*, 1987; *Lichten*, 1990; *Webb and Zumberge*, 1993; *Lichten et al.*, 1995] to estimate daily site positions in the global reference frame ITRF-96 (a global Cartesian coordinate system [*Sillard et al.*, 1998]). GIPSY-OASIS II yields highly accurate results which is useful when the velocity gradients are very small (as in the NMSZ). The data were subsequently converted into geographic coordinates and are listed with estimated daily geographic coordinates in appendices A, B and C.

2.3.2 Estimating Site Velocities

I estimated horizontal velocities for each site from least squares fits to daily positions weighted by errors, following methodology of *Mao et al.* [1999]. Since GPS daily positions are plagued by occasional spurious outliers, daily positions that fell more than 2 σ outside a first order least squares fit were removed and a new velocity (by a second fit) was then determined. The final fits, with corrected error and root mean squared (rms) scatters are shown in figures 2.3, 2.4, 2.5 and 2.6.

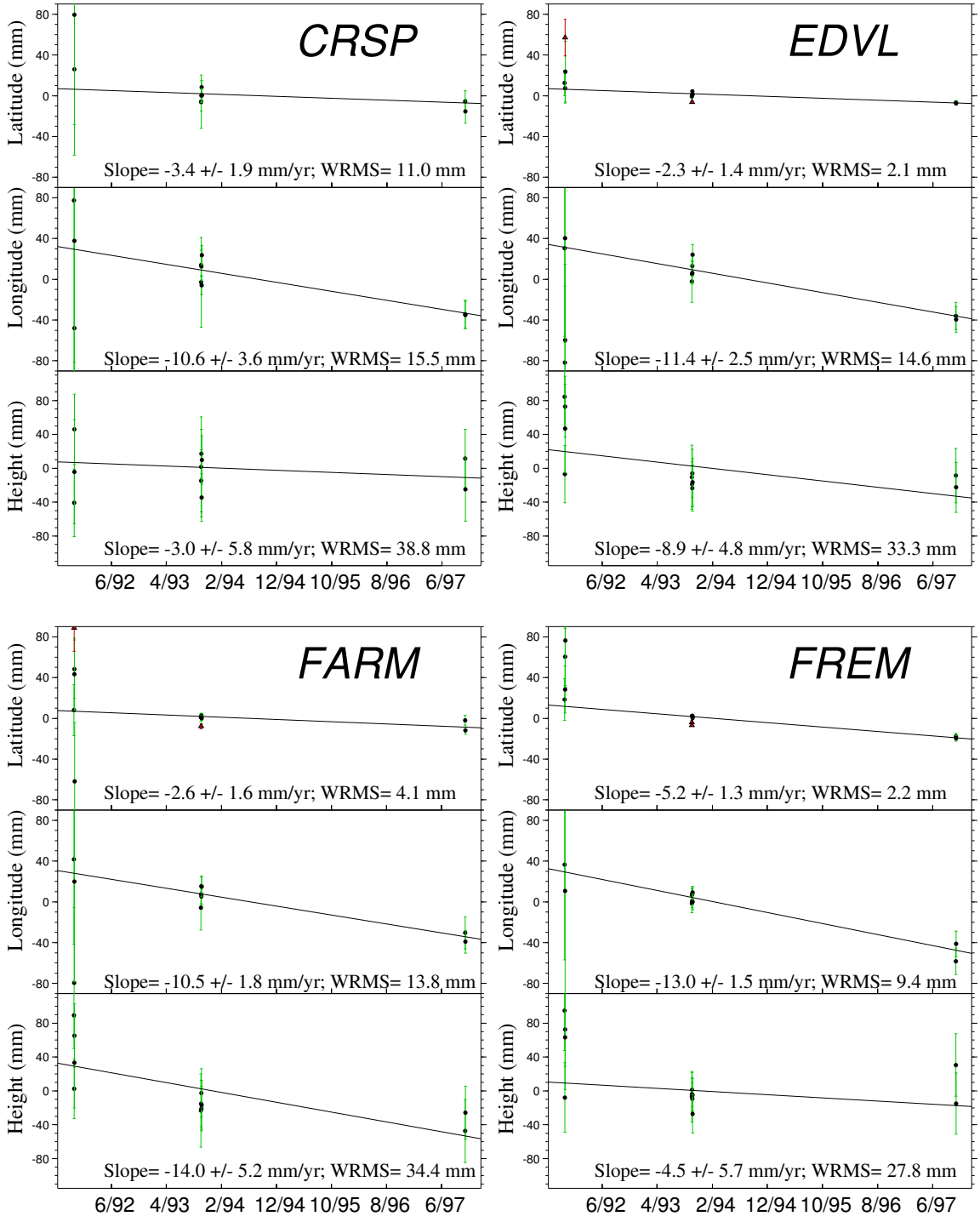

Figure 2.3: Estimated velocities for sites CRSP - FREM. The vertical component is represented for completeness; no major effort has been made to reduce the formal errors in velocities.

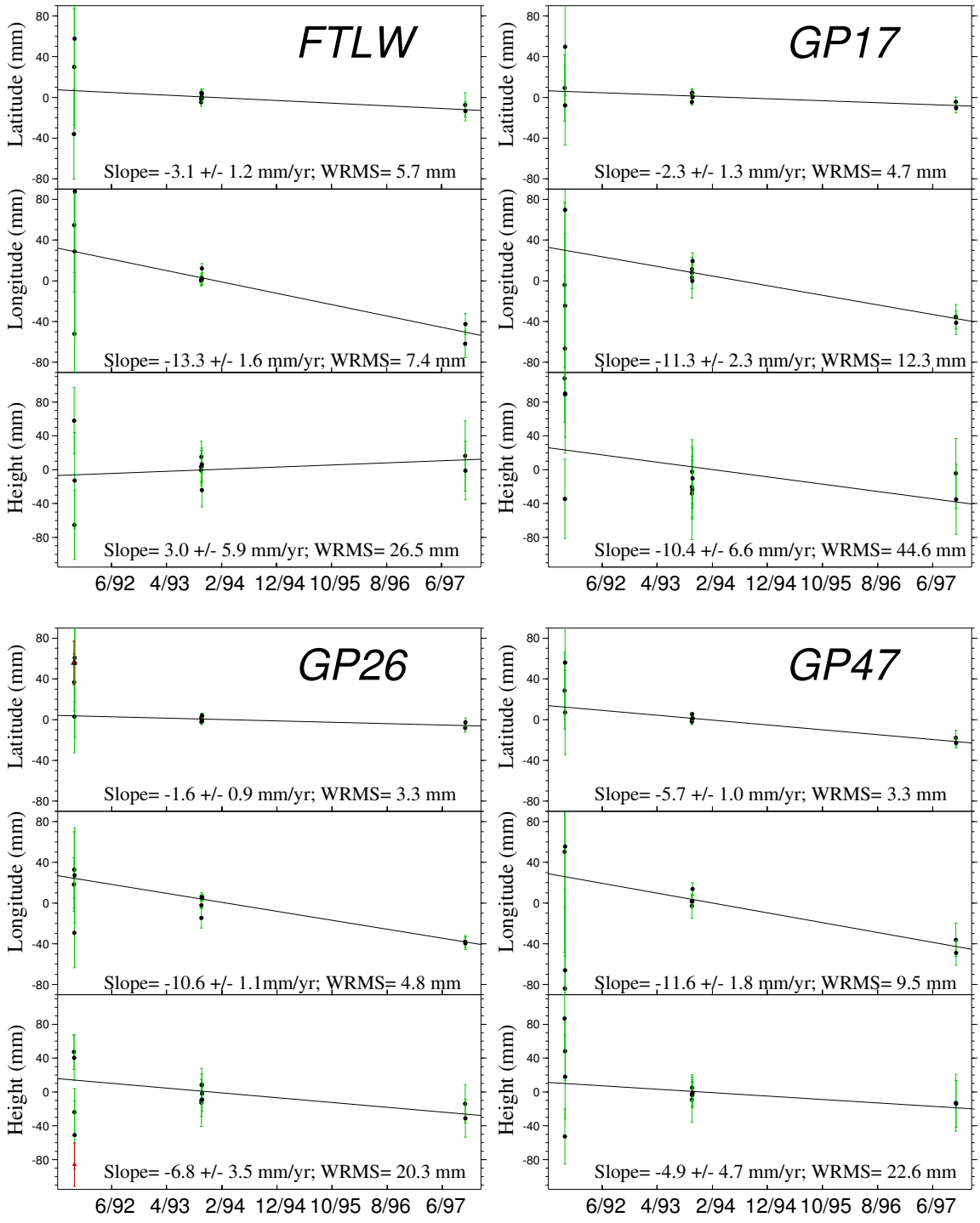

Figure 2.4: Estimated velocities for sites FTLW - GP47. The vertical component is represented for completeness; no major effort has been made to reduce the formal errors in velocities.

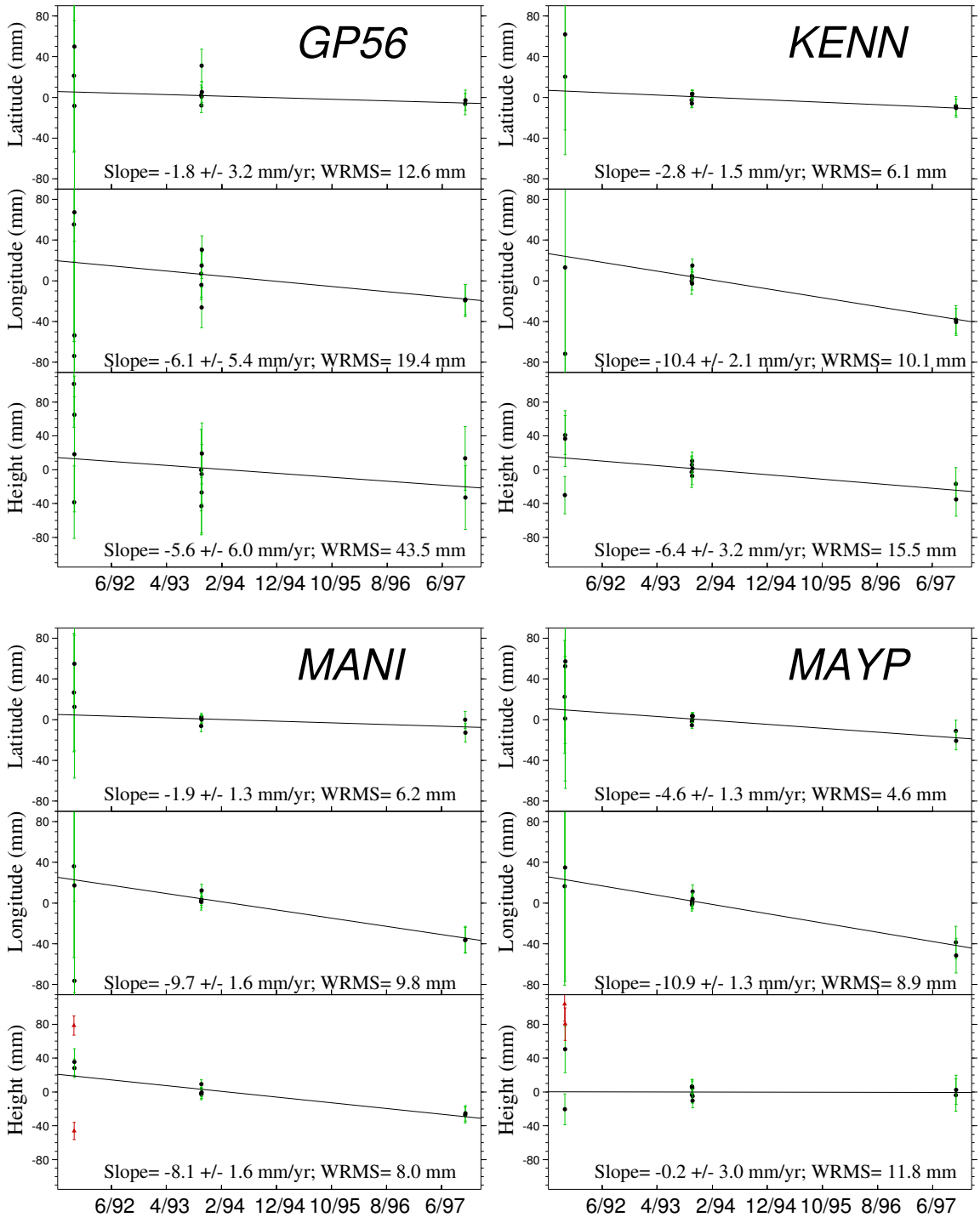

Figure 2.5: Estimated velocities for sites GP56 - MAYP. The vertical component is represented for completeness; no major effort has been made to reduce the formal errors in velocities.

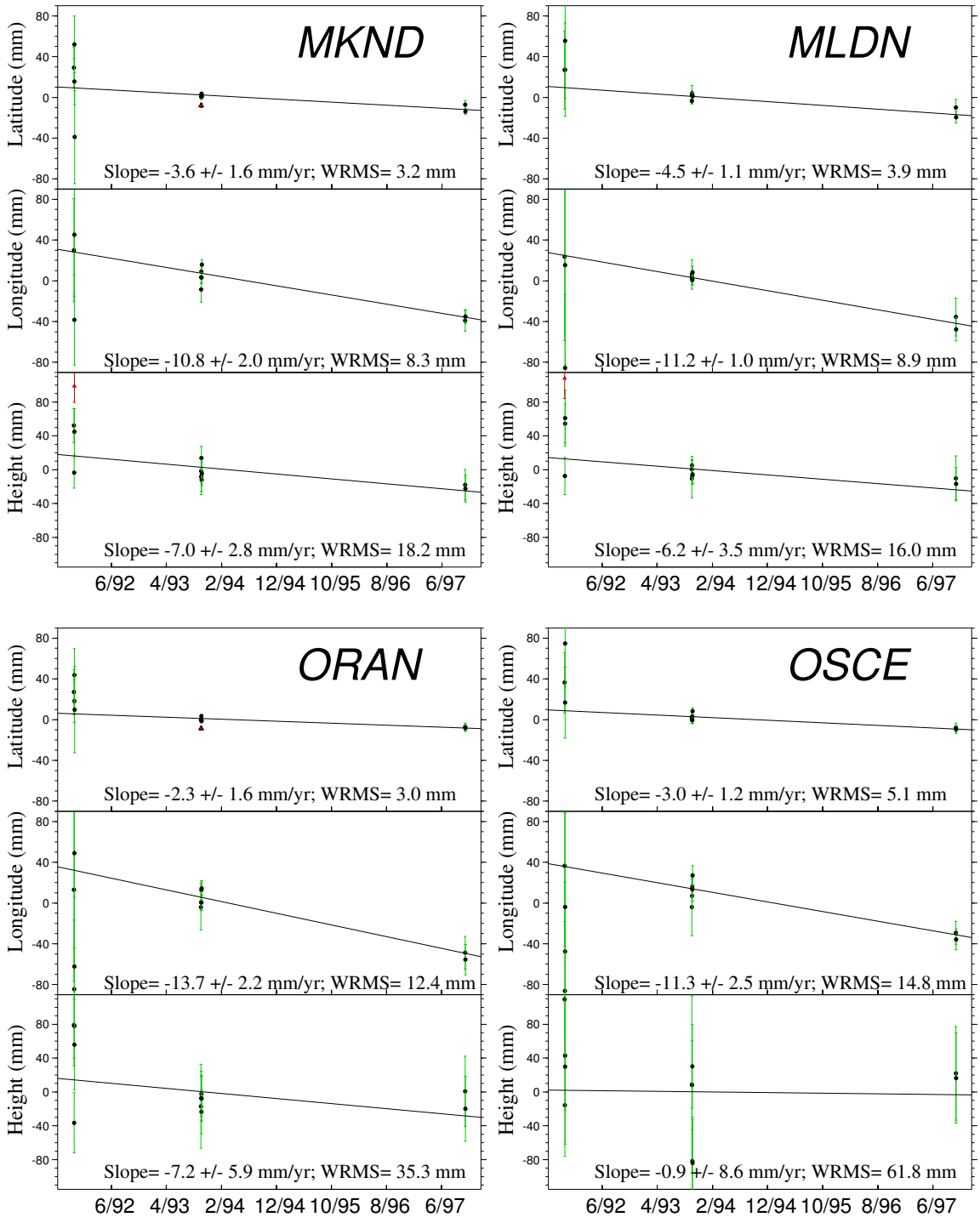

Figure 2.6: Estimated velocities for sites MKND - OSCE. The vertical component is represented for completeness; no major effort has been made to reduce the formal errors in velocities.

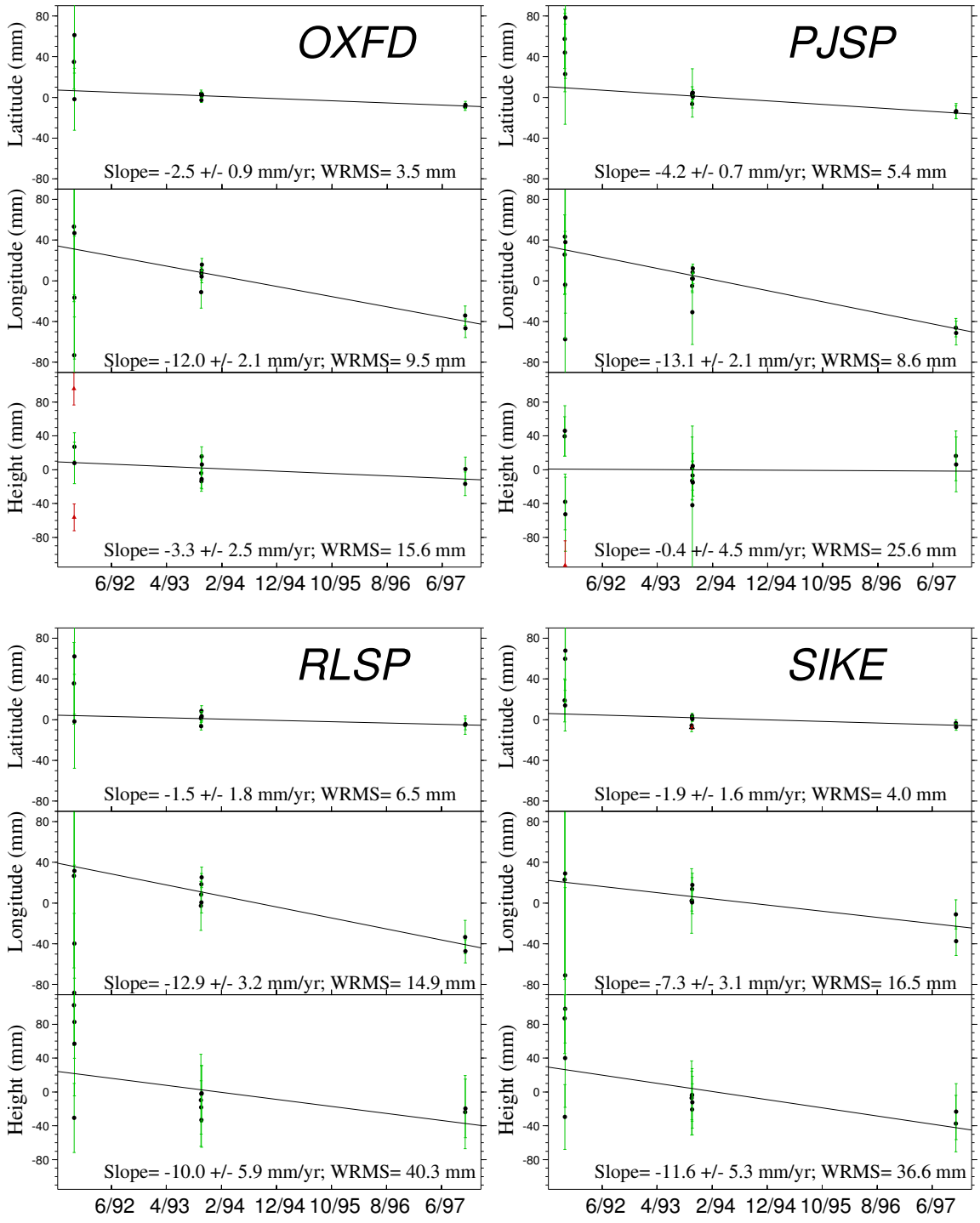

Figure 2.7: Estimated velocities for sites OXFD - SIKE. The vertical component is represented for completeness; no major effort has been made to reduce the formal errors in velocities.

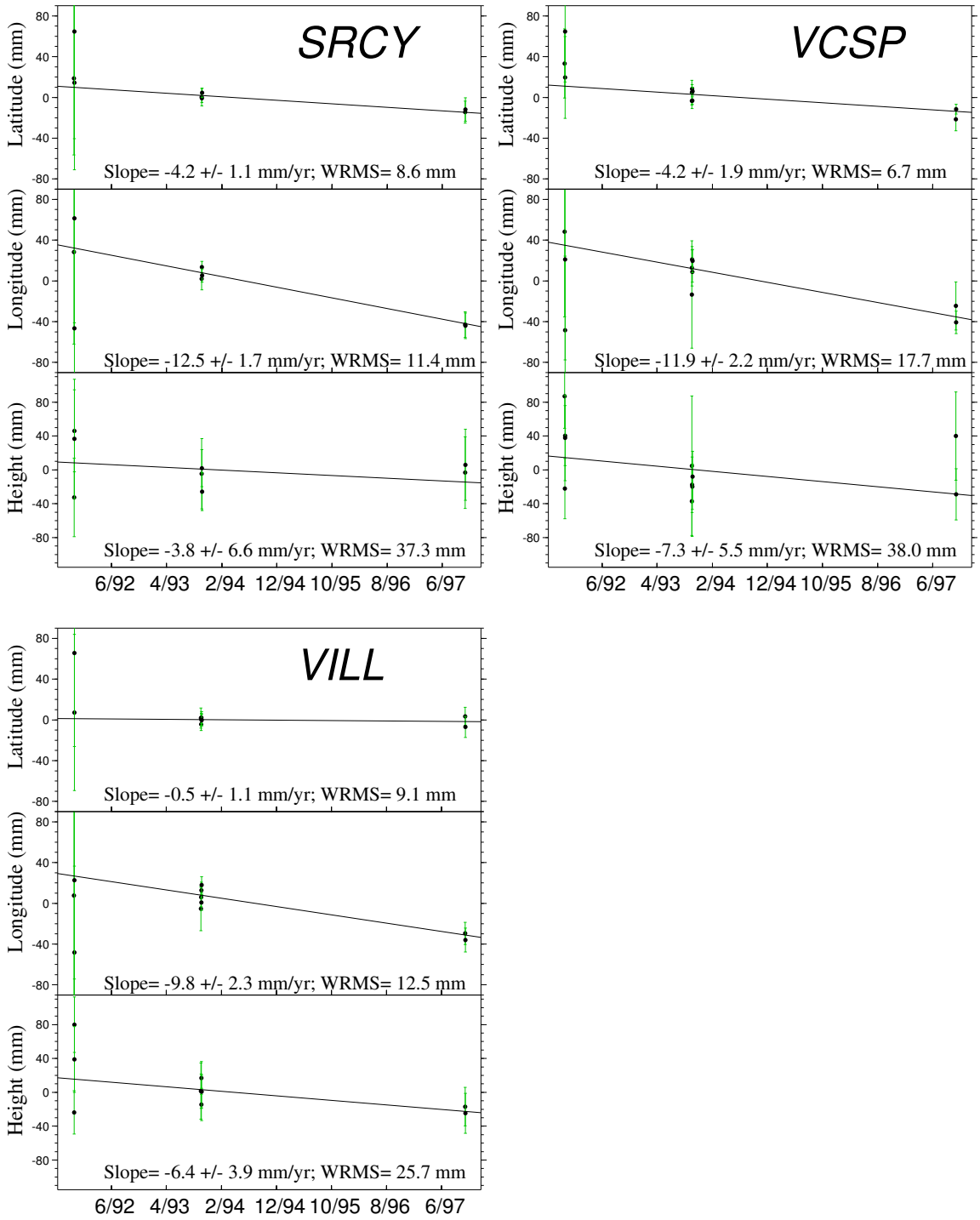

Figure 2.8: Estimated velocities for sites SRCY - VILL. The vertical component is represented for completeness; no major effort has been made to reduce the formal errors in velocities.

SITE	Lat. (°)	Long. (°)	Site Vel. North (mm/yr)	Site Vel. East (mm/yr)	Exp. Plate Vel. North (mm/yr)	Exp. Plate Vel. East (mm/yr)	σ_N	σ_E	$Corr_{NE}$
CRSP	36.05	-90.67	-3.4	-10.6	-4.3	-12.9	1.9	3.6	0.37
EDVL	36.92	-87.79	-2.3	-11.4	-3.2	-13.2	1.4	2.5	0.46
FARM	37.82	-90.46	-2.6	-10.5	-4.2	-13.4	1.6	1.8	0.43
FREM	36.95	-91.10	-5.2	-13.0	-4.4	-13.2	1.3	1.5	0.45
FTLW	37.69	-92.17	-3.1	-13.3	-4.8	-13.3	1.2	1.6	0.48
GP17	36.28	-89.20	-2.3	-11.3	-3.7	-13.0	1.3	2.3	0.43
GP26	36.01	-86.36	-1.6	-10.6	-2.7	-13.0	0.9	1.1	0.46
GP47	35.59	-89.59	-5.7	-11.6	-3.9	-12.8	1.0	1.8	0.45
GP56	35.23	-88.19	-1.8	-6.1	-3.3	-12.8	3.2	5.4	0.40
KENN	36.23	-90.04	-2.8	-10.4	-4.0	-13.0	1.5	2.1	0.40
MANI	35.89	-90.15	-1.9	-9.7	-4.1	-12.9	1.3	1.6	0.41
MAYP	36.77	-88.58	-4.6	-10.9	-3.5	-13.1	1.3	1.3	0.48
MKND	37.55	-89.22	-3.6	-10.8	-3.7	-13.4	1.6	2.0	0.34
MLDN	36.61	-89.99	-4.5	-11.2	-4.0	-13.1	1.1	1.0	0.50
ORAN	37.09	-89.62	-2.3	-13.7	-3.9	-13.2	1.6	2.2	0.54
OSCE	35.69	-90.01	-3.0	-11.3	-4.0	-12.8	1.2	2.5	0.38
OXFD	34.35	-89.51	-2.5	-12.0	-3.8	-12.4	0.9	2.1	0.36
PJSP	35.12	-92.94	-4.2	-13.1	-5.1	-12.5	0.7	2.1	0.38
RLSP	36.47	-89.35	-1.5	-12.9	-3.8	-13.1	1.8	3.2	0.39
SIKE	36.89	-89.57	-1.9	-7.3	-3.8	-13.1	1.6	3.1	0.43
SRCY	35.28	-91.66	-4.2	-12.5	-4.6	-12.6	1.1	1.7	0.44
VCSP	35.16	-90.72	-4.2	-11.9	-4.3	-12.6	1.9	2.2	0.33
VILL	35.94	-89.83	-0.5	-9.8	-4.0	-12.9	1.1	2.3	0.37

Table 2.1: For the 23 remaining GPS sites in the NMSZ north and east velocities (with errors) are shown as measured from GPS and as predicted from a single Euler pole (in ITRF96 reference frame). $Corr_{NE}$ is the correlation between the North and the East error.

Until recently, most GPS studies assumed that geodetic noise is uncorrelated in time. However recent work has shown that the noise is time-correlated, and that assuming noise is uncorrelated can yield underestimates of velocity errors by up to an order of magnitude [*Mao et al.*, 1999]. In order to better assess the uncertainties in this early data I scaled the position errors using the correlations between weighted rms and white and colored noise, which effectively de-weights them compared to later data. The higher rms scatter in the 1991 data as compared to 1993 and later data is primarily due to the lower precision of the orbit estimates. Almost all residual velocities are small, and within the 2 σ error ellipses estimated from the repeatability of daily site positions, scaled to include the effects of time-correlated errors [*Dixon et al.*, 1997; *Mao et al.*, 1999] (see Table 2.1).

The vertical daily positions and first order fits for velocities are included in figures 2.3, 2.4, 2.5, 2.6, 2.7 and 2.8 for completeness, howevever, I did not consider them for further analysis. This was for two reasons: First, errors in the vertical component can be considerably higher than those for horizontal components due mainly to atmospheric propogation uncertainties and perhaps antenna height changes during the various occupations [*Dixon*, 1991]. Second, since the New Madrid faults are considered to be mostly strike-slip, offset by a smaller thrust segment [*Johnston and Schweig*, 1996], vertical tectonic signals are expected to be smaller as compared to horizontal signals away from the thrust segment as evidenced in boundary-element modeling by *Gomberg* [1992] and *Gomberg and Ellis* [1994]. This can also be inferred from work by *Liu* [1997] on moment-tensor inversions of small recent earthquakes in the New Madrid. He noted that the current activity's major compressional and

tensional axes lie primarily in a horizontal plane, hence the majority of expected motion is horizontal.

Removal of North American Plate Motion

I removed the motion predicted by an Euler vector for stable North America (1.16°S, 80.2°W, 0.193°/Myr) that I determined by an inversion of GPS data from 16 continuous stations, following work by *Dixon et al.* [1996] and *Mao* [1998]. These stations, the same ones that I use below to attempt to differentiate motion between the southeastern and northwestern portions of the North American plate (see section 2.5), have been selected because they were considered most stable (lowest rms scatter). The resulting motion at each of the campaign sites is listed along with the estimated velocities from the GPS campaigns in Table 2.1.

By removing the North American plate motion, we remove most network-wide motion, although a small (though not statistically significant) eastward drift remains and is visible in figure 2.9. Whether this drift is tectonically significant is unclear though it has no effect on our fault motion analysis (Table 2.2, Figures 2.11, 2.12 and 2.13) since we are only concerned with the velocity gradient (differential motion) across a northeast linear fault trend, rather than "absolute" velocity.

2.4 Locked-Fault Model

Since all the observed motions in this study are small, and within the 2σ error ellipse (see Figure 2.9), it is unlikely that any motion is resolvable across the fault trend. To test this claim, I use a simple model that has been shown to work well in other

SITE	Lat. (°)	Long. (°)	North Velocity (mm/yr)	East Velocity (mm/yr)	σ_1	σ_2	Azimuth CW from N
CRSP	36.05	269.33	0.9	2.3	3.7	1.7	75.81
EDVL	36.92	272.21	0.9	1.8	2.6	1.2	71.78
FARM	37.82	269.54	1.6	2.9	2.1	1.3	53.62
FREM	36.95	268.90	-0.8	0.2	1.7	1.1	55.17
FTLW	37.69	267.83	1.7	0.0	1.8	1.0	61.66
GP17	36.28	270.80	1.4	1.7	2.4	1.2	72.58
GP26	36.01	273.64	1.1	2.4	1.3	0.8	58.96
GP47	35.59	270.41	-1.8	1.2	1.9	0.9	72.66
GP56	35.23	271.81	1.5	6.7	5.6	2.8	71.92
KENN	36.23	269.96	1.2	2.6	2.3	1.3	65.77
MANI	35.89	269.85	2.2	3.2	1.7	1.1	56.03
MAYP	36.77	271.42	-1.1	2.2	1.6	1.0	46.49
MKND	37.55	270.78	0.1	2.6	2.2	1.4	62.52
MLDN	36.61	270.01	-0.5	1.9	1.3	0.8	41.79
ORAN	37.09	270.38	1.6	-0.5	2.5	1.2	60.87
OSCE	35.70	269.99	1.0	1.5	2.6	1.1	77.53
OXFD	34.35	270.49	1.3	0.4	2.2	0.9	79.77
PJSP	35.12	267.06	0.9	-0.6	2.2	0.7	82.19
RLSP	36.47	270.65	2.3	0.2	3.3	1.6	73.71
SIKE	36.89	270.43	1.9	5.8	3.2	1.4	74.51
SRCY	35.28	268.34	0.4	0.1	1.8	1.0	68.70
VCSP	35.16	269.28	0.1	0.7	2.4	1.7	57.66
VILL	35.94	270.17	3.5	3.1	2.4	1.0	77.87

Table 2.2: Locations and horizontal velocities (with corresponding errors) relative to North American plate (NAP) motion are shown for each of 23 campaign GPS sites in the NMSZ. σ_1 and σ_2 are the major and minor axis of error in velocity estimates. σ_1 is rotated by the azimuth (reported in degrees clockwise from north). This is similar to table 2.1 without NAP motion and errors set to north and east.

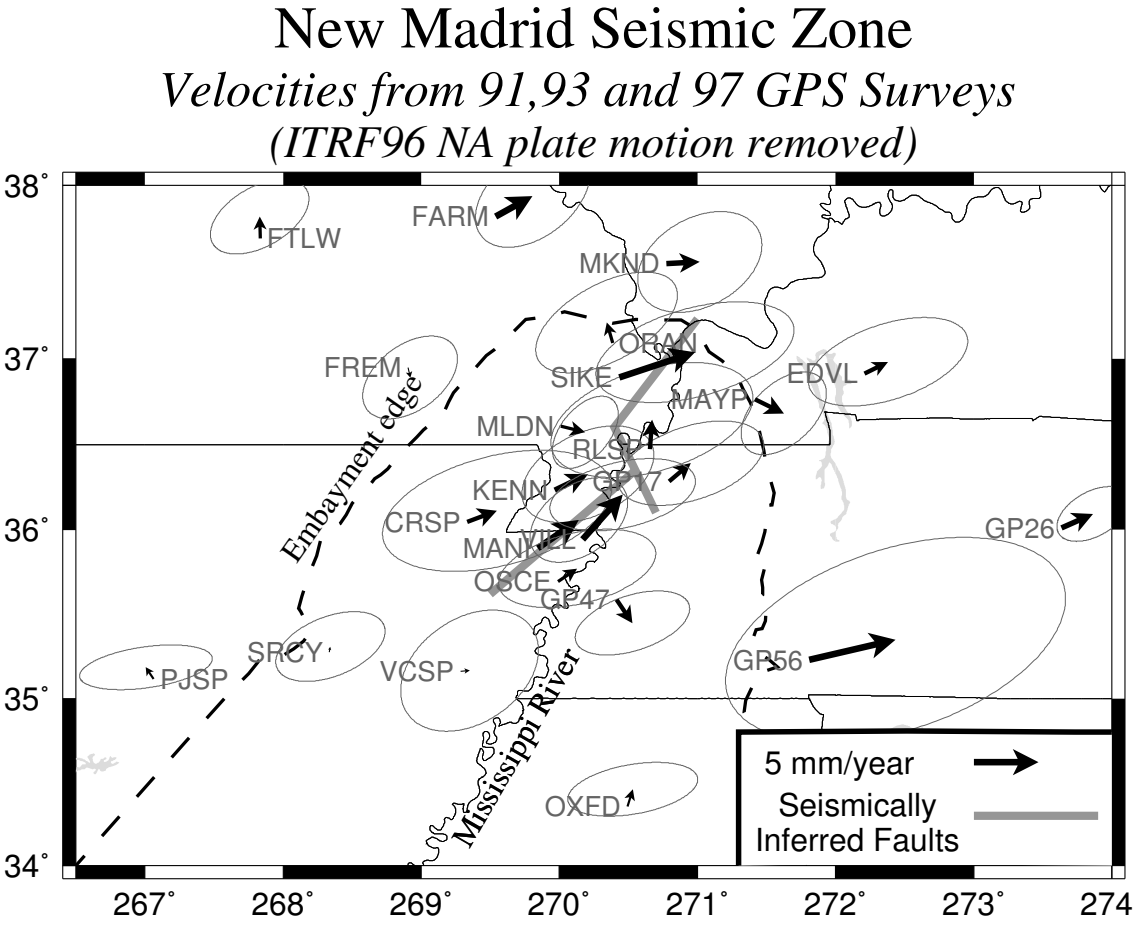

Figure 2.9: Residual horizontal site velocities (1997-1991) for the New Madrid GPS network, after removal of the motion of the North American plate. The 23 site GPS network spans the NMSZ, with sites both in the Quaternary alluvium and semi-consolidated Tertiary strata near the seismic zone, and on more stable Paleozoic-Precambrian bedrock sites outside [*Newman et al.*, 1999a]. The velocities are small and within the 2 σ error ellipses estimated from the repeatability of daily site positions, scaled to include the effects of time-correlated errors.

regions of strike-slip faulting. *Savage and Burford* [1973] have shown that a simple screw dislocation model [*Weertman and Weertman*, 1964] can be fit to geodetic data across an infinitely long locked-fault. The velocity field is defined by:

$$v_{\parallel} = \frac{2v_{\infty}}{\pi} \arctan\left(\frac{x}{D}\right), \tag{2.1}$$

where the fault parallel velocity, $v_{\parallel}$, at some distance from the fault, x, is controlled only by the far-field motion, v_{∞}, and the locking depth, D. This creates a steep velocity gradient near the fault that asymptotically approaches the far-field interseismic rate away from the fault (Figure 2.10); hence, as x/D increases $v_{\parallel}$ goes to v_{∞}. It can be argued that the New Madrid fault complex cannot be modeled this way since it lies within a plate interior [*Schweig et al.*, 1999] and does not have infinite length. However, in the absence of compelling alternative models, and given that this works well on on other seismogenic faults, this simple model makes the least assumptions.

To assess the possible fault parallel motion, I projected the site velocities along N42°E, the approximate strike of the strike-slip segments of the faults. Assuming strain accumulation on a locked right-lateral strike-slip fault, this geometry should give the greatest interseismic motions (motion expected between large earthquakes). I then removed the mean velocity and compared the residual data to the predicted velocity profile for a locked vertical strike-slip fault.

I used a fault locking depth of 25 km equivalent to the maximum depth of current seismicity [*Chiu et al.*, 1992; *Liu*, 1997; *Pujol et al.*, 1997]. Because the assumed locking depth affects only the shape of the steep central part of the profile, a reasonable range of depth has little effect on the far-field velocities (Figure 2.10).

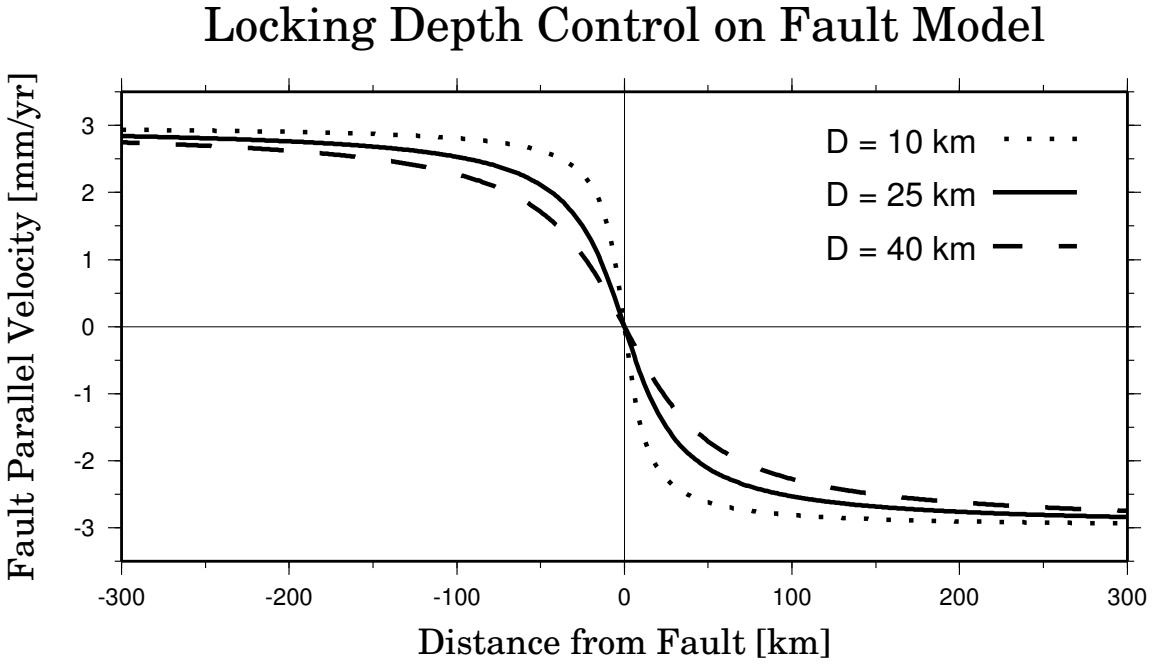

Figure 2.10: Curves illustrate the control of locking depth on the velocity gradient across an analytic locked-fault model [*Savage and Burford*, 1973] (Equation 2.1). This assumes the fault is infinitely long and motion is right-lateral.

I then varied the far-field velocity over rates of ± 6 mm/yr (negative rates denote left-lateral motion) to allow a full range of plausible lateral motion, and calculated the misfit to the model as a function of rate. To estimate uncertainties in the best-fitting rate, I rescaled the misfit to have reduced χ^2 =1 at the minimum, and used a χ^2 test to find 95% (2 σ) confidence limits for each site selection.

Figure 2.11 shows a profile of all the site velocities, with their 1 σ errors, projected parallel to the approximate trend of the major strike-slip faults (N42°E) in the NMSZ. I also show the best fit model profile using the 23 sites for a locked vertical strike-slip fault driven by far-field motion. Misfit as a function of interseismic rate is shown (bottom) with ± 2 σ range. The best fit for all sites is -0.2±2.4 mm/yr of right-lateral strike-slip far-field motion. Thus, the predicted velocities and errors are small, consistant with essentially zero motion. I also examined several sections of the network to attempt to discriminate fault motion not seen over the entire network.

2.4.1 Separation of Near- and Far-field Sites

I divided the stations into near-field and far-field sites and determined best fitting interseismic velocities. The near-field monuments are soft sediment sites within the Mississippi Embayment, and thus are expected to have greater error due to monument instability [‡]. These sites are also the most likely to have a significant tectonic signal (such as from post-seismic relaxation from the 1811-12 earthquake series [*Rydelek and Pollitz*, 1994]), as they are nearest the fault zone. The far-field sites are further away

[‡]I looked briefly into the possibility of soil effects from the 1993 Mississippi river flood on our network and determined that the flood region was located too far north of the network to have caused any significant effects [*Izenberg et al.*, 1996].

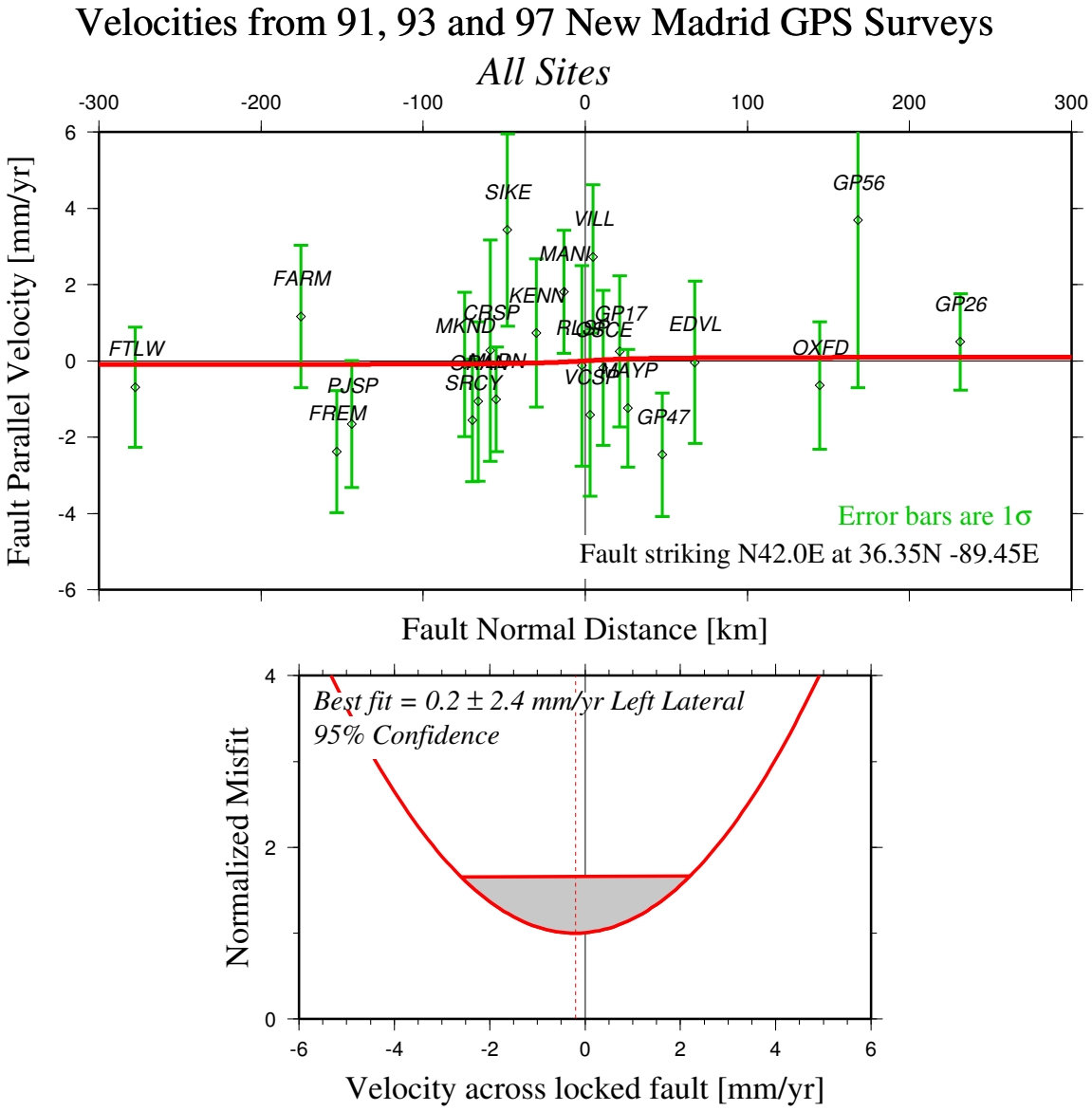

Figure 2.11: Profile of all site velocities with one σ errors (top), projected parallel to the approximate strike of the major strike-slip faults (N42°E) in the NMSZ is shown. Also shown is the best fit model profile using all 23 sites for a locked vertical strike-slip fault driven by far-field motion. Misfit as a function of interseismic rate is shown (bottom) with $\pm$ 2 σ range. The best fit for all sites is -0.2$\pm$2.4 mm/yr of right-lateral strike-slip far-field motion.

from the fault and are in Paleozoic bedrock [§]. Thus, the motion expected from these sites should have smaller error and more resemble rigid plate motions. Independently fitting these subsets to the locked fault model yields 0.6 ± 3.2 and -0.9 ± 2.2 mm/yr, respectively (Figures 2.12 and 2.13).

2.4.2 Southern Sites

The southern subnet of stations was also fit to the locked fault model independently to determine if an increased velocity field was present as suggested by previous work [*Liu et al.*, 1992; *Weber et al.*, 1998]. The sites were the same ones used by *Weber et al.* [1998] with the exception of CRVL. The best fitting model to this data show -0.4±3.2 mm/yr of right-lateral motion (Figure 2.14), considerably less than was previously estimated. This is, however, in agreement with new findings by *Kerkela et al.* [1998], who have re-occupied sites previously studied by *Liu et al.* [1992] (the same group), and have now found no resolvable strain.

None of the values for far-field motion, including the slightly higher one in the near-field where noise might be highest, differ significantly from zero. Because the rates are low, even their small uncertainties permit a range of interpretations (they are consistent with both 0 and 2 mm/yr at 2 σ). Although velocity uncertainties will be reduced by longer observation periods, the present data show little, if any, steady fault-parallel far-field motion expected prior to future strike-slip earthquakes. Note, however, the slightly higher near-field values: these might reflect a small but

[§]Here, I use *far-field sites* to represent the campaign sites furthest away from the New Madrid seismic zone. In the next section, however, I examine plate-wide continuous GPS sites which would truly be far-field; however, I denote these as continuous or platewide.

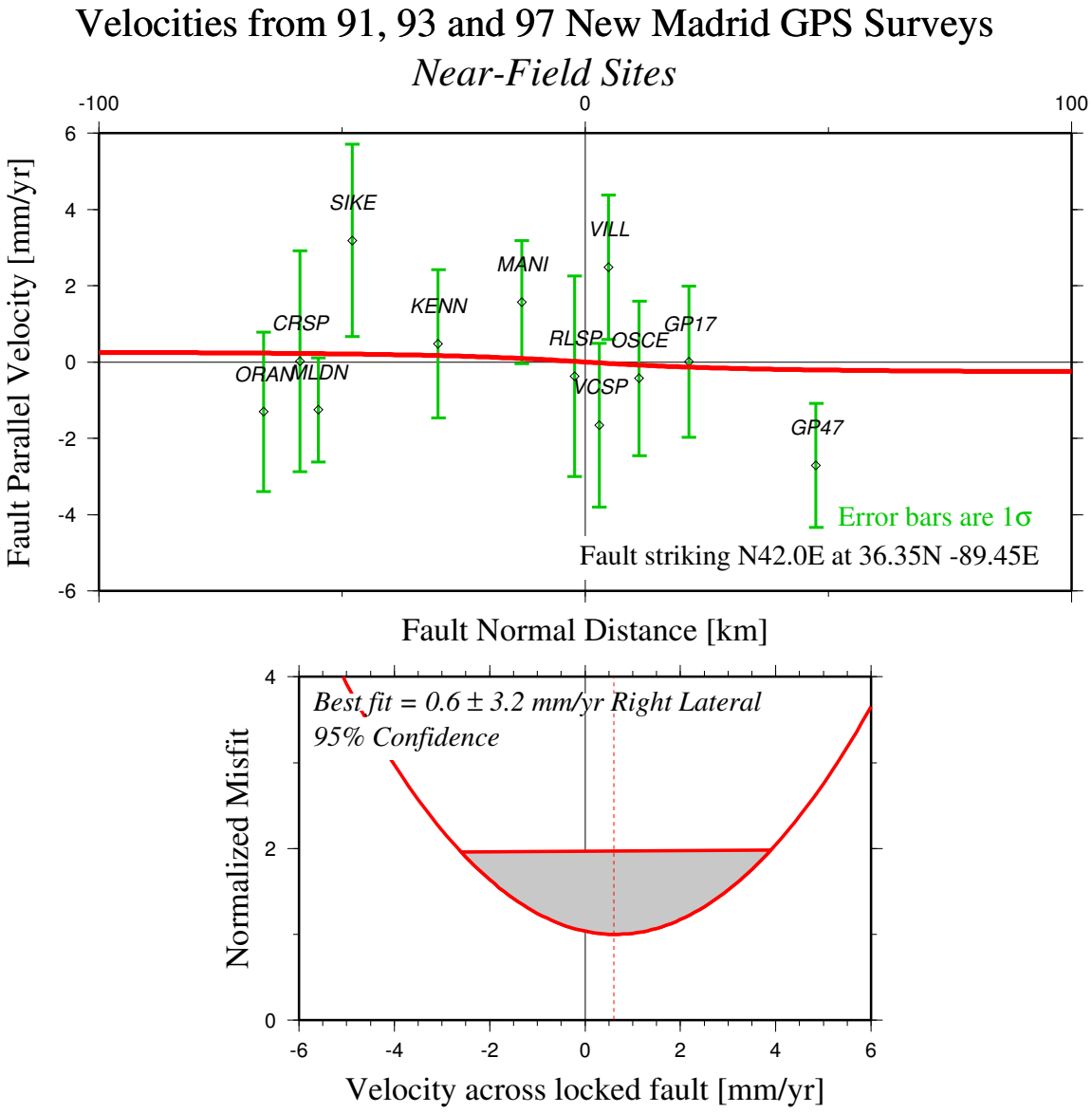

Figure 2.12: As in figure 2.11, the profile of the near-field site velocities (top) with the best fit model profile for a locked vertical strike-slip fault is shown (note: this figure is scaled differently than others). Misfits as a function of interseismic rate is shown (bottom) with $\pm$ 2 σ range. The best fit for the near-field sites is 0.6$\pm$3.2 mm/yr of right-lateral strike-slip far-field motion (higher error probably due to the less stable soil monuments).

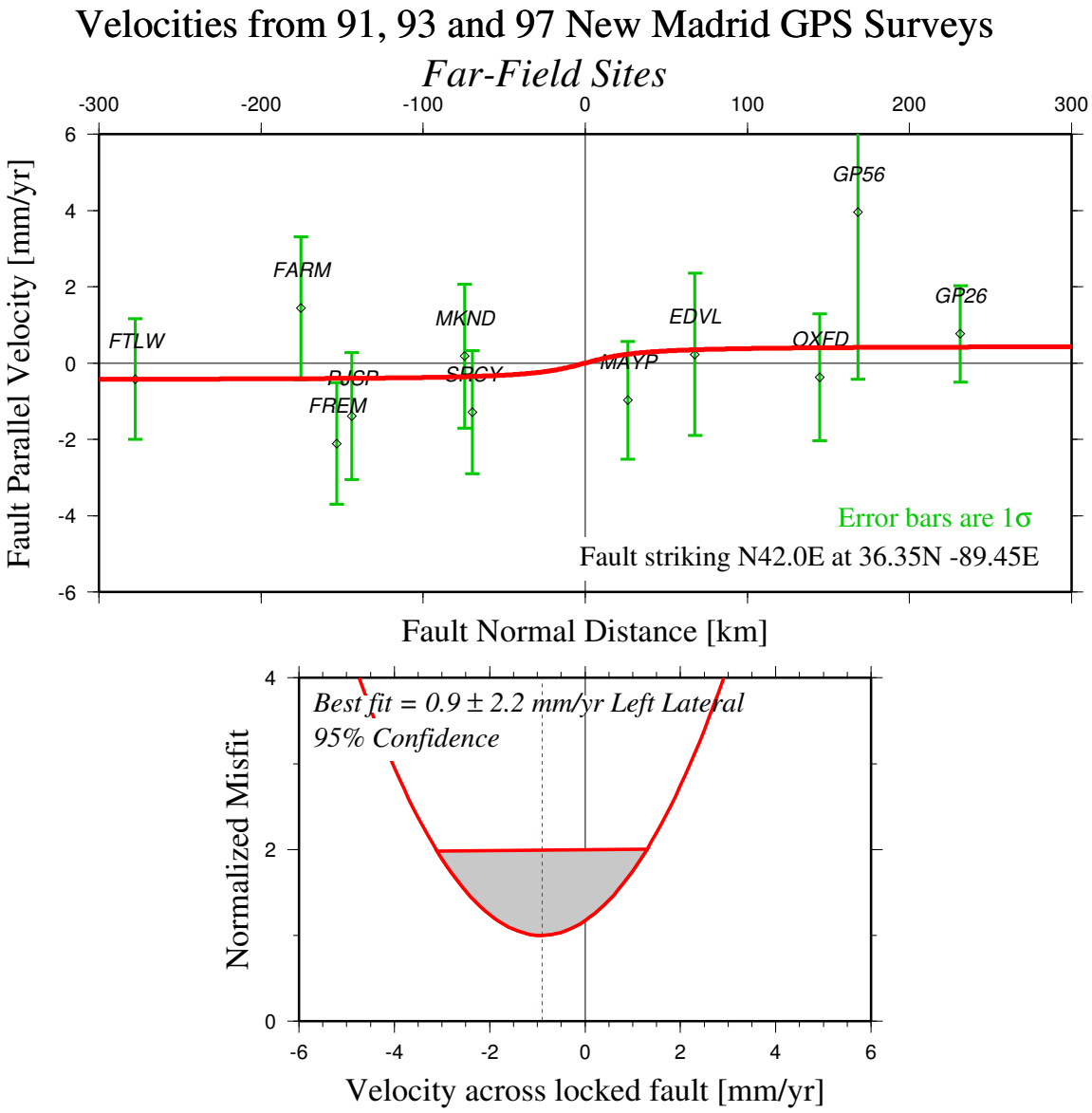

Figure 2.13: As in figure 2.11, the profile of the far-field site velocities (top) with the best fit model profile for a locked vertical strike-slip fault is shown. Misfits as a function of interseismic rate is shown (bottom) with $\pm$ 2 σ range. The best fit for the far-field sites is -0.9$\pm$2.2 mm/yr of right-lateral strike-slip motion. None of the best fitting rates differ significantly from zero.

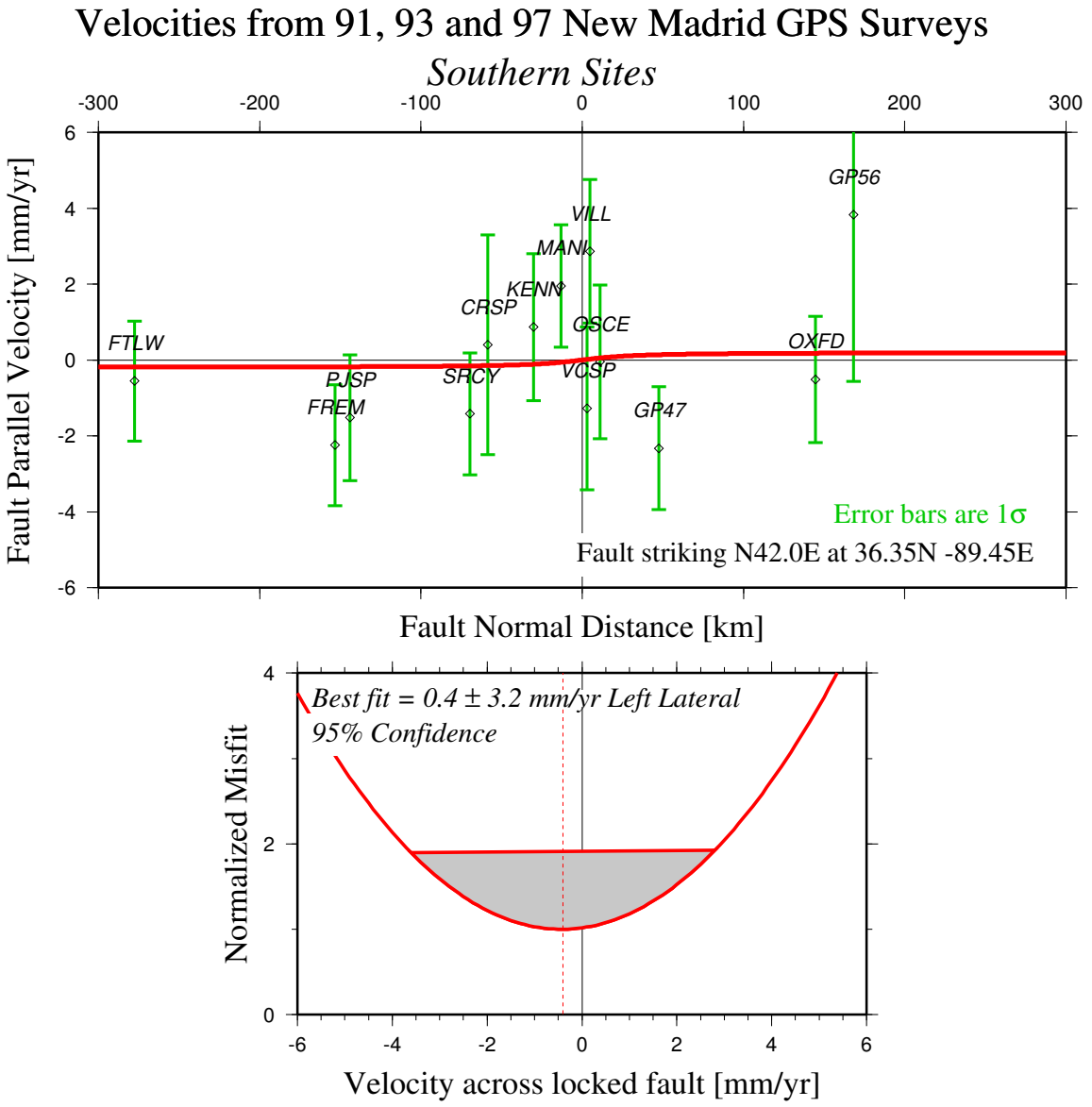

Figure 2.14: (Similar to figure 2.11), the profile of the southern network (where possible higher strain was inferred in the earlier campaigns by *Weber et al.* [1998]) site velocities (top) with the best fit model profile for a locked vertical strike-slip fault is shown. Misfits as a function of interseismic rate is shown (bottom) with ± 2 σ range. The best fit for the far-field sites is -0.4±3.2 mm/yr of right-lateral strike-slip motion. There is no resolvable motion in this section.

real signal, not consistant with a simple strike-slip fault model but possibly more indicative of real motion. For example, it could represent post-seismic deformation from the 1811-12 earthquakes [*Rydelek and Pollitz*, 1994], though there is no observed direction change across the fault structure.

Kenner and Segall [2000] explained the lack of significant motion detected by GPS with relaxation of a ductile weak zone which transfers stress to the overlying brittle crust. Although this model can create frequent large earthquakes, a mechanism capable of initiating this transient relaxation process has not been proposed, and it must not be operative at most plate boundaries where GPS routinely measure steady strain accumulation.

2.5 Continuous Platewide GPS motions

The 1991, 1993 and 1997 GPS campaigns, over a 600 km range, show little ($\leq$ 2 mm/yr), if any far-field motion across the New Madrid seismic zone. Therefore it may be possible that the far-field strain is taken up across greater distances. Thus, I examined the horizontal velocities of continuous GPS sites across the stable North America plate (NAP), in order to determine whether any resolvable motion is present across across the entire plate. Using continuous GPS from 8 sites across the plate, *Dixon et al.* [1996] found that the North American plate was extremely rigid, with site velocities fitting a single plate model with a mean residual of only 1.3 mm/yr. Following their work and including another 8 continuous stations that were found to be in the stable plate [*Mao*, 1998], I determined Euler vectors for the North American plate using three configurations of the 16 continuous sites. First, I solved for the Euler

vector for the entire plate and subtracted the site motions it predicted to determine residual site velocities (Figure 2.15, Table 2.3). Next, I separated the sites into NW and SE "blocks" divided by a simple line defining the northeasterly trending diffuse seismicity from Texas to New Brunswick (see Figure 2.15). The rms misfits of this Euler vector are not reduced by assuming the separate "blocks" east and west of the NMSZ (Figure 2.15 [Inset]), and the predicted motion across the NMSZ is indistinguishable from zero.

2.6 Implications from GPS Geodesy

The GPS results shown here have interesting implications for earthquake recurrence in the New Madrid seismic zone. It has been assumed that the 1811-1812 earthquakes were magnitude 8 events, with 5-10 m of horizontal slip [*Johnston*, 1996]. Hence, the earlier geodetic results which indicated surprisingly rapid near-field strain accumulation, 5 -7 mm/yr of horizontal motion, were interpreted as consistent with 500-800 yr recurrence for such great earthquakes (see section 2.2.1). Howeverm he estimate of far-field interseismic motion derived here, less than 2 mm/yr, implies a recurrence period for such earthquakes well exceeding 2500 yr (Figure 2.16). This period is a minimum, because it is derived from the maximum rate (at 2 σ), rather than the best fitting near-zero value which predicts a much longer period. This analysis is based on the assumption that all interseismic motion will be released seismically, without any aseismic creep or afterslip, as is commonly found in more tectonic regions [*DeMets*, 1997]. Since deformation rates here are less than a few mm/yr, compared to tens of mm/yr on plate boundaries, the recurrence times for similar large earthquakes must

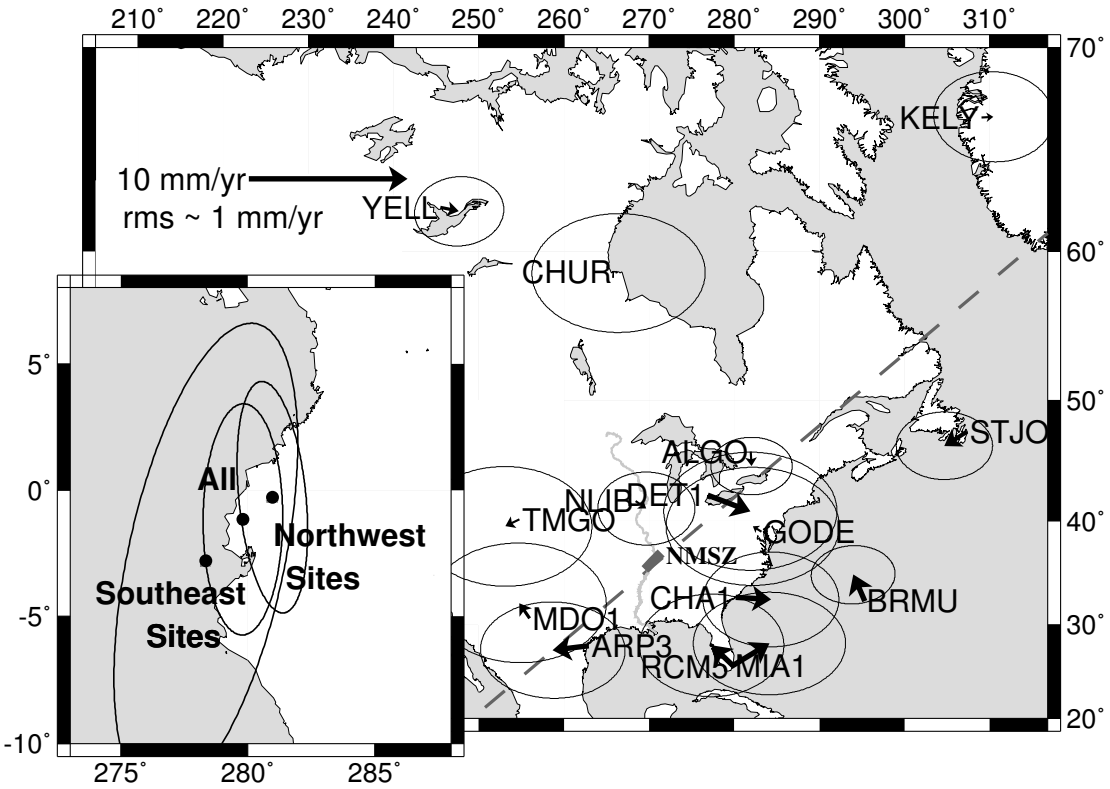

Figure 2.15: Locations of continuously recording GPS sites used to estimate an Euler vector for the presumably-stable portion of North America. For each, the misfit between the observed velocity and that predicted for a single plate is shown.
Inset: Euler poles for the eastern and western subsets of the sites (divided by dashed line) compared to that for the entire set. East and west poles overlap at 95% confidence, thus showing no resolvable motion across the NMSZ (after *Mao* [1998]).

SITE	"block"	Lat.	Long.	North Vel. (mm/yr)	East Vel. (mm/yr)	σ_1	σ_2	Azim. CW from N
ALGO	NW	45.96	281.93	-0.9	0.1	1.1	0.7	89.99
ARP3	SE	27.84	262.94	-0.3	-2.3	1.9	1.2	-88.81
BRMU	SE	32.37	295.30	1.7	-0.7	1.1	0.8	87.55
CHA1	SE	32.76	280.16	-0.1	2.2	1.8	1.2	90.00
CHUR	NW	58.76	265.91	-0.1	0.3	2.2	1.5	89.45
DET1	NW	42.30	276.90	-1.0	2.7	2.2	1.5	-89.98
GODE	SE	39.02	283.17	0.3	-0.5	2.2	1.5	89.95
KELY	NW	66.99	309.06	0.0	0.7	1.5	1.2	-86.53
MDO1	NW	30.68	255.99	1.0	-0.7	2.2	1.5	-88.94
MIA1	SE	25.73	279.84	1.3	-1.3	1.9	1.3	-89.96
NLIB	NW	41.77	268.43	-0.5	0.7	1.2	0.9	-89.58
RCM5	SE	25.61	279.62	1.5	2.4	2.0	1.3	-89.95
STJO	SE	47.60	307.32	-0.9	-1.4	1.2	0.9	89.92
THU1	NW	76.54	291.21	0.2	-0.3	1.6	1.1	-87.99
TMGO	NW	40.13	254.77	-0.4	-0.9	2.2	1.5	-89.49
YELL	NW	62.48	245.52	-0.2	1.2	1.1	0.9	84.58

Table 2.3: Location and horizontal residual velocities are shown for continuous North American GPS sites. Position and velocity (with corresponding errors) are shown for each of 16 North American Plate continuous sites and are divided into either NW or SE "blocks" separated by a 1st order line defining the Northeasterly trending diffuse seismicity from Texas to New Brunswick (see Figure 2.15). σ_1, σ_2 and azimuth are reported in the same manner as in Table 2.2.

"block"	Euler Pole		Rotation	σ_1	σ_2	Azimuth	σ
	Lat.	Long.	$^\circ\ myr^{-1}$			from N	rms
ALL	-1.16	-80.20	0.1929	1.86	0.64	0.4	1.41
southeast(SE)	-2.80	-81.66	0.1927	3.90	1.26	12.1	2.16[a]
northwest(NW)	-0.28	-79.04	0.1904	1.87	0.54	-5.6	1.33[a]

[a]rms values for SE site are calculate from the Euler vector describing the NW site, and vise-versa. This was done to illustrate better the rigidity of the North American plate.

Table 2.4: Estimated Euler Vectors for the North American plate and NW and SE "blocks", determined using the sites listed in Table 2.3.

be correspondingly longer.

Previous work by *Liu et al.* [1992], in which they had used GPS to re-measure monuments previously used for by triangulation, reported rapid strain accumulation in the southern section of the New Madrid Seismic Zone (corresponding to 5-7 mm/yr slip). A similar study across the northern NMSZ yielded strain rates indistinguishable from zero [*Snay et al.*, 1994]. The study of *Weber et al.* [1998], based on the first two GPS occupations of presumably more stable monuments, reported a far-field rate of 3±3 mm/yr, indistinguishable from zero at 2 σ. Unless the uncertainties are well understood, the estimated velocity may appear unduly significant [*Savage and Burford*, 1973]. For New Madrid, the older triangulation data were presumably less accurate than GPS, due to limitations of the technique, possibly compounded by instability of shallow-rooted triangulation pillars. Moreover, for low strain rate areas a few measurements can change triangulation results significantly [*Snay*, 1986]. The monuments used in my study were deeper-rooted and presumably more stable. They also had extend outside the Embayment and into competent bedrock. Unfortunately geodetic GPS technology was still immature in 1991. By 1993, improved GPS receivers and an improved network of global tracking sites yielded better data, as measured by improved repeatability of site positions between successive days. GPS velocity analysis is also less sensitive to site-specific errors than the triangulation analysis. Hence, we consider the GPS results here more accurate than earlier surveys. With improved geodetic techniques and longer time series, studies have found successively slower motion. This is presumably because the far-field velocity is small (or possibly zero) and since the data are uncertain, early studies with short time series

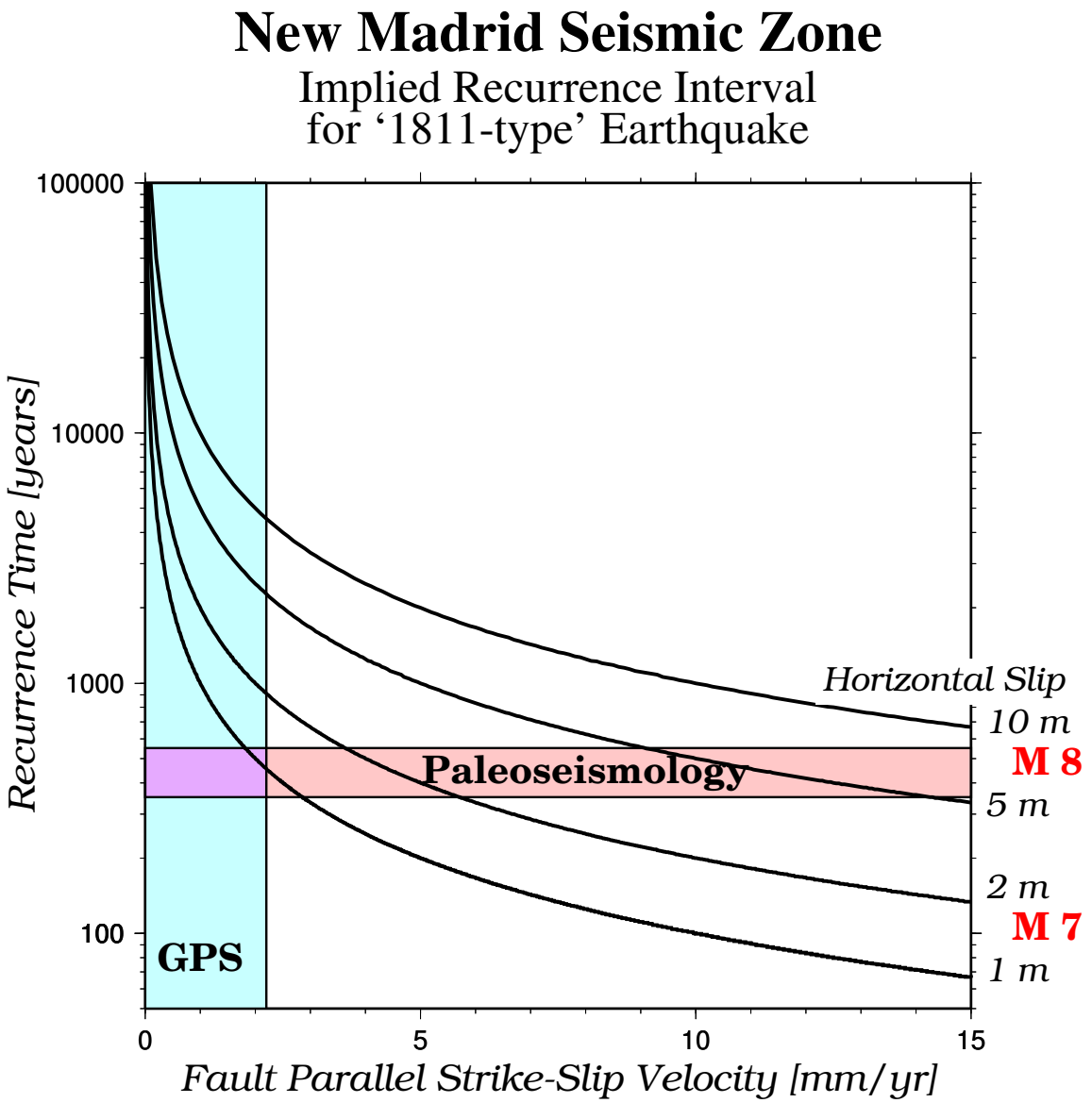

Figure 2.16: Relation between interseismic motion and the recurrence time of large New Madrid earthquakes. For an assumed horizontal slip in 1811-1812 of 5-10 m, the geodetically observed interseismic motion of less than 2 mm/yr (blue vertical bar) discussed here implies recurrence times greater than 2500 yr. Also shown are recurrence estimates from paleoseismic studies (salmon horizontal bar). The paleoseismic and geodetic data are jointly consistent with slip in 1811-1812 being about 1 m, corresponding to a Magnitude 7 earthquake (magenta box).

will allow large velocities which may appear significant if errors are underestimated. With successive measurements over longer time periods, and improved understanding of the inherent uncertainties, we should be better able to determine the true motions across the New Madrid seismic zone.

Recurrence intervals of 400-600 years, significantly shorter than those found in my study, have been estimated from the geologic record [*Wesnousky and Leffler*, 1992; *Tuttle and Schweig*, 1995; *Kelson et al.*, 1996]. However, these paleoseismologic results can be reconciled with the geodesy and frequency-magnitude relation. It is possible that the 1811-1812 and earlier large earthquakes in the paleoseismic record were significantly smaller than previously assumed, perhaps magnitude 7 with slip of about 1-2 m. If so, 1-2 mm/yr of interseismic motion would correspond to a 500-2000 yr recurrence (Figure 2.16). Later (Chapter 3), I will show that this is consistent with the recurrence for **M** 7 earthquakes from the frequency-magnitude relation (Figure 3.2). Although this magnitude is smaller than that previously inferred from the felt area of the 1811-1812 earthquakes and the spatial extent of the paleoseismic deformation [*Johnston*, 1996], it is still significant from a seismic hazard point of view. Note also that both techniques have considerable uncertainties in estimating earthquake magnitude. A recent re-evaluation of the felt-area from the 1811-12 shocks has found that earlier estimates may have been too high and that the 3 major events were more likely 7.25, 7.0, 7.45, all $\pm$ 0.3 [*Hough et al.*, 2000]. Recent paleoseismic results that estimate slip rate directly from fault-related folding yield about 6 ± 0.7 mm/yr of slip on the uppermost portion of the thrust segment over the last 2300 ± 1000 years, equivalent to $2 - 3$ mm/yr of right-lateral strike-slip motion [*Mueller et al.*,

1999]. This value, though on the high end, is still consistent with our results at 95% confidence.

In comparing the fault length of the NMSZ (∼225 km), it is difficult to understand how an **M** 8.3 could occur since the global distribution for strike-slip earthquakes predicts a subsurface rupture length greater than 370 km for that magnitude of rupture [*Wells and Coppersmith*, 1994] (see Section 1.2.1 and Figure 1.5). Hence, it is plausible that smaller 1811-1812 earthquakes can reconcile the different techniques, given uncertainties.

It is also possible that 1811-1812 style earthquakes may never recur. If more accurate future surveys continue to find essentially no interseismic slip, and the smaller earthquakes stop occurring, it is possible that we may be near the end of a seismic sequence. It has been suggested that since topography in the New Madrid region is quite subdued, the fault zone is complex and finite, and no evidence exists for earthquakes more than 2000 years ago. The New Madrid seismic zone may be a feature no older than a few Myr and perhaps as young as several thousand years [e.g., *Schweig and Ellis*, 1994]. Hence New Madrid seismicity might be a transient feature, and the present locus of intraplate strain release may migrate with time between fossil weak zones.

Although much remains to be learned about this intriguing example of intraplate tectonics, the current GPS data strongly imply that 1811-1812 size earthquakes are either much smaller (**M** 7 instead of **M** 8) or far less frequent than previously assumed (recurrence $>$ 2,500 years). In either case, it seems that accelerations predicted by current seismic hazard maps in the New Madrid zone [e.g., *Frankel et al.*,

1996] are significantly overestimated. The effects of different maximum earthquakes and recurrence times, along with different ground motion models will be discussed in chapter 4.

Chapter 3

Earthquake Recurrence from Current Seismicity

Although recent geodetic studies show no resolvable motion across the fault system (see Chapter 2), the New Madrid seismic zone (NMSZ) continues to have a large number of small earthquakes compared to other regions in eastern North America. These small events are useful because the frequency at which they occur predicts recurrence of larger events [*Gutenberg and Richter*, 1954]. Using this data, *Johnston and Nava* [1985] derived a surprisingly short recurrence time, T_r, of 550 - 1100 years for the large "1811-12 style" New Madrid events.

The recurrence interval given by *Johnston and Nava* [1985] seems short given that there has not been an earthquake greater than **M** 6 in the last 100 years. It has received much attention in the New Madrid seismological community [e.g., *Schweig and Ellis*, 1994], and has been used to constrain the recurrence of maximum magnitude events in the NMSZ for recent national seismic hazard maps [*Frankel et al.*, 1996], as discussed in Chapter 4. Here, I re-examine the assumptions made in previ-

ous extrapolations of recurrence of the large earthquakes in the New Madrid seismic zone and find a strikingly different result.

3.1 Location and Sense of Current Seismicity

In the nearly two centuries that followed the 1811-12 NMSZ earthquake series, the frequency of occurance of smaller earthquakes has not considerably changed (Figure 1.6). Thus, it seems likely that the newer seismicity is not composed of aftershocks of the 1811-12 sequence, but rather created by continuing platewide stresses or motions. Figure 3.1, which shows the epicenters of seismicity in the central United States from 1974-1999, inidicates that the New Madrid is still active. The majority of seismicity is localized on what are interpreted as three buried, discrete fault planes that have been interpreted as the fault ruptures of the three largest 1811-12 earthquakes [*Chiu et al.*, 1992; *Pujol et al.*, 1997]. There is much speculation about which of the fault segment ruptured when [e.g., *Johnston*, 1996]. A reinterpretation of felt reports from the 1811-12 series interprets the December 16^{th}, January 23^{rd}, and the February 7^{th} events as rupturing the SW strike-slip segment, NE strike-slip segment and the central thrust segment, respectively [*Hough et al.*, 2000].

Focal mechanisms from recent earthquakes are a valuable source of information, giving the sense of motion across the fault zone. The mechanisms show right-lateral strike-slip motion across the two main northeast trending vertical faults and thrusting along the west dipping fault [*Street et al.*, 1974; *Herrmann and Canas*, 1978; *Liu*, 1997]. The overall fault motions imply east-west compression consistent with inferences from well breakouts and hydrofracture data [*Zoback and Zoback*, 1981].

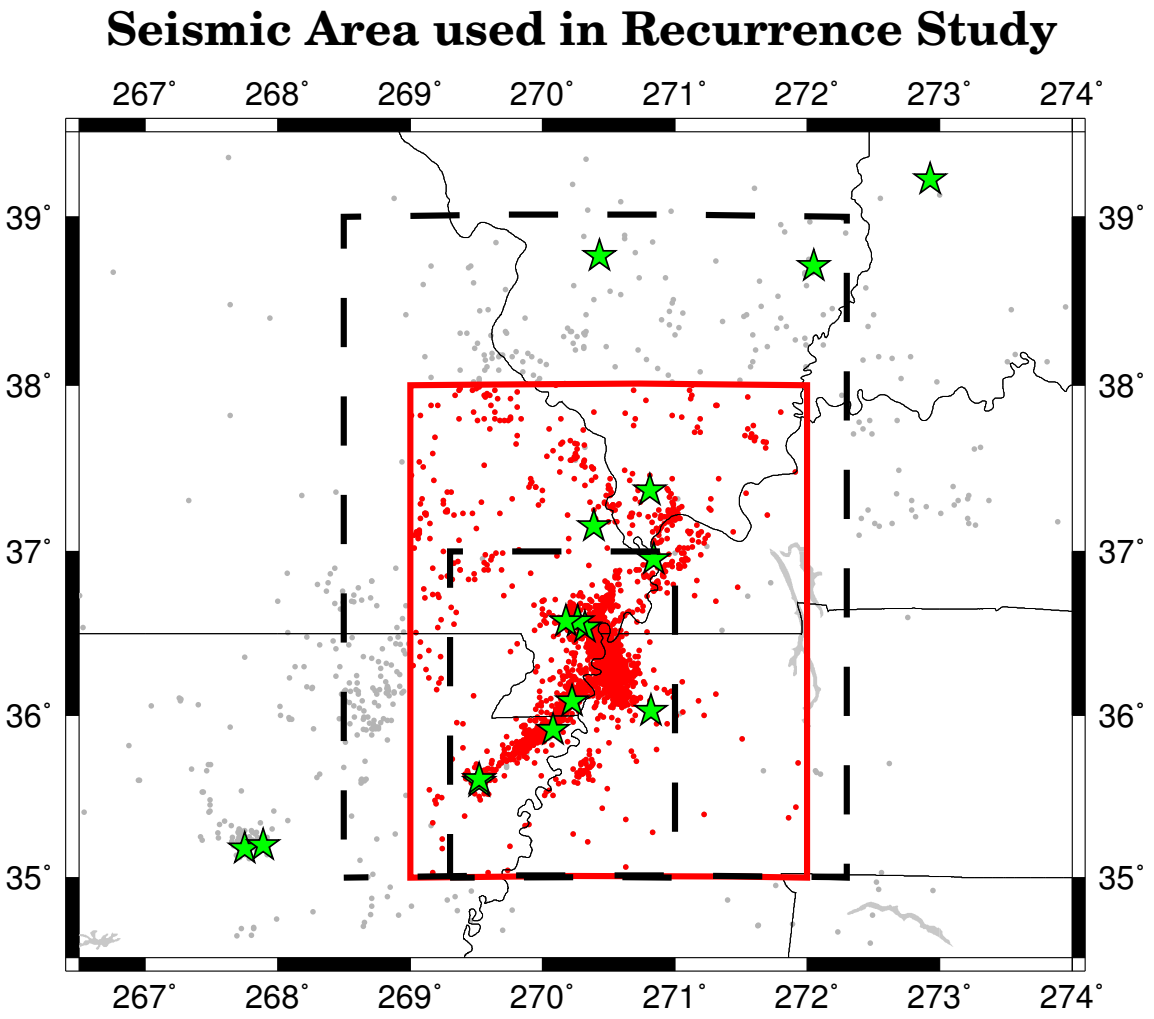

Figure 3.1: Instrumentally recorded earthquake epicenters in the Mississippi Valley from 1974 - 1999. Stars ★ represent earthquakes greater than m_b 4. Within the solid box, 35.0°- 38.0°N/88.0°- 91°W, are the events used in this Gutenberg-Richter seismic recurrence study. The dashed larger and smaller boxes are the regions that *Johnston and Nava* [1985] used to obtain the lower and higher bounds on the recurrence interval, T_r, respectively. Note, the seismicity within the region differs from *Johnston and Nava* [1985] because my study includes another 15 years of earthquake data. Seismicity data comes from same source as Figure 1.3.

3.2 NMSZ Earthquake Frequency-Magnitude Relationship

One of the problems associated with earthquake prediction is that earthquakes seem to have a temporally chaotic behavior. This behavior, however aids in understanding the frequency with which smaller events occur with respect to larger ones, through a phenomenon known as self-similarity*. Thus, earthquake populations approximately follow

$$log_{10}N = a - bM, \tag{3.1}$$

where N is the number of earthquakes (total or annual) whose magnitude exceeds M. The absolute number of earthquakes that occur within a unit time is the activity a, and the slope, b, also called the b value describes the frequency at which smaller earthquakes occur with respect to larger ones [*Ishimoto and Iida*, 1939; *Gutenberg and Richter*, 1944, 1954].

It has long been understood empirically that the relation between magnitude and frequency of occurrence is well ordered, without much understanding as to why. However, *Rundle* [1989] shows, theoretically, that the b value should be equal to 1 using the following three steps [reorganized by *Okal and Romanowicz*, 1994]:

First: Along any given fault, earthquake rupturing is considered to be scale independent (i.e., small earthquake rupture areas and slip look like miniature versions

Morris [1992] defines *self-similarity*, from chaos dynamics as "a characteristic of fractals that, when magnified, may resemble their unmagnified image."

of large ruptures and slip). Hence, the number of shocks of a certain size N_s, is inversely proportional to their rupture areas S, or

$$N_s \propto \frac{1}{S}. \tag{3.2}$$

Second: The scaling laws predict a dependence between area and seismic moment M_0,

$$S = M_0^{\beta}, \tag{3.3}$$

therefore,

$$\log_{10} N = a - \beta \log_{10} M_0 \ . \tag{3.4}$$

Third: Earthquake magnitude, M scales as

$$\mathbf{M} = a - \alpha \log_{10} M_0, \tag{3.5}$$

making the b value

$$b = \frac{\beta}{\alpha}. \tag{3.6}$$

As long as the earthquake dimensions do not saturate, $\beta = \frac{2}{3}$ [*Geller*, 1976]. *Hanks and Kanamori* [1979] empirically set α to $\frac{2}{3}$ in order to convert M_0 to the moment magnitude, M_w, such that M_w is consistent with other magnitude scales, using the

equation

$$M_w = \frac{2}{3} \log_{10} M_0 - 10.73, \tag{3.7}$$

making $b = 1$.

Because b is about one, earthquakes of a given size number approximately ten times less than those the next magnitude unit lower. Hence, a region with 100 earthquakes greater than **M** 2 per year, should have about 10 earthquakes greater than **M** 3 per year, and we would expect an earthquake greater than **M** 6 once every 100 years.

Okal and Romanowicz [1994] pointed out that b values change significantly when earthquakes become large, because fault width cannot extend to depths below the upper crust. In other words, as the failure plane elongates the b value changes. At this point, m_b saturates and β goes to 1 from $\frac{2}{3}$, increasing the b value. Also, it has been empirically shown that for smaller earthquakes, in which M_s does not saturate, α should go to one [*Ekström and Dziewonski*, 1988; *Okal*, 1989], thus lowering the b value.

After fitting multiple global data sets of Harvard's Central Moment Tensor (CMT) solutions, *Okal and Romanowicz* [1994] found that using a single magnitude scale for a full range of earthquake sizes does not yield a constant b value. Instead it is less than one for smaller magnitudes and greater than one for the largest events. However, they suggest that b is often about one because of a common practice of using a non-uniform magnitude scale, reporting M_s for large events, m_b for smaller events, and M_L for local earthquakes.

3.3 Previous Earthquake Recurrence Estimates for the NMSZ

Early studies of earthquake recurrence for the New Madrid region used modified Mercalli intensities to infer earthquake magnitude [e.g., *Mann et al.*, 1974], yielding average return periods of 175 to 700 years for large earthquakes ($MMI_0 \geq X$) [*Nuttli*, 1974]. Later, by combining smaller instrumentally recorded earthquakes from the Saint Louis University seismic network [*Stauder*, 1974-1983] with historical seismicity after 1816, in which MMI values were used to infer magnitude [*Nuttlie and Brill*, 1981], *Johnston and Nava* [1985] extrapolated a recurrence, T_r=550-1100 yr for earthquakes with $M_s > 8.3$. The shorter and longer T_r come mostly from the size of the area used to calculate the a value. Longer T_r occurs for the smaller, highly-active fault zone, and shorter T_r results from including additional background seismicity in the larger area (see Figure 3.1). For m_b, *Johnston and Nava* [1985] find a = 3.43, 3.32 and b = 0.88, 0.91, for the large and small zones, respectively.

This rapid recurrence comes from treating magnitude 7 earthquakes from the b value analysis as body-wave magnitude, m_b= 7, and then equating these to surface-wave magnitude, M_s, 8.3[†] following an m_b to M_s conversion developed by *Nuttli* [1983] for the central U.S. Recent results [*Okal and Romanowicz*, 1994] indicate that these are better treated as surface-wave magnitude 7 because b is only constant when a catalog combines M_L and m_b for smaller events and M_s where body-wave magnitudes saturate above m_b 6.4 [*Geller*, 1976](see Section 3.2).

[†] *Johnston and Nava* [1985] assume that the largest 1811-12 New Madrid events were M_s 8.3, a value which now seems a considerable overestimate.

3.4 Re-evaluation of Earthquake Recurrence at the NMSZ

Here, I determine frequency-magnitude relations for both current instrumental seismicity and historic earthquakes with inferred magnitudes. For current seismic activity, I use the New Madrid catalog of earthquakes, compiled by the Center for Earthquake Research and Information (CERI), with seismicly determined magnitudes for 1974-1998 (obtainable at http://www.ceri.memphis.edu/∼seisadm). This catalog is a compilation of data from several small early and continuing networks that have been merged in an effort to avoid duplicating events. The historical data, more likely to contain aftershocks from the 1811-12 series thus skewing the slope and activity, comes from Nuttli's catalog (http://www.eas.slu.edu/Earthquake_Center), in which many events (especially prior to 1962) were converted from modified Mercalli Intensity (MMI) to a magnitude that is comparable to m_b. For each catalog, I calculate the activity per year, a, and slope, b, for all earthquakes within the solid box (35.0°-38.0°N/ 88.0°- 91°W) in Figure 3.1, and made no additional assumptions about the earthquake magnitudes. This was done because conversion factors for magnitudes vary with every network, and magnitude scales are essentially empirical relations that are supposed to be similar to the original Richter magnitude. Although, deviations in magnitude scales are great for large earthquakes, the events that are used here are all smaller than **M** 5.1 for current seismicity and smaller than **M** 6.2 for historical seismicity.

The current seismicity yields a and b values of 3.446 ± 0.041 (1 σ) and 0.954

$\pm$ 0.013. The older seismicity from the Nuttli catalog, spanning the years from 1816 to 1984 with magnitudes prior to 1962 inferred from the intensities and less complete (few earthquakes reported below **M** 3.5), yields a and b values of 3.619 $\pm$ 0.176 and 0.979 $\pm$ 0.036 (Figure 3.2). Since the second catalog's values are comparable to the current seismicity, with slightly increased a possibly due to aftershock activity, with larger errors, I use the values for current seismicity to extrapolate T_r (with 2 σ uncertainties) for magnitude 7 and 8 earthquakes of between 1,120-2,590 and 9,500-25,000 years, respectively.

Since I use catalogs similar to those used by *Johnston and Nava* [1985], my a and b value*s* are similar. The differences in recurrence times come from the assumption that *Johnston and Nava* [1985] made by extrapolating to m_b 7.0 and converting this to an M_s 8.3. First, m_b 7.0 is not a real entity since body-waves saturate completely before by m_b 6.4. Second, *Okal and Romanowicz* [1994] found that the b value is essentially constant when m_b or M_L is used for smaller earthquakes and M_s for larger events.

The values I obtain for recurrence time seem plausible: since 1816, there have been 16 earthquakes with magnitude greater than 5 (about a 10-yr recurrence), and two with magnitude greater than 6 (about a 100-yr recurrence), so magnitude 7 and 8 earthquakes should have about 1000 and 10000 yr recurrence (see Figure 1.6).

A note on extrapolation

Extrapolation of the recurrence of larger earthquakes from the rate of smaller earthquakes, used because of the limited data available for earthquakes prior to this century,

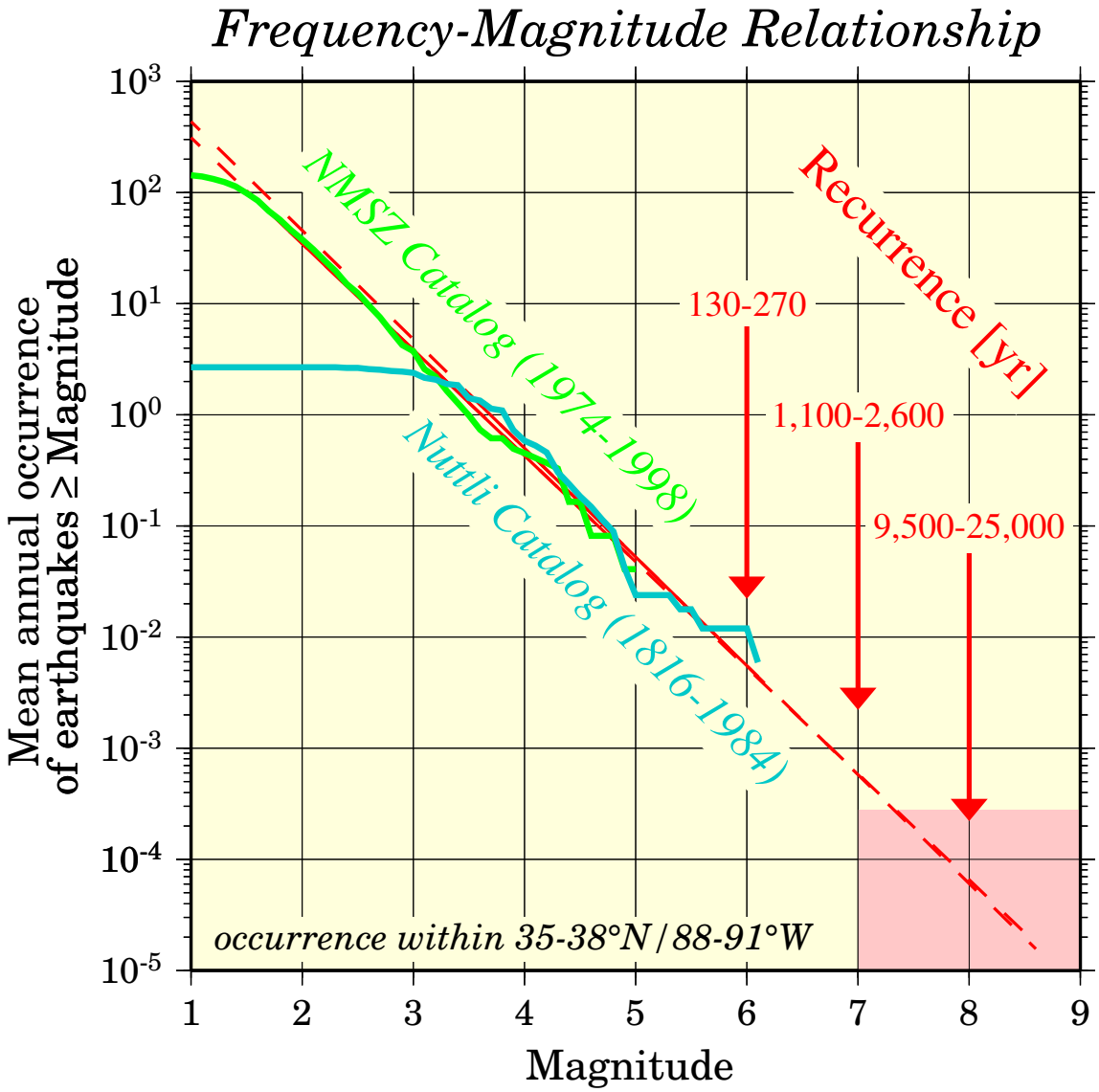

Figure 3.2: Earthquake frequency-magnitude data for the New Madrid zone. The recent (1974-1998) and historic (1816-1984) data have similar a (3.446 ± 0.041 and 3.619 ± 0.176) and b values (0.954 ± 0.013 and 0.979 ± 0.036), though the recent data have much smaller errors which are likely due to more complete earthquake reporting. Recurrence interval predicted from the current seismicity are between 1,100-2,600 yr for **M** 7 earthquakes and between 9,500-25,000 yr for **M** 8 earthquakes. Recurrence ranges, as predicted by the recent seismicity for **M** 6, 7, and 8 are shown, in red, with 2 σ uncertainties.

is affected by various uncertainties: *Stirling et al.* [1996] find that such extrapolation overestimates recurrence times of large "characteristic earthquakes" inferred from geological data, in contrast, *Triep and Sykes* [1997] and *Okal and Romanowicz* [1994] find that a linear extrapolation under-predicts recurrence times for large intra-continental and shallow earthquakes, as determined by current global seismicity.

3.5 Implications for Earthquake Recurrence from Frequency-Magnitude Relations

I reach a similar conclusion from estimating the recurrence of future larger earthquakes from the observed rate of smaller earthquakes (Figure 3.2), as I did from the geodetic study (see Chapter 2, and Figure 2.16). From recent (1974-1998) seismicity, when the earthquake catalog should be most complete and magnitudes are seismologically determined, we expect magnitude 7 and 8 earthquakes on average every 1,700 and 15,000 yrs. Similar values (1,000 and 13,000 yr) emerge from consideration of the post-1816 seismicity. These estimates are consistent with my GPS results (Chapter 2), but far exceed those in an earlier study (500 to 1,100 years [*Johnston and Nava*, 1985]), because they assumed that a linear extrapolation of the b valuefrom m_b earthquakes is just and that an m_b 7 = M_s 8.3. Both this and the GPS results thus strongly imply either **M** 7 events every 1,000 years or **M** 8 events every 10,000 years. These recurrence times are significantly longer than those previously used in seismic hazard estimates for the New Madrid seismic zone. I examine the consequences of these recurrence intervals in the following chapter.

Chapter 4

Uncertainties in Seismic Hazard Maps for the New Madrid Seismic Zone

4.1 Motivation

The U. S. Geological Survey National Seismic Hazard maps [*Frankel et al.*, 1996] predict that the seismic hazard for parts of the central U.S. due to earthquakes in the New Madrid Seismic Zone (NMSZ) in some ways exceeds that in California. The predicted ground accelerations in these maps reflect crucial parameter assumptions, many of which have considerable uncertainty due to the absence of seismological data from any but small earthquakes. For example, the *Frankel et al.* [1996] seismic hazard maps assume that the largest NMSZ earthquakes of 1811-1812 were **M** 8 events, and should recur every 1000 years. Alternatively, my GPS results (Chapter 2) and earthquake frequency-magnitude re-analysis (Chapter 3) suggest that these earthquakes may have been significantly smaller (low **M** 7) [*Newman et al.*, 1999a]. Similarly, the *Frankel et al.* [1996] maps incorporate a relation developed for the mapping project

that predicts ground motion for large earthquakes that is significantly different (and significantly higher away from the source) than other alternative published relations [e.g., *Atkinson and Boore*, 1995; *Toro et al.*, 1997].

Thus, in this chapter, I explore alternative plausible parameter assumptions (maximum magnitude M_{max}, recurrence time T_r, and alternative ground motion models), in order to determine how each affect predicted 1 Hz and peak ground accelerations in the New Madrid region. The work herein has been a cooperative effort between John Schneider and Andres Mendez of Impact Forecasting, L. L. C, Seth Stein (thesis advisor), and myself and has been recently submitted for publication, thus serving as a more concise review of this study [*Newman et al.*, 2000]*.

4.2 Introduction

Earthquake risk assessment has been described as "a game of chance of which we still don't know all the rules" [*Lomnitz*, 1989]. At present, most such assessment is done using the probabilistic seismic hazard analysis (PSHA) approach developed by *Cornell* [1968] and widely applied in engineering design [*Reiter*, 1990; *McGuire*, 1995]. Major studies of seismic hazard in the central and eastern United States, including the New Madrid Seismic Zone (NMSZ), were conducted in the 1980s by Lawrence Livermore National Laboratory [*Bernreuter et al.*, 1985] and the Electric Power Research Institute [*EPRI*, 1986] for application to nuclear power plant licensing. A

*Much of the probabilistic seismic hazard code was developed at Impact Forecasting, L. L. C., as part of a product developed for individual clients in the New Madrid region considering seismic risks to their properties or developments, and is therefore proprietary. Thus I will only give general descriptions of probabilistic Seismic Hazard Analysis (PSHA), as it will not effect the nature of this work.

detailed study of the NMSZ was also carried out for the U.S. Department of Energy for the Gaseous Diffusion Plant in Paducah, Kentucky [*Toro et al.*, 1994]. Based on these and related efforts, and motivated by the design and licensing needs of critical facilities, detailed consensus recommendations have been developed for conducting PSHA [*SSHAC*, 1997]. Unfortunately, the bulk of this work is not generally known (or easily accessible) to the broader community of seismologists because it is generally written up in technical reports published by the U.S. government, private research institutes, or conference proceedings [*Abrahamson and Shedlock*, 1997]. For the uninitiated, a beginners guide by *Hanks and Cornell* [1994], provides an informative (and entertaining) overview of the principles and implications of PSHA, although, it too, has only been published in the proceedings of an obscure (at least to seismologists) engineering conference.

Meanwhile, it has become common practice to apply the PSHA method to develop seismic hazard maps for input to regional planning and building codes [e.g., *Youngs et al.*, 1997; *Petersen et al.*, 1996; *Wong and Olig*, 1998; *Frankel*, 1995; *Frankel et al.*, 1996]. Among the recent studies, the National Seismic Hazard Maps developed by the U.S. Geological Survey [*Frankel et al.*, 1996] have gained much attention. Although the products of these efforts are widely used and accepted, few practitioners, let alone users, have an in-depth understanding of the limits of applicability of such hazard maps, or the sensitivity of such maps to assumptions in the underlying parameters.

An intriguing feature of the National Seismic Hazard maps is the high accelerations predicted for parts of the central U.S., due to earthquakes in the NMSZ. In

SHAKING EXCEEDING	AREA OF SHAKING (1,000 km^2) for: San Francisco Bay	Southern California	Central U.S.	Central U.S(a)
0.5 g	80	80	70	60
1.2 g	16	12	20	23

Table 4.1: Areal coverage of strong ground shaking for California and the central U.S. as estimated by *Frankel et al.* [1996] for peak ground acceleration at a 2% probability of exceedance in 50 years with "firm rock" site conditions. Central U.S.(a) is from this study's quantification of hazard using similar maximum magnitudes, recurrence times, and ground shaking formulations (i.e., Equal weighting of Toro and Frankel ground shaking, using $M_{max} = 8$ and $T_r = 1{,}000$ years).

parts of the NMSZ, the predicted accelerations exceed that in high-risk portions of California (Table 4.1): peak ground acceleration (PGA) predicted in 50 years at 2% probability exceeds that in San Francisco; and the area predicted to experience very high acceleration (exceeding 1.2 g) for the NMSZ exceeds that for Los Angeles. These predictions seem surprising because California is within a plate boundary zone, and thus accommodates most of the approximately 45 mm/yr net motion between the Pacific and North American plates [*DeMets et al.*, 1990; *Bennett et al.*, 1999]. In contrast, the NMSZ is within the generally stable plate interior, which GPS data show to be rigid to better than 2 mm/yr [*Dixon et al.*, 1996; *Newman et al.*, 1999a]. Hence large (magnitude 7 or greater) earthquakes taking up the interplate motion typically occur on major faults in California with mean recurrence of 100-200 yr [e.g., *Sieh et al.*, 1989]; whereas the small intraplate deformation appears to give rise to earthquakes of this size about every 500-1000 yr [*Johnston and Schweig*, 1996; *Newman et al.*, 1999a].

The ground acceleration estimates of *Frankel et al.* [1996] are based on the

assumption that the largest New Madrid earthquakes are of comparable magnitude to, though less frequent than, those in California, and thus will eventually produce ground motion exceeding that in California at comparable distances. Thus, this comparison is to evaluate the effects of assumptions made in determining the largest ground motions that are expected in a time interval of approximately 2,500 years ($\sim$ 2% probability in 50 yr).

Smaller earthquakes can still cause significant damage ($\mathbf{M} \gtrsim 5$) at close distances. Although I do not consider specific parameter assumptions that affect the size or recurrence, of these smaller events, their inclusion is necessary, since the predicted acclerations for these smaller events is affected by the ground shaking parameter chosen.

The National Seismic Hazard Maps for probabilities of 5% and 10% in 50 years predict that the ground accelerations in the NMSZ is reduced relative to high-hazard areas of California, but scientific and public attention have focused on lower probability maps in part, because these are now being used to formulate building-codes. In addition, the fact that the maps do not include site effects is often overlooked. These effects can dramatically modify the distribution of ground motion for areas of heterogeneous soil types, such as those of the Mississippi Valley, where soil type and thickness can magnify ground motions between 0.5 - 3.0 times that of hard rock [*Toro et al.*, 1994]. Nonetheless, these maps are used as a basis for policy decisions on issues ranging from building codes to science funding. Thus, the needs of engineers, insurance companies, policy makers and funding agencies would be better served by an appreciation of the uncertainties and limiting assumptions underlying these maps.

Typically, hazard maps (including the *Frankel et al.* [1996]) address primarily the aleatory uncertainty (due to inherent randomness of nature), and incorporate some aspects of the epistemic uncertainty (due to lack of data or understanding) within the overall expression of probabilities. For instance, the *Frankel et al.* [1996] maps address aleatory uncertainty by treating the occurrence time of earthquakes as a Poisson (time-independent) process. In this model, the probability of occurrence and magnitude of a major or characteristic earthquake is presumed known and constant through time. In reality, there may be significant epistemic uncertainty in the magnitude and the underlying probability of occurrence, which is not treated in the maps. On the other hand, the uncertainty in ground motion predictions for a given earthquake and distance is treated at least in part by incorporating two different ground motion attenuation relations[†]. The resulting variability or uncertainty in ground motion is combined with aleatory effects in the final probabilistic ground motion distributions. The issue of how uncertainty is treated prompted me to explore alternative plausible values for the key parameters used in making seismic hazard maps, and to illustrate the sensitivity of the differences in estimated accelerations to the parameters chosen. The variation in the estimated ground accelerations due to differences in plausible values of these parameters is a measure of the epistemic uncertainty associated with any particular such map. A more exhaustive explanation of these uncertainties can be found in *Toro et al.* [1997].

[†]In the field of seismic hazard it is common to use the term *attenuation* to refer to the ground shaking expected at some distance away from an event. This differs from what is generally called seismic attenuation, because it includes not only the effect of internal-friction, but also geometric spreading. Through the rest of this chapter I will refer to the parameter as "ground motion model" or "ground shaking relation" in order to differentiate it from seismic attenuation.

The New Madrid Seismic Zone is a natural focus for this discussion since, although the uncertainties in a few parameters have been openly discussed [e.g., *Schweig et al.*, 1999; *Newman et al.*, 1999b], their implications for hazard maps have not. Specifically, although there has been much discussion of the maximum earthquake magnitude, M_{max}, and return period, T_r, these parameters affect the estimated accelerations via the predicted ground motion, which depends on other factors as well. Hence my goal here is not to analyze specific features of the *Frankel et al.* [1996] maps, but in general terms to illustrate the sensitivity on such maps from the underlying assumptions and associated uncertainties, and to make some suggestions about the use of such maps. Thus I have not attempted to replicate the *Frankel et al.* [1996] hazard model, or make refined estimates of predicted accelerations for use in risk analyses.

4.3 Models

Probabalistic seismic hazard maps giving the predicted ground acclerations can be produced for various ground motion parameters, probabilities, and various time intervals. Each of these choices describes the predicted accelerations in a different way, and in turn depends on a number of parameters that characterize the hazard model. To illustrate this effect, I examined the effects on peak[‡] and 1 Hz ground accelerations

[‡] *Peak ground accleration (PGA)* is a somewhat confusing term, refering to the highest frequencies of ground shaking and NOT the frequency at which maximum shaking occurs. Unfortunately, PGA is not a constant,depending on geographical region. For example, since California attenuates faster than the eastern U.S., so while 50 Hz might be meaningless in California it may still have significant energy in the NMSZ [*A. Mendez, personal communication*, 2000]. For the central U.S. PGA may be considered to be approximately $\geq$ 40 Hz [e.g., *Hanks*, 1978, 1981].

of three crucial parameters: the relation used to predict ground acceleration with distance (ground shaking model); the size of the maximum earthquake expected, M_{max}; and the recurrence time of these largest events, T_r.

4.3.1 Ground Shaking

In recent years much work has been done in trying to derive better relations for predicting ground motions from earthquakes in North America, east of the Rocky Mountains [e.g., *Ou and Herrmann*, 1990; *Atkinson and Mereu*, 1992; *Boatwright and Choy*, 1992; *Atkinson*, 1993a, b; *Boatwright*, 1994; *Atkinson and Somerville*, 1994; *Horton*, 1994; *Atkinson and Boore*, 1995; *Frankel et al.*, 1996; *Atkinson and Boore*, 1997; *Toro et al.*, 1997; *SSHAC*, 1997]. Ground motion relations reflect the combined effects of the earthquake source spectra and propagation effects, including geometric spreading, crustal structure, and anelastic attenuation. Their predicted ground accelerations differ significantly, due to the lack of ground motion data for large earthquakes with magnitudes greater than 6. Here, I focus on differences between three of these relations used for central United States: *Atkinson and Boore* [1995], *Frankel et al.* [1996], and *Toro et al.* [1997]. The later two attenuation models were used (equally weighted) in developing the National Seismic Hazard maps. For convenience, throughout this chapter I refer to these three relations as AB95, Frankel and Toro, respectively.

The AB95, Frankel and Toro formulations all use a stochastic model originally developed by *Hanks and McGuire* [1981], who showed that earthquake ground motions at high frequencies can be approximated by finite-duration band-limited Gaus-

sian noise. The Frankel and Toro models each assume a *Brune* [1970] source model with a single corner frequency, which has been shown previously to work well with the stochastic model in California at frequencies higher than 1 Hz [*Hanks and McGuire*, 1981; *Boore*, 1983; *Boore et al.*, 1992; *Silva and Darragh*, 1995]. However, *Boatwright and Choy* [1992] have shown, from teleseismic spectra, that intraplate earthquakes deviate from the Brune model and exhibit two corner frequencies.

Because of this, *Atkinson and Boore* [1995] felt it was necessary to develop a new model for ground motion in eastern North America with a more complex source model having two corner frequencies. The AB95 model thus predicts significantly smaller accelerations at intermediate frequencies ($\sim$ 1 Hz) than previous single corner frequency Brune models (with stress drop, $\Delta\sigma$=100 bars). *Frankel et al.* [1996] felt it necessary to develop a new model instead of including the AB95 model in their seismic hazard maps for eastern North America because a prior "workshop participants were not comfortable" with the AB95 model. The AB95 model is also the only one of the three models that has been validated with empirical data (up to **M** 5), and is consistant with the Saguenay (**M** 5.8; north of Quebéc City) and Nahanni (**M** 6.8; southwestern Northwest Territories) earthquakes, which are recent large intraplate earthquake in Canada [*Atkinson and Boore*, 1995, 1997].

Frankel et al. [1996] developed a new ground motion model for the Central United States to be incorporated into the U.S.G.S. Seismic Hazard Mapping project. They saw the need for a new model to incorporate the possibility of large earthquakes that exhibit significantly higher stress drops, $\Delta\sigma$, such as the Saguenay, Quebec, earthquake (**M** 5.8, $\Delta\sigma \approx 500$ bars [*Boore and Atkinson*, 1992; *Boatwright and Choy*,

1992]). To achieve this, they started with $\Delta\sigma = 180$ bars, shown to fit high frequency spectral data [*Atkinson*, 1993a], but chose to convert it for a different source shear velocity and site amplification factors. Thus, *Frankel et al.* [1996] calculated a new stress drop, $\Delta\sigma$=137, using

$$\Delta\sigma_{fr.} = \Delta\sigma_{atk.} \left(\frac{\beta_{So_{fr.}}}{\beta_{So_{atk.}}} \sqrt{\frac{\beta_{NS}}{\beta_{So_{fr.}}}} \right)^{\frac{3}{2}}, \tag{4.1}$$

where $\Delta\sigma_{atk.}$ and $\beta_{So_{atk.}}$ are Atkinson's stress drop and source shear wave velocity (3.8 km/s), $\beta_{So_{fr.}}$ is Frankel's source shear velocity (3.6 km/s), and β_{NS} is the assumed near-surface shear velocity (2.8 km/s). They then chose to use $\Delta\sigma$= 150 bars, rather than 137 in order to be conservative[§].

The Toro model uses a lower $\Delta\sigma$ (120 bars), determined from a similar conversion (as Equation 4.1) from *Atkinson* [1993a]'s $\Delta\sigma$, using a different path and near-surface velocity model. This is the primary difference between the Toro and Frankel models and is why the Toro model predicts significantly smaller shaking than does the Frankel model.

The *Frankel et al.* [1996] relation predicts higher ground motions for "firm rock" site conditions than that of *Toro et al.* [1997] and *Atkinson and Boore* [1995] (Figures 4.1 and 4.2). A "firm rock" site condition (V_s=760 m/s in the upper 30 meters, and corresponding to NEHRP B-C boundary [*Frankel et al.*, 1996]), equivalent to moderately fractured bedrock, was used in the U.S.G.S. maps. This was

[§]Here, and throughout the hazard literature, the term *conservative* refers to being cautious, meaning it is better to predict higher ground accelerations than what expected, just in case! One could argue that these choices should be left in the hands of the policy makers and that scientists should report unbiased results.

chosen in order to produce consistent hazard maps across the United States. Thus the site conditions are more representative of western rather than eastern U.S. rock conditions and should be converted to a hard rock site condition (V_s =1830 m/s) before use at bedrock sites east of the Rocky Mountains. In order to compare the three models directly, I thus converted the Toro and AB95 ground motion relations from hard rock to "firm rock" by multiplying by 1.52 for PGA (Figure 4.1) and 1.34 for 1 Hz acceleration (Figure 4.2), which are magnitude and distance independent constant correction proposed by *Frankel et al.* [1996]. This conversion factor should probably be reduced substantially for large accelerations due to high-strain weakening of surficial soils, especially above 0.5 *g* [*J. Schneider, personal communication*, 2000]. However, because the AB95 and Toro ground accelerations are lower at most distances (Figures 4.1 and 4.2), the assumed constant factors of 1.52 and 1.34 actually underestimate the differences between models.

4.3.2 Maximum Earthquake Size and Recurrence

Along with ground shaking models, the predicted seismic acceleration also depends significantly on the assumed size of the largest earthquakes. The present maps assume that the three largest New Madrid earthquakes of 1811-1812 were **M** 8 events, and will recur every 1,000 years[¶]. The assumed maximum magnitude M_{max}, is based mainly on a study by *Johnston* [1996] of the area over which various Modified Mercalli Intensity levels were reported for the earthquakes. The recurrence period for such events was

[¶]Magnitudes for the largest New Madrid earthquakes are typically discussed as moment magnitude, although the data used to indirectly infer magnitudes of the 1811-1812 events are non-instrumental [*Nuttli*, 1973; *Nuttli and Herrmann*, 1984].

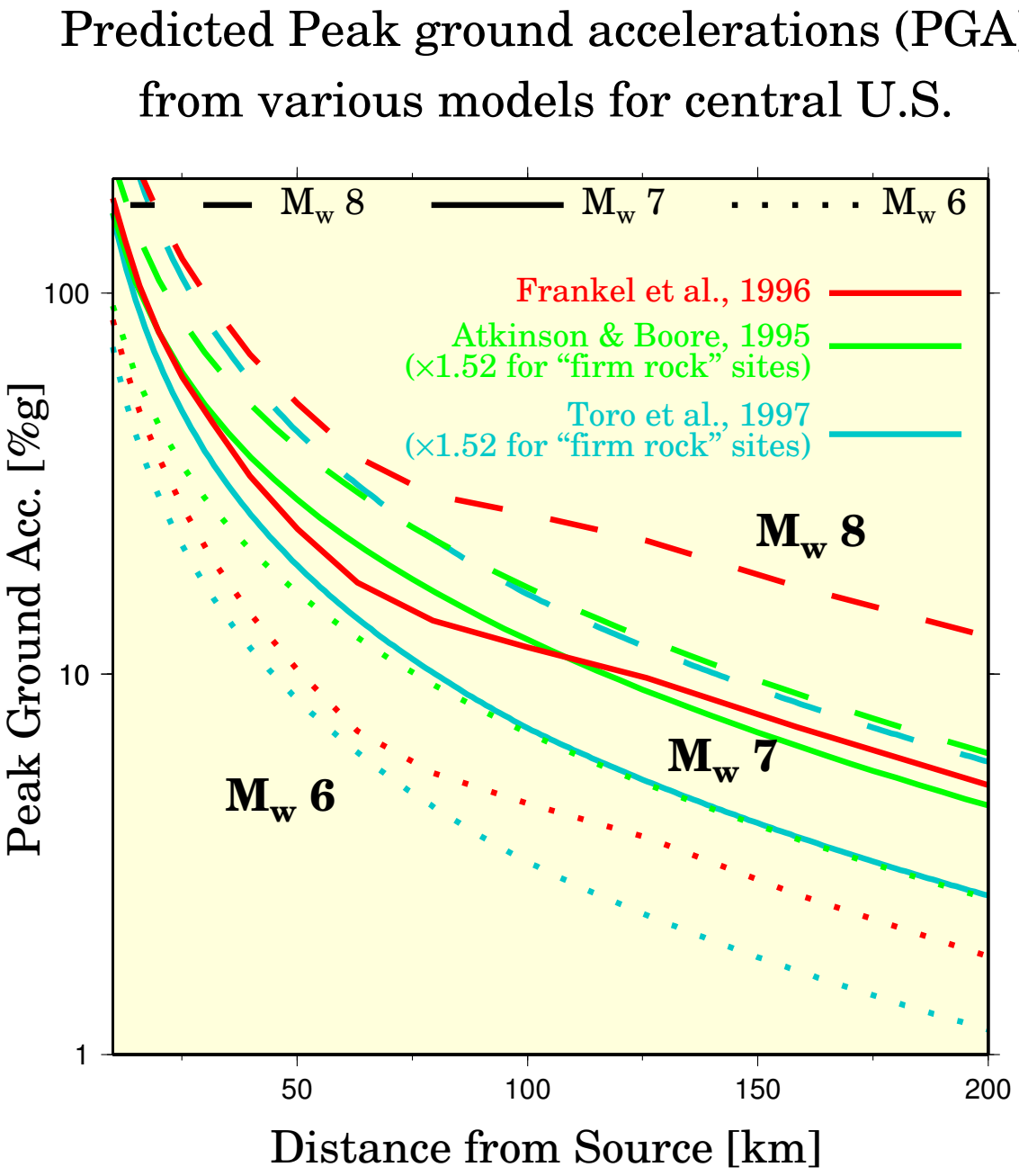

Figure 4.1: Comparison of peak ground acceleration (PGA) as a function of distance for different earthquake magnitudes predicted by *Frankel et al.* [1996], *Atkinson and Boore* [1995], and *Toro et al.* [1997] relations for ground motion published for eastern United States. Accelerations are reported in percent g (one earth acceleration).

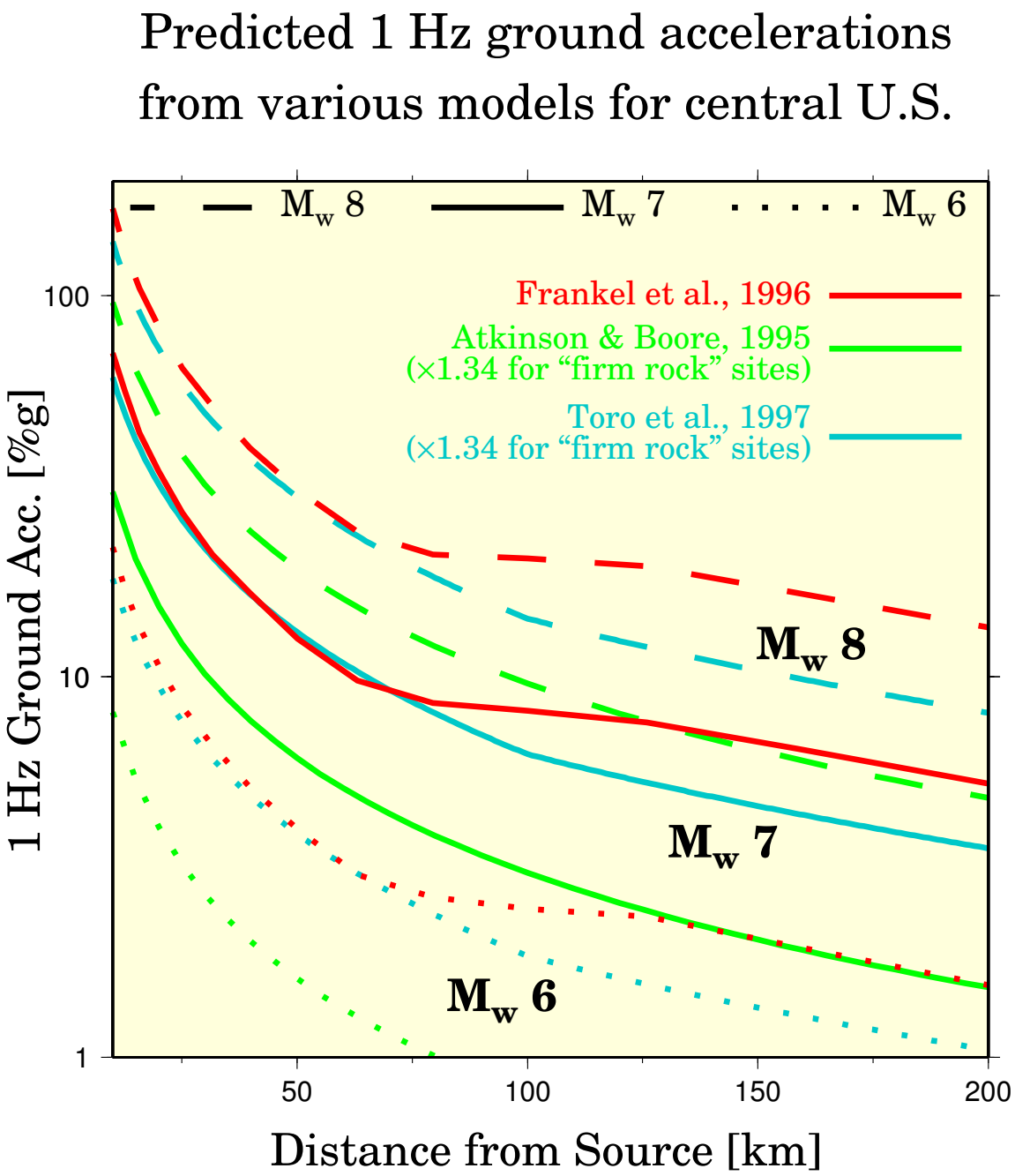

Figure 4.2: Comparison of 1 Hz ground acceleration as a function of distance for different earthquake magnitudes (similar to Figure 4.1) predicted by *Frankel et al.* [1996], *Atkinson and Boore* [1995], and *Toro et al.* [1997] relations for ground motion published for eastern United States. Accelerations are reported in percent g (one earth acceleration).

originally estimated from an interpretation of the frequency-magnitude distribution of modern smaller earthquakes [*Johnston and Nava*, 1985]. More recently, paleoliquefaction studies have been interpreted as indicating that the 1811-1812 earthquakes were preceded by a similar sequences in about 1500 and 900 AD, implying a recurrence interval of about 500 yr for large events [e.g., *Tuttle and Schweig*, 1995; *Kelson et al.*, 1996; *Tuttle*, 1999; *Tuttle et al.*, 1999].

Several recent studies, however, find that a lower M_{max} is more likely for the New Madrid region. In previous chapters, I have argued from recent GPS results and from a re-interpretation of frequency-magnitude data that the earlier large earthquakes were likely to be significantly smaller than previously assumed, perhaps low magnitude 7 (See sections 2.6 and 3.4, also [*Newman et al.*, 1999a]). Similar suggestions emerge from a paleoseismic study of fault-related folding [*Mueller et al.*, 1999], which indicates a thrust slip rate of 5-6 mm/yr across the Reelfoot scarp, corresponding to about 2 mm/yr of strike-slip, or about 1 m (likely low **M** 7) for a major earthquake every 500 yr. It has also been noted that the relatively short fault lengths thought to have been involved in the 1811-12 earthquakes are probably too small for an **M** 8 event [*Schwartz et al.*, 1999]. Moreover, reevaluation of intensities from the three main shocks [*Hough et al.*, 2000] indicates lower magnitudes (7.2-7.3, 7.0, 7.4-7.5, all $\pm$ 0.3) for the three major events.

The effect of magnitude is also illustrated by Figures 4.1 and 4.2, showing that assuming that an **M** 7 earthquake had been **M** 8 overstates the expected ground accelerations by a factor of two or more, depending on the ground motion relation used. Hence ground acceleration estimates include a tradeoff between the assumed earth-

quake size and ground motion relation. As shown, the PGA for an **M** 7 earthquake predicted by the Frankel relation at distances greater than 100 km is comparable to that predicted for an **M** 8 earthquake by the AB95 and Toro relations. Thus, the predicted ground motions can depend as significantly on the ground motion relation as on the maximum magnitude. It is important to note that substantial differences in ground motion will result from local ground motion amplification. However, these effects, while contributing to large spatial variations in ground motions, approximately scale with differences in the base ground motion estimated from the rock attenuation relations. Therefore, a comparison of maps constructed to include site effects would show relative differences in acceleration similar to those illustrated here for rock motions.

4.4 Source Contribution to Seismic Ground Accelerations

In order to evaluate the effects of potentially different seismic sources in the central Mississippi Valley, the predicted ground shaking is modeled as resulting from two distinct earthquake populations: smaller earthquakes occurring over a distributed area, and larger events occurring along discrete fault source.

4.4.1 Treatment of the New Madrid Fault Source

The first earthquake population is a simple northeast striking, 90° dipping, strike-slip New Madrid fault source extending from N35.4, W90.55 to N37.1, W89.2 (Fig-

ure 4.3[left]). The fault was assumed to be 20 km wide (bounded by lower limit of current seismicity [*Pujol et al.*, 1997]) and starts at a depth of 1 km because of a deep sediment layer in the Mississippi and the lack of clear surface ruptures for the 1811-12 earthquake sequence. The simple strike-slip fault representation was chosen over a more complex and realistic fault with strike-slip segments separated by a thrust segment (Figure 4.3[right]), because of limitations in our PSHA code that would not allow a single event to rupture the 3 individual segments simultaneously. Complications in the fault source have no substantial effect at sites greater than 50 km from its nearest point (e.g., St. Louis), though this parameter choice become increasingly important when sites are closer to the rupture zone (e.g., Memphis and the Missouri Bootheel). I allow an M_{max}event to occur randomly on the fault, with rupture size dictated by the empirical relationship with **M** *Wells and Coppersmith* [1994] (see Figure 1.5). However, when calculating the accelerations of M_{max} 8 events, the empirically derived rupture area ($\approx 1000\ km^2$) is greater than my defined fault. Thus, the entire space is allowed to rupture (but no more). Other damaging earthquakes, smaller than M_{max} and following the *Gutenberg and Richter* [1944] frequency-magnitude relationship for recurrence, were not included in the fault source but were assumed to occur off the fault within the New Madrid segment of the area source model.

4.4.2 Treatment of Area Sources

Area sources, which compose the second population of earthquakes, are randomly occurring smaller events away from the principal fault source. Area sources thus predict more uniform regions of ground shaking. I used a set of nine area sources

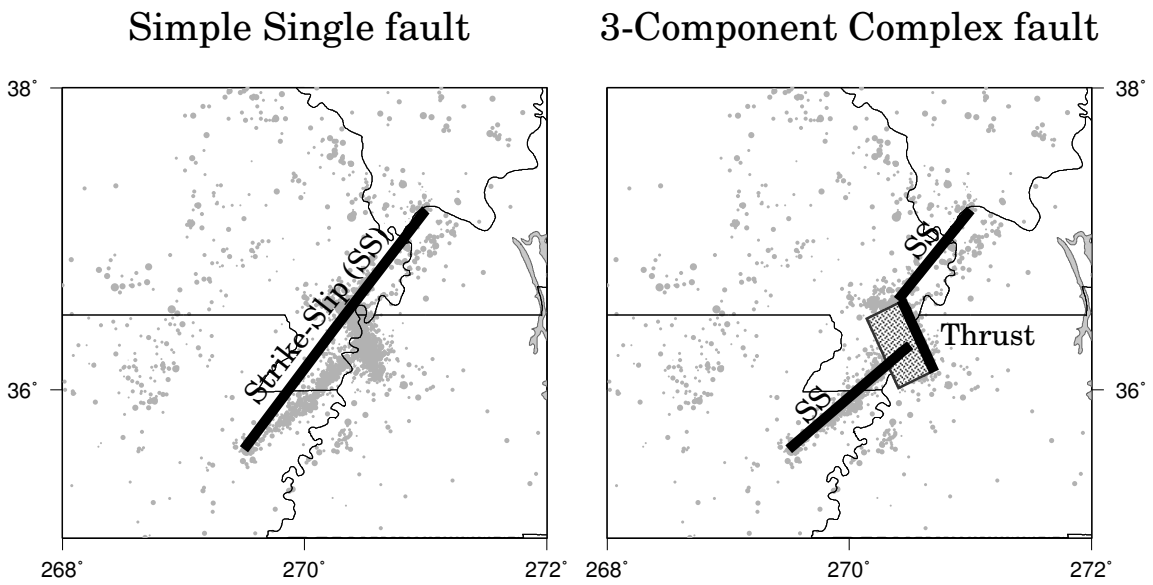

Figure 4.3: Simplified NE-SW trending strike-slip fault geometry [left], extending the length of the majority of the current seismicity, was used for the recurrence of M_{max} earthquakes, instead of a more realistic complex fault geometry with two NW-SE trending strike-slip faults separated by a SW dipping thrust fault [right].

developed by *EPRI* [1986] and Lawrence Livermore National Laboratory researchers [*Bernreuter et al.*, 1985] and compiled by *Toro et al.* [1994]. The area geometries (Figure 4.4) were chosen to represent differences in underlying geology, and their seismicity is described by a maximum magnitude, an activity rate specifying the occurrence of $\mathbf{M} > 4.6$ ($m_{bLg} > 5$) earthquakes within each geometry per year, and a b value (~ 1). I use the Gutenberg-Richter frequency-magnitude relation to estimate the time-independent probability of earthquakes of different sizes within each area. Within each area, earthquakes were distributed according to the frequency-magnitude relation. The events were then assumed to occur uniformly over a distributed area and with a randomly oriented distribution of earthquake strike. The variations in activity rates create spatial variability in the resulting hazard map. For example, in some of the maps increased accelerations in the St. Louis Arm and the Wabash Valley (elongated area sources trending NW and NE of the NMSZ; Figure 4.4) appear as prominent "bunny ears".

For simplicity, I did not explore the effects of variability in these sources, but instead focused only on the effects of varying the main NMSZ fault source. It is worth noting that although the largest predicted accelerations are due to the fault source, area sources represent a significant portion of the ground accelerations at greater distances from the fault, and provide most of the predicted high-frequency acceleration for St. Louis. The area sources contributions to individual acceleration maps vary depending on the ground motion relation used, but are independent of the variable New Madrid sources.

The spatial trends in ground acceleration vary with period of vibration and

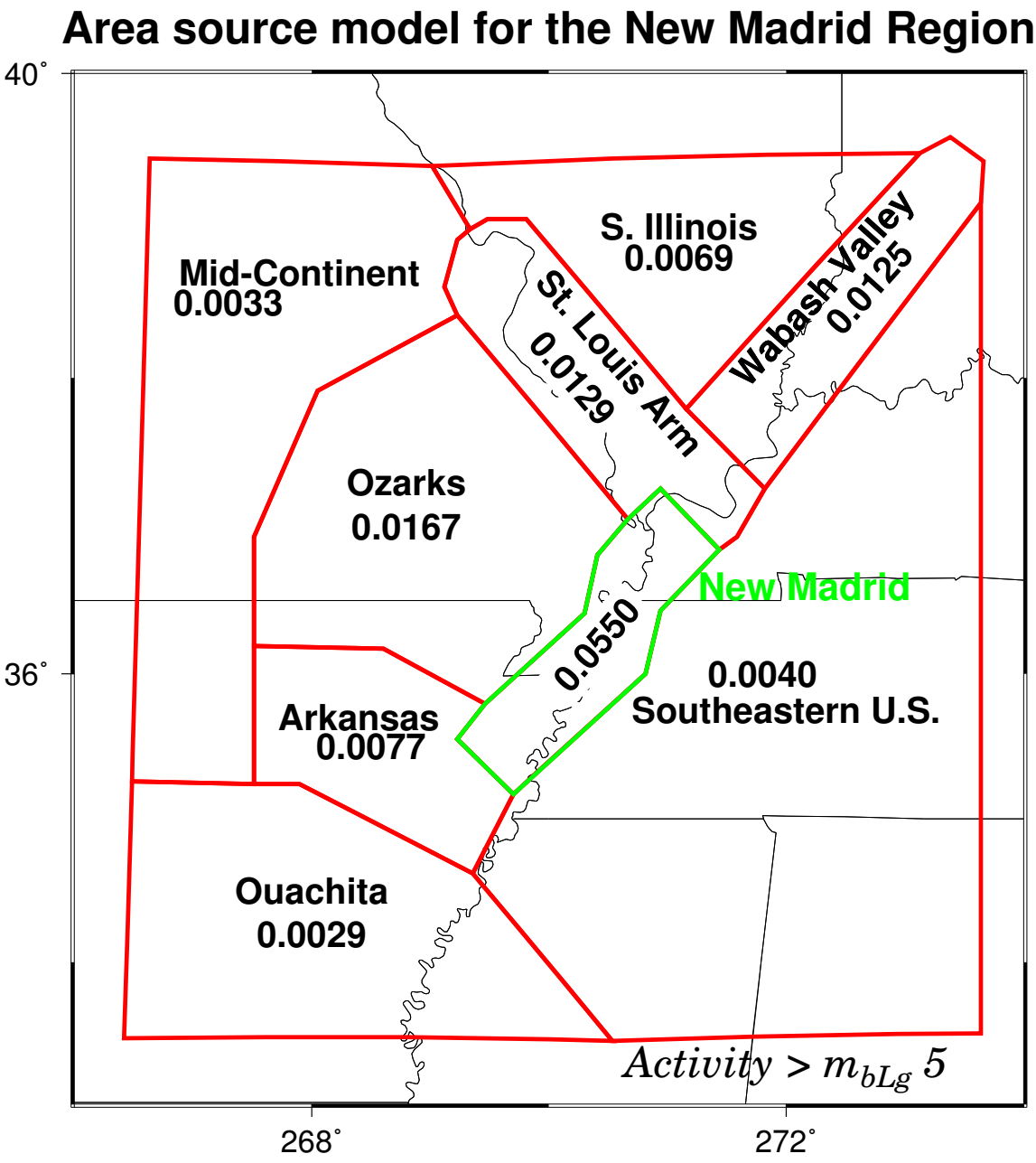

Figure 4.4: Area source geometry used in hazard modeling. Areas represent differences in underlying geology. Their seismicity is described by the annual activity rates of $m_{bLg} > 5$ earthquakes (shown within geometries) and b value (~ 1) [*Toro et al.*, 1994].

exposure window. For instance, at longer vibration periods (or lower frequencies), large earthquakes from the New Madrid fault source have a relatively greater impact than area sources on the accelerations out to greater fault distances (e.g., 0.3 and 1 sec) [e.g., *Frankel et al.*, 1996; *Harmsen et al.*, 1999]. Conversely, outside the NMSZ, area sources have a relatively greater impact on the acceleration for shorter exposure windows, which correspond to lower levels of ground shaking but higher probabilities (or rates) of occurrence.

4.5 Hazard Maps

I calculated maps at both PGA and 1 Hz acceleration for one of the probabilities mapped by the *Frankel et al.* [1996] group, the 2% probability of exceedance in 50 years. The earthquake return period, $\frac{1}{\nu}$, that this corresponds to is

$$\frac{1}{\nu} = \frac{-t}{\ln\left(1 - \frac{ptrg}{100}\right)}, \tag{4.2}$$

where $ptrg$ is the percent probability of exceedance, over t years. Thus, the maps illustrate the predicted ground shaking expected over approximately the next 2,500 years, and are currently recommended for use in building codes for earthquake resistant design.

The parameters used here differ somewhat from those in the U.S.G.S. hazard maps (Figures 4.5 and 4.7), due in part by my use of an alternative area source model and a non-distributed fault source. However, the predicted accelerations are comparable when I assume the same M_{max}, T_r, and ground shaking models (**M** 8,

1000 yr, and equally weighted Toro and Frankel ground shaking models; Figures 4.6 and 4.8).

4.5.1 Maps for Peak Ground Acceleration

For the hazard models, I considered several parameter choices that I believe essentially span the likely range of variability. For maximum magnitude of the New Madrid fault source, I use either **M** 8 or **M** 7, values that span the range of proposed values. I computed maps (Figure 4.9) for the *Frankel et al.* [1996], *Toro et al.* [1997] and *Atkinson and Boore* [1995] ground motion relations. I also considered recurrence times, T_r, for the largest earthquakes on the New Madrid fault of both 500 and 1000 yr. As discussed below, this range seems reasonable but is hard to assess given the short earthquake time series. I denote models by these three parameters, e.g., "Frankel/**M** 8/1000 yr". Following *Frankel et al.* [1996], all hazard models are truncated at 2 g, since larger accelerations have not been observed during earthquake ruptures anywhere in the world and therefore seem, unlikely here. This keeps the predicted accelerations in the region directly over the assumed fault zone constant when assuming M_{max} 8 and varying T_r and ground shaking model, since the models would all otherwise predict $\geq$ 2 g accelerations here.

For a given ground motion relation (rows in Figure 4.9), assuming that a **M** 7 earthquake had been **M** 8 overestimates the expected peak ground acceleration by a factor of two or more, depending on the distance. This effect is largest near the fault on which the maximum earthquake is presumed to occur. For a given maximum magnitude (columns in Figure 4.9), the choice of ground motion model

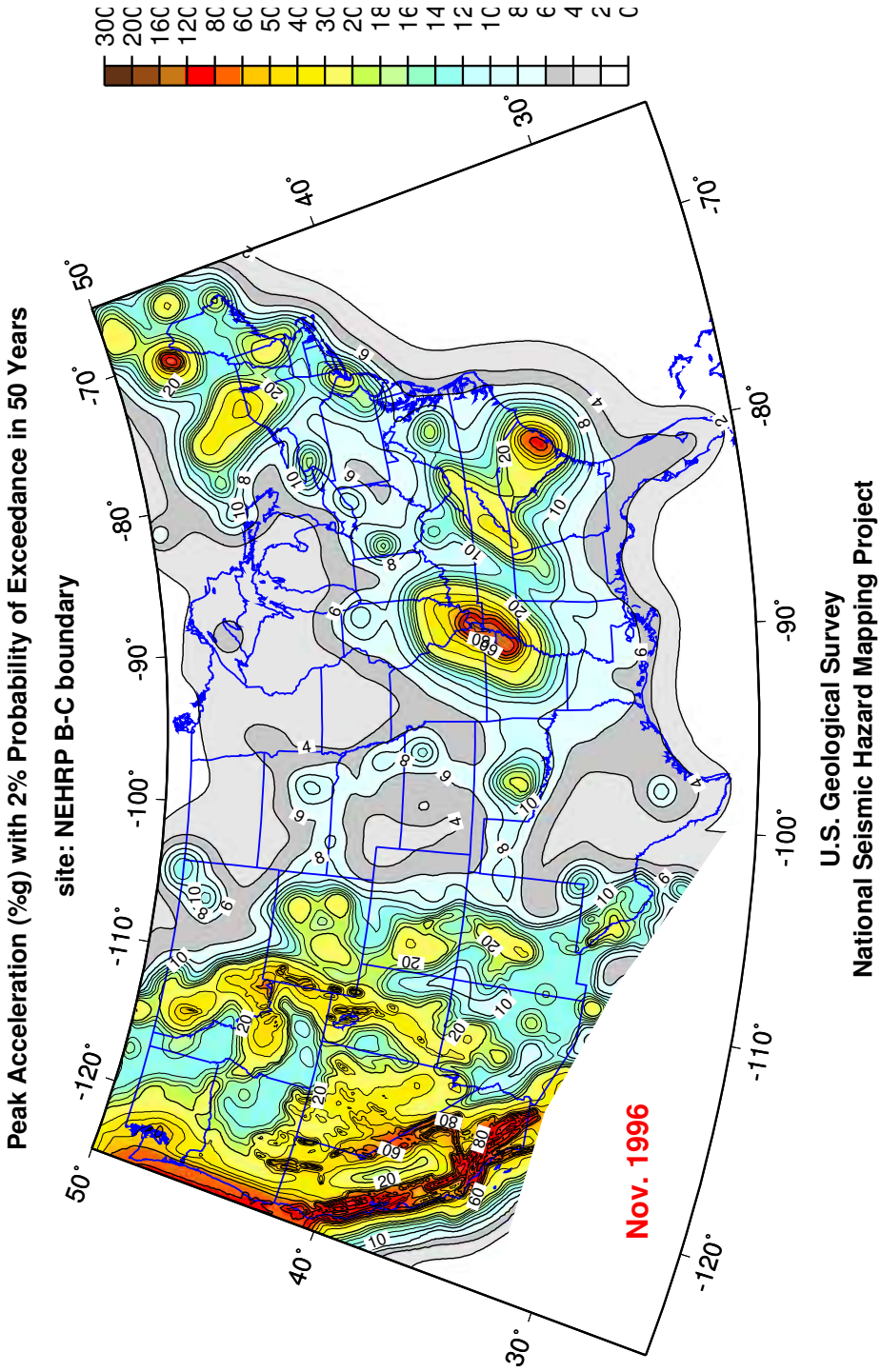

Figure 4.5: U.S.G.S. National Hazard Mapping Project predicted peak ground accelerations (%g) for the U.S. at 2% probability of exceedance in 50 years [*Frankel et al.*, 1996] Note: Color scale and units (%g) are different than used in this study (units of g).

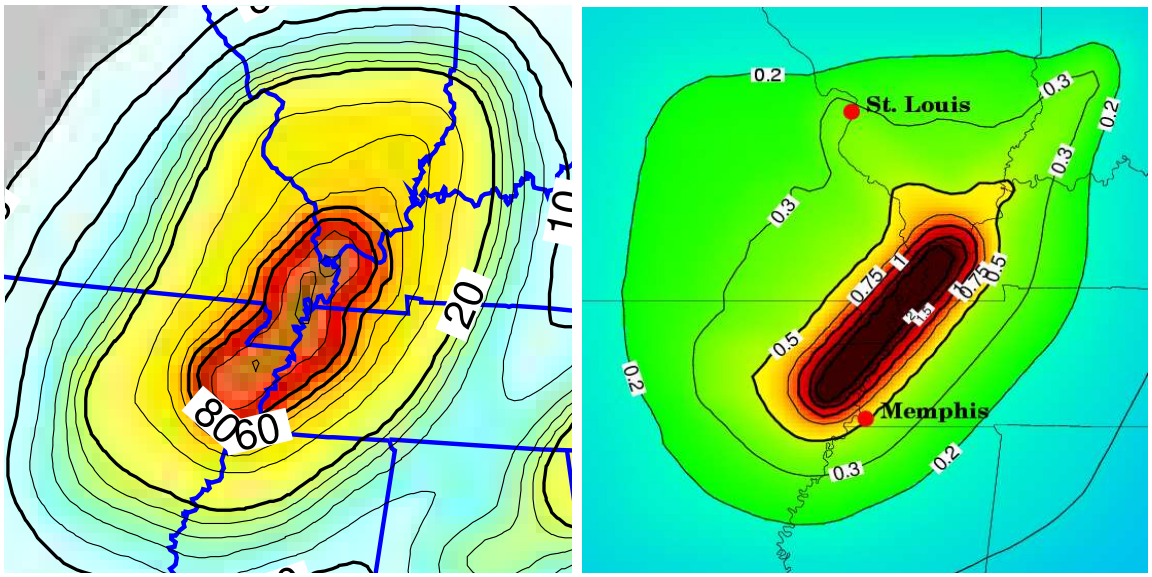

Figure 4.6: Comparison between peak ground accelerations (in $\%g$, left) predicted by the U.S.G.S. National Hazard Mapping project [*Frankel et al.*, 1996] and this study (in g, right). Both maps were generated using M_{max} 8 with T_r of 1000 years with equally weighted Frankel and Toro ground shaking models for 2% probability of exceedence in 50 years for "firm rock" site conditions. Though, these maps differ in shape (and color scale) areas of equal predicted accelerations are similar. It is likely that differences are mostly due to different area source assumption and the use of a complex fault source distributed across the Reelfoot rift by the U.S.G.S. maps as compared to a simple fault source considered in this study.

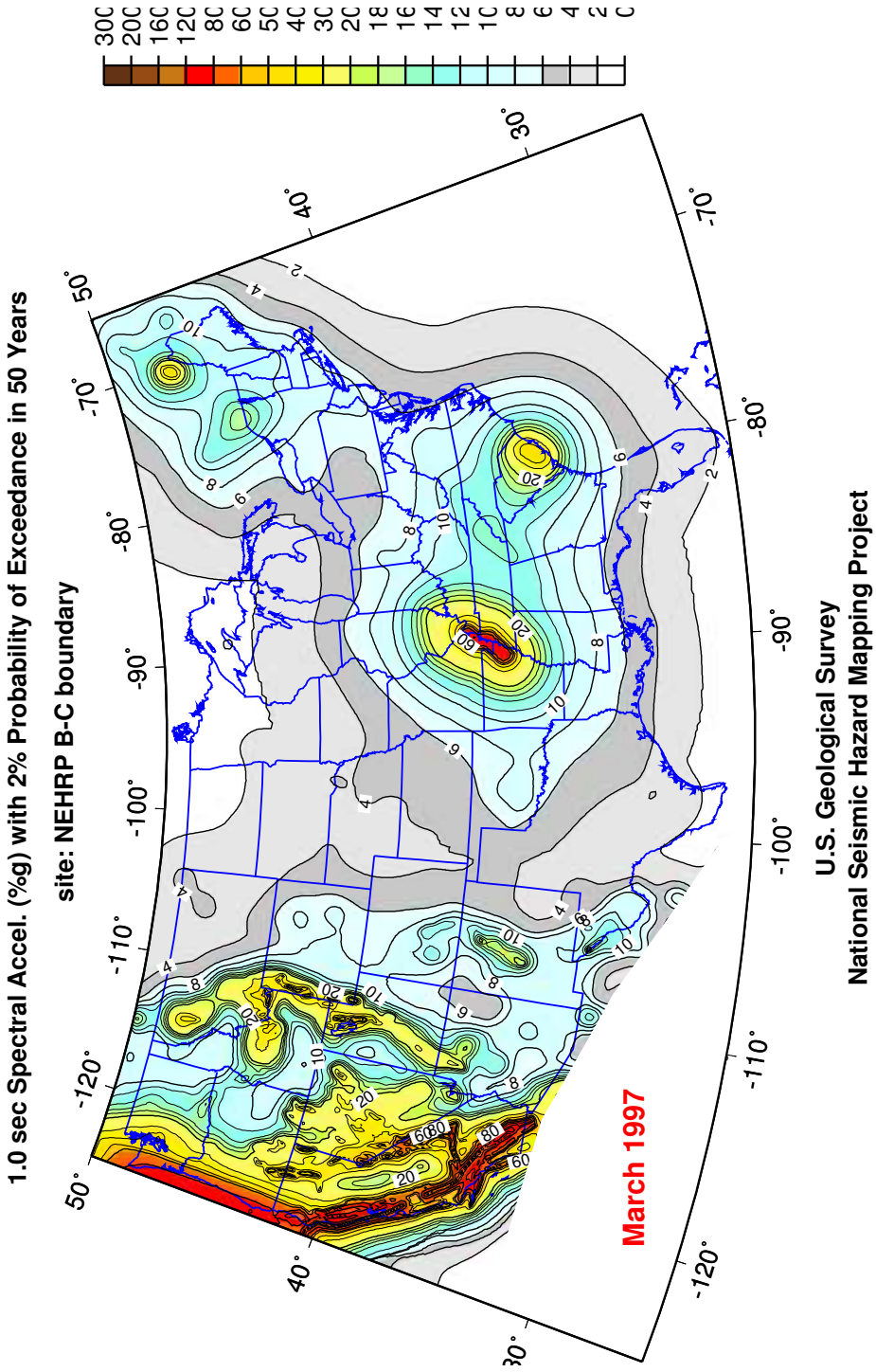

Figure 4.7: U.S.G.S. National Hazard Mapping Project predicted 1Hz ground acclerations (%g) at 2% probability of exceedance in 50 years [*Frankel et al.*, 1996]. Note: Color scale and units (%g) are different than used in this study (units of g).

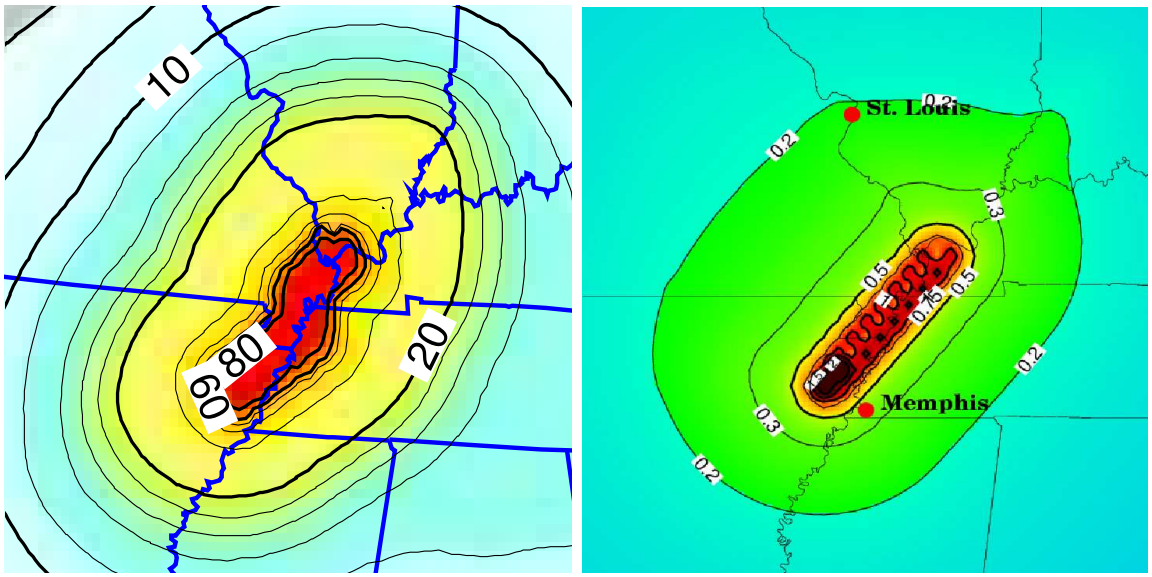

Figure 4.8: Comparison between 1Hz ground accelerations (in $\%g$, left) predicted by the U.S.G.S. National Hazard Mapping project [*Frankel et al.*, 1996] and this study (g, right). Both maps were generated using M_{max} 8 with T_r of 1000 years with equally weighted Frankel and Toro ground shaking models for 2% probability of exceedence in 50 years for "firm rock" site conditions. Though the maps differ, in shape (and color scale) areas of equal predicted accelerations are similar. It is likely that differences are mostly due to different area source assumption and the use of a complex fault source distributed across the Reelfoot rift by the U.S.G.S. maps as compared to a simple fault source considered in this study.

has similar consequences, but over a larger area. The lower ground motions for the "Toro/**M** 7/1000 yr" model may be more consistent with the lower MMI values determined recently by [*Hough et al.*, 2000] for the 1811-1812 earthquakes. However, a proper comparison can only be made through the estimation of M_{max} scenario ground motions, including site effects and ground failure. The different parameters affect the hazard maps in various ways. A detailed deaggregation (seperation of individual contributions to predicted acclerations) of the U.S.G.S. seismic hazard maps, showing the individual contributions to the predicted seismic accelerations for many cities in the eastern U.S. was developed by *Harmsen et al.* [1999], and thus serves as a good example for understanding individual contributions to estimated accelerations in hazard maps. It is useful to compare the effects near the fault at Memphis ($\sim$ 50 km) and farther away ($\sim$ 230 km), in St. Louis (Table 4.2). For a given ground motion relation and maximum earthquake recurrence time, the assumed maximum magnitude primarily affects the predicted acceleration near the fault. Hence for all three ground motion relation and T_r of 1000 yr, lowering M_{max} from 8 to 7 reduces PGA at Memphis by approximately one half. However, the effects at St. Louis are less: for the Frankel relation PGA drops from about 0.4g to about 0.3g, and this effect is even smaller for the AB95 and Toro relations.

In contrast, differences in the assumed ground motion relations primarily affect the predicted acceleration at greater distances. Hence the predicted acceleration at Memphis is only slightly less for the Toro relation than for either AB95 of Frankel relation, whereas, at St. Louis, peak ground accleration is significantly less for the Toro relation.

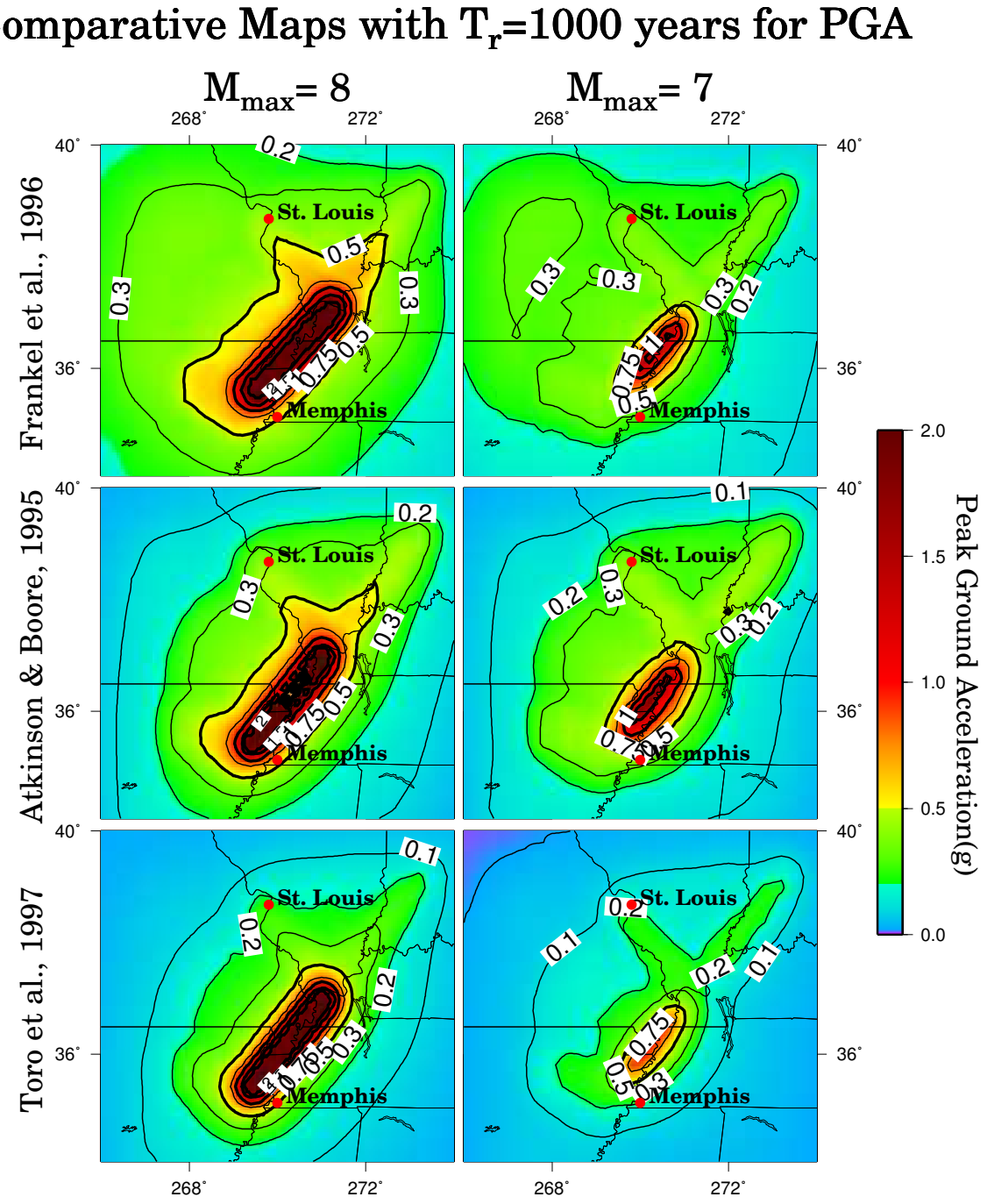

Figure 4.9: Comparison of the predicted acceleration (PGA for 2% probability in 50 years) for "firm rock" sites, corresponding to different ground motion relations and maximum magnitudes of the New Madrid fault source, for T_r of 1000 yr. Each model assumes a simple strike-slip fault source.

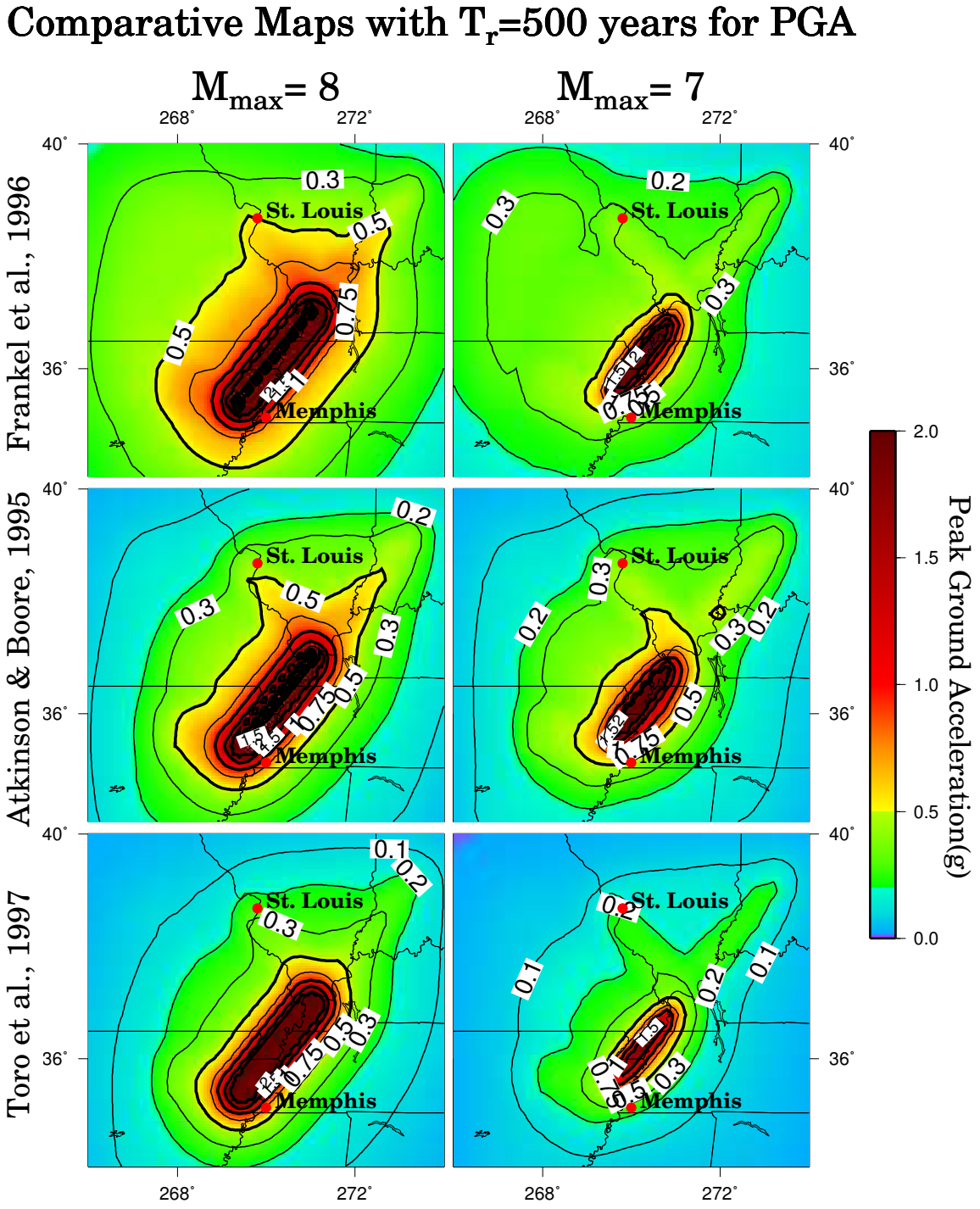

Figure 4.10: Comparison of the predicted acceleration (PGA for 2% probability in 50 years) for "firm rock" sites, corresponding to different maximum magnitude and ground motion relations, for T_r of 500 yr. Each model assumes a simple strike-slip fault source.

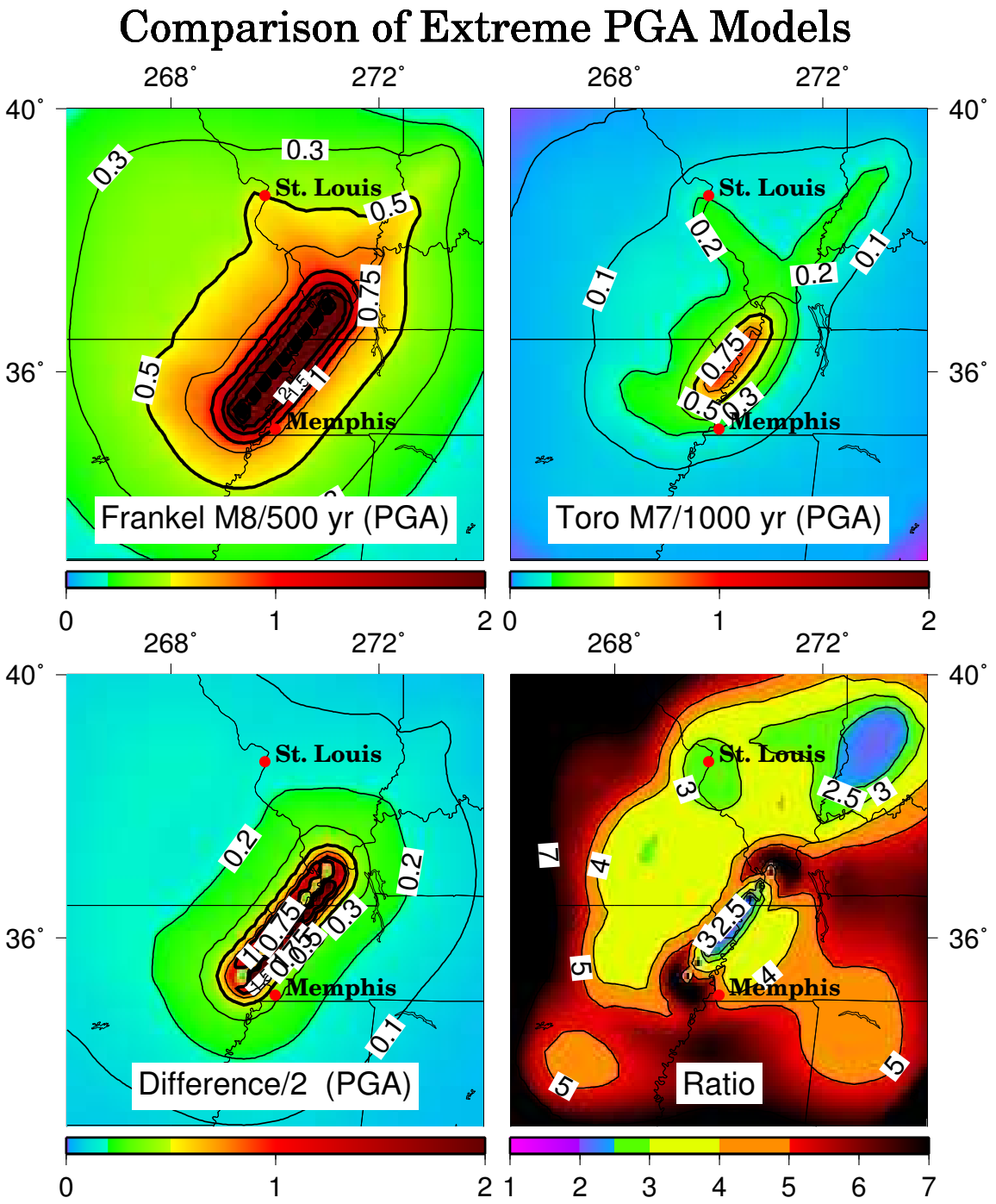

Figure 4.11: Illustration of the variability between extremal models at predicted peak ground acceleration. The extremal models are Frankel/**M** 8/500 yr (top left) and Toro/**M** 7/1000 yr (top right). Lower left is the variation in models as shown by half the difference between them. Lower right illustrates the ratio of the extremal models.

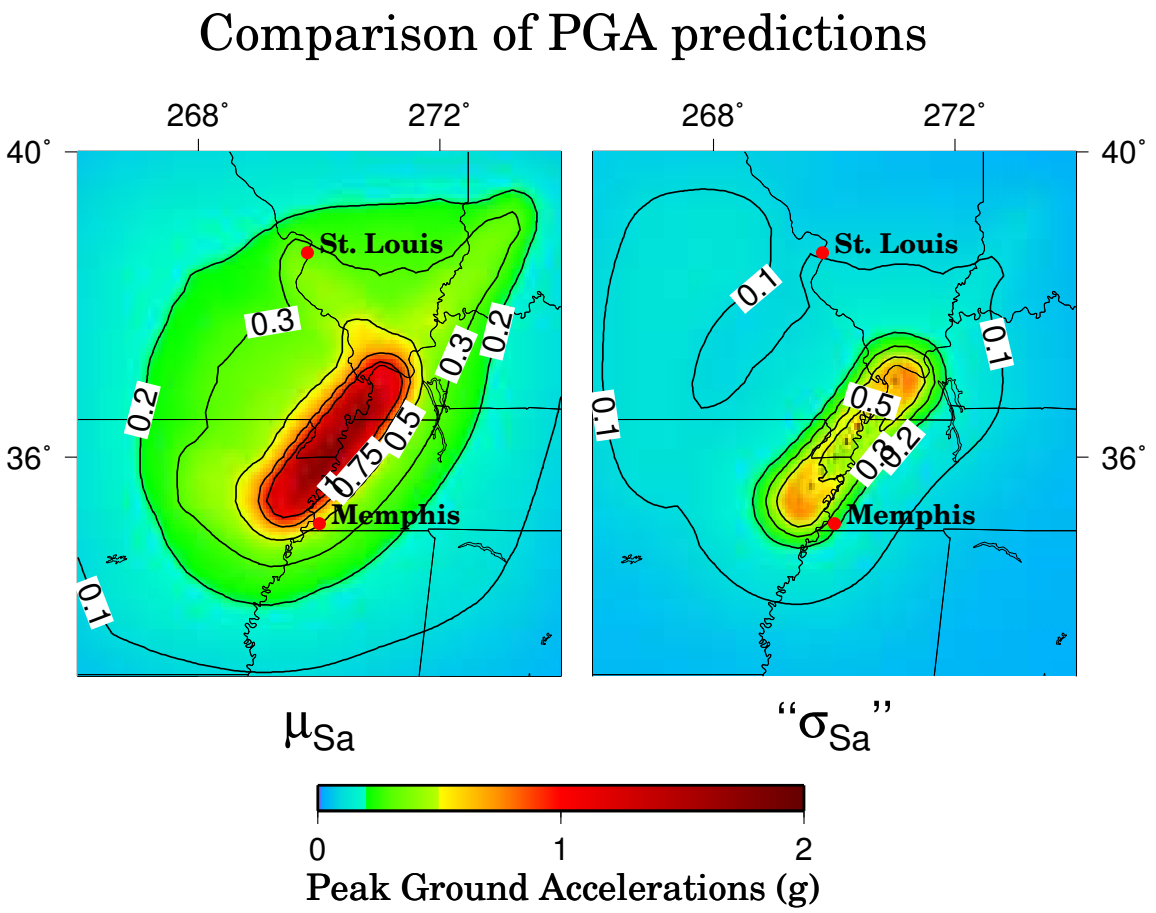

Figure 4.12: The mean predicted peak ground accelerations and uncertainties, given the 12 possible combinations of maps discussed (varying T_r, M_{max}, and ground shaking model) for 2% probability in 50 years is illustrated for hard rock site conditions. The mean acceleration μ_{Sa} map (left) shows moderate accelerations at St. Louis and Memphis (0.34 and 0.51 g) and have a considerable uncertainty ("1 σ_{Sa}" errors are 0.10 and 0.23g).

	PEAK GROUND ACCELERATIONS (g)					
CITY	St. Louis			Memphis		
lon.,lat.	90.2°W,38.7°N			90°W,35.1°N		
	Frankel	AB95	Toro	Frankel	AB95	Toro
M8/1000 yr	0.43	0.39	0.23	0.55	0.61	0.52
M7/1000 yr	0.34	0.36	0.19	0.27	0.37	0.20
M8/500 yr	0.50	0.42	0.27	0.92	0.83	0.74
M7/500 yr	0.36	0.38	0.20	0.38	0.48	0.27
μ_{Sa}	0.34 ± 0.10			0.51 ± 0.23		

Table 4.2: Predicted peak ground accelerations (g), including mean, μ_{Sa}, for major cities (St. Louis and Memphis) near New Madrid seismic zone (at 2% probability in 50 years) for various parameters sets. Using the parameter choices of *Frankel et al.* [1996] (M_{max} 8 and T_r 1000 yr with equally weighted Toro and Frankel models) yields 0.33 and 0.54 g for St. Louis and Memphis.

The general pattern of the maps persists for a shorter, 500 year recurrence time for the M_{max} events (Figure 4.10). The predicted ground shaking increases overall, but the variation with M_{max} and ground motion relation is similar to that for the 1000 yr recurrence (Figure 4.9).

In order to illustrate the extreme variability in predicted peak ground acceleration better, I plotted and examined the variation between the extremal models (Figure 4.11). Frankel/**M** 8/500 yr and Toro/**M** 7/1000 yr models (Figure 4.11 (top)), are extremal in that they predict the highest and lowest accelerations of the models I considered. The range of values is shown by the variation (the difference divided by 2) between the extremal models, and the ratio of these models. These models differ in predicted PGA by 0.3 g or more at distances greater than 100 km from the fault, and much more closer in. As shown, the predicted acceleration at Memphis varies by a factor of 5, whereas that for St. Louis varies by a factor of 3.

Because the appropriate parameter choices are unlikely to be known soon due to the low seismicity rate, these uncertainties should be recognized when making and using hazard maps. This variation between models is typical for most sites in the region, except for sites at either end of the main fault zone, which show higher fractional changes because they are at the fault ends.

Since these models are extremal, thus showing the greatest variability, it was necessary to do a more robust examination of the variability between the individual sites of all possible maps. Figure 4.12 illustrates the combined effects of the different parameter choices. I compared each of the 12 possible maps, given the $(2 \times 2 \times 3)$ parameter choices that I varied, each weighted equally to determine a mean map μ_{Sa} and a "standard deviation" map "σ_{Sa}". This is not a true standard deviation since the parameters used for the individual data points are not independent, nor can they be shown to have a Gaussian distribution about a mean since there are only 12 data points per site. With this in mind, the maps still serve to illustrate the extreme variability in peak ground accelerations expected from the range of possibilities given the few parameter choices. Thus, given the variation in maps from the selected parameter choices, mean peak ground accelerations at St. Louis (0.34 ± 0.10) and Memphis (0.51 ± 0.23) are reasonable, and the sizable variations between models are represented.

4.5.2 Maps for 1 Hz Ground Acceleration

Though peak ground accelerations (PGA) are used frequently by the U.S.G.S. and others when illustrating seismic hazards, this parameter is of limited design use,

mostly affecting smaller structures such as single family residences and unreinforced masonry [*G. Atkinson, personal communication*]. Therefore, it is useful to examine the uncertainty in maps generated also at a lower frequency. Here, I do the same analysis as in the previous section, but for accelerations due to 1 Hz (1 second) ground shaking, which would be expected to be important for larger structures such as high rise buildings.

Figure 4.2 illustrates the considerable differences between AB95, Toro and Frankel ground motion relationships. Toro's ground shaking was converted from hard rock to Frankel's "firm rock" (1830 to 760 m/s in upper 30 meters) by a magnitude and frequency independent multiplicative factor (1.34) developed by *Frankel et al.* [1996]. Although these relations are comparable near (< 60 km) an M_{max}=8 earthquake source they differ further away and at lower M_{max}=7. Thus, the Frankel relation predicts accelerations 50% greater than for Toro and considerably more than for AB95. The AB95 model predicts considerably smaller accelerations due to the use of the two-corner spectral source model [*Atkinson and Boore*, 1995].

I calculated the predicted seismic acceleration for the 2% probability of exceedance in 50 years of 1 Hz accelerations using 12 combinations of the three parameter choices (M_{max}, T_r, and ground shaking) described earlier. Figure 4.13, showing the predicted ground accelerations for T_r = 1000 year, resembles Figure 4.9 but depends less on the small, distributed events making up the area sources and more on large events on the New Madrid fault source. This is because lower-frequency ground motions attenuate more slowly with distance than higher frequency motions. Because the Toro and Frankel relations for ground motion at 1 Hz are comparable at close

ranges, the predicted area above 0.6 g, and closest to the proposed New Madrid fault source is similar for an M_{max} of 8 and T_r of 1000 years. The differences, however, become extreme away from the fault. Using the Toro rather than Frankel ground motion relationship reduces the predicted 1 Hz accelerations significantly in Memphis or St. Louis, and much less if assuming the AB95 relation. Reducing the size of the largest predicted earthquakes in New Madrid to M_{max} 7 significantly decreases the predicted area of strong 1 Hz shaking. This is indicated by the reduction in the area of ground shaking greater than 0.2 g to a quarter of its size if M_{max} were 8.

Table 4.3 shows the variations in predicted 1 Hz accelerations for St. Louis and Memphis. Using the Frankel ground motion model instead of the Toro model at St. Louis almost doubles the predicted accelerations at **M** 8/500 yr (the most conservative parameter choice). These effects occur even with **M** 7/1000 yr (the least conservative choice). At Memphis, which is closer to the fault, the differences are lesser between accelerations predicted by the Frankel and Toro relations, although both are still significantly higher than that for the AB95 relation.

Figure 4.14 (similar to Figure 4.10), shows the predicted acceleration at 1 Hz for T_r of 500 year instead of 1000 years. The shapes of the exceedance contours are similar to those in Figure 4.13, but encompass a larger areas. For the same ground shaking model and estimated M_{max}, a decrease of this nature would significantly increase the predicted 1 Hz ground shaking near the fault source.

For the parameters that I considered, the highest predicted ground accelerations would result from an M_{max} 8 recurring every 500 years, using the Frankel ground shaking relation (Figure 4.14 [top-left]). Alternatively, the lowest 1 Hz shak-

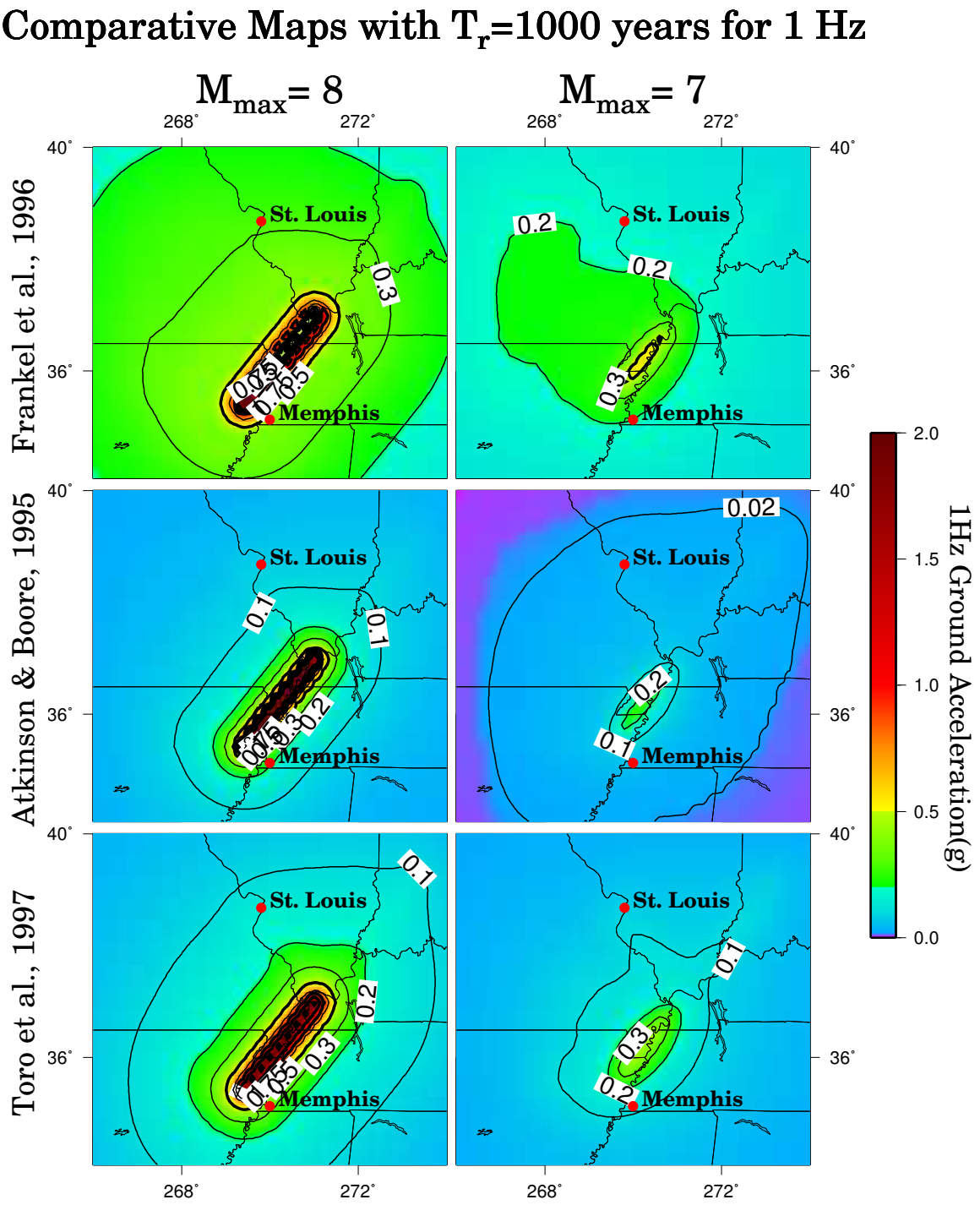

Figure 4.13: Comparison of the predicted acceleration (1Hz for 2% probability in 50 years) for "firm rock" sites, corresponding to different ground motion relations and maximum magnitudes of the New Madrid fault source, for T_r of 1000 yr.

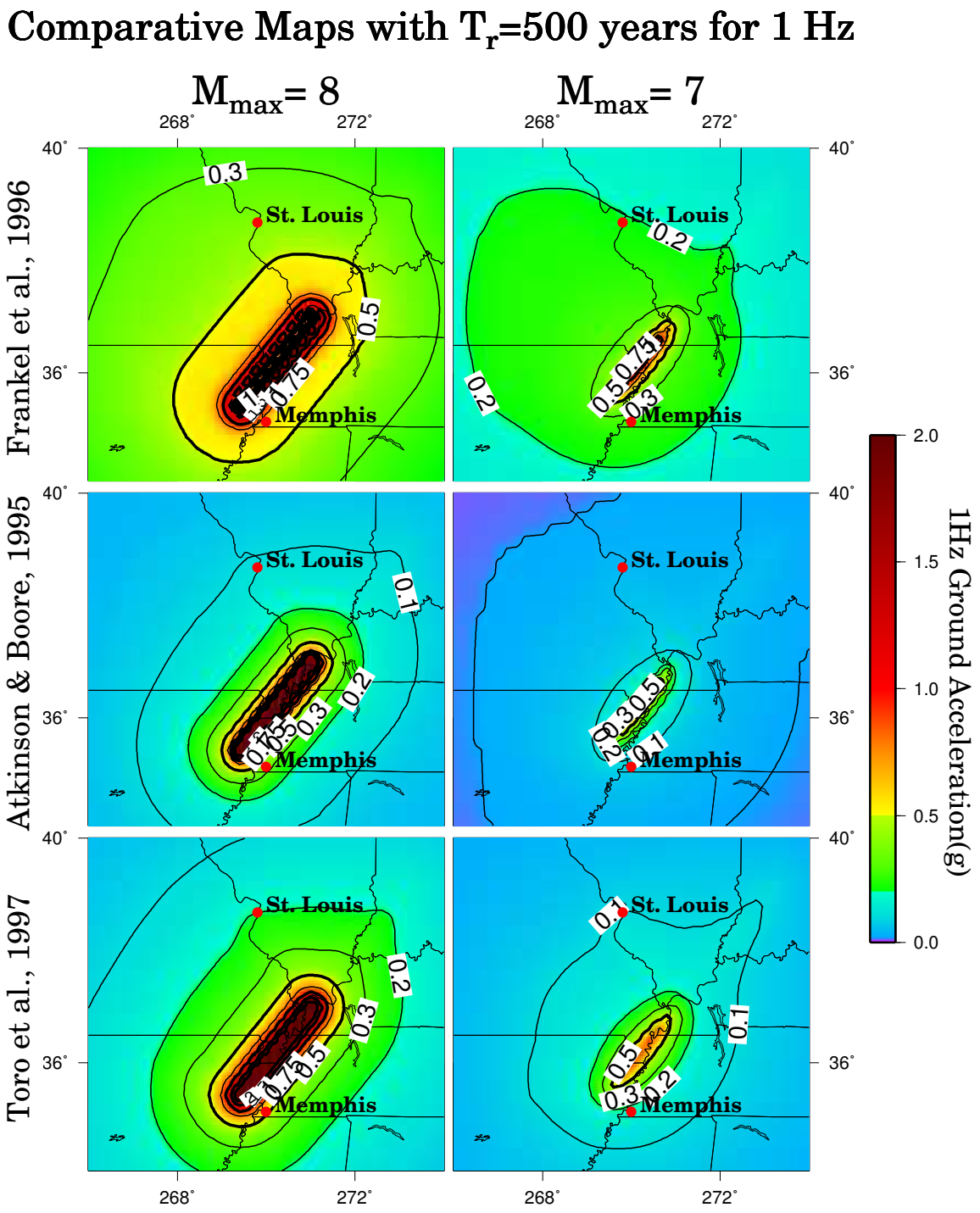

Figure 4.14: Comparison of the predicted acceleration (1 Hz for 2% probability in 50 years) for "firm rock" sites, corresponding to different maximum magnitude and ground motion relations, for T_r of 500 yr.

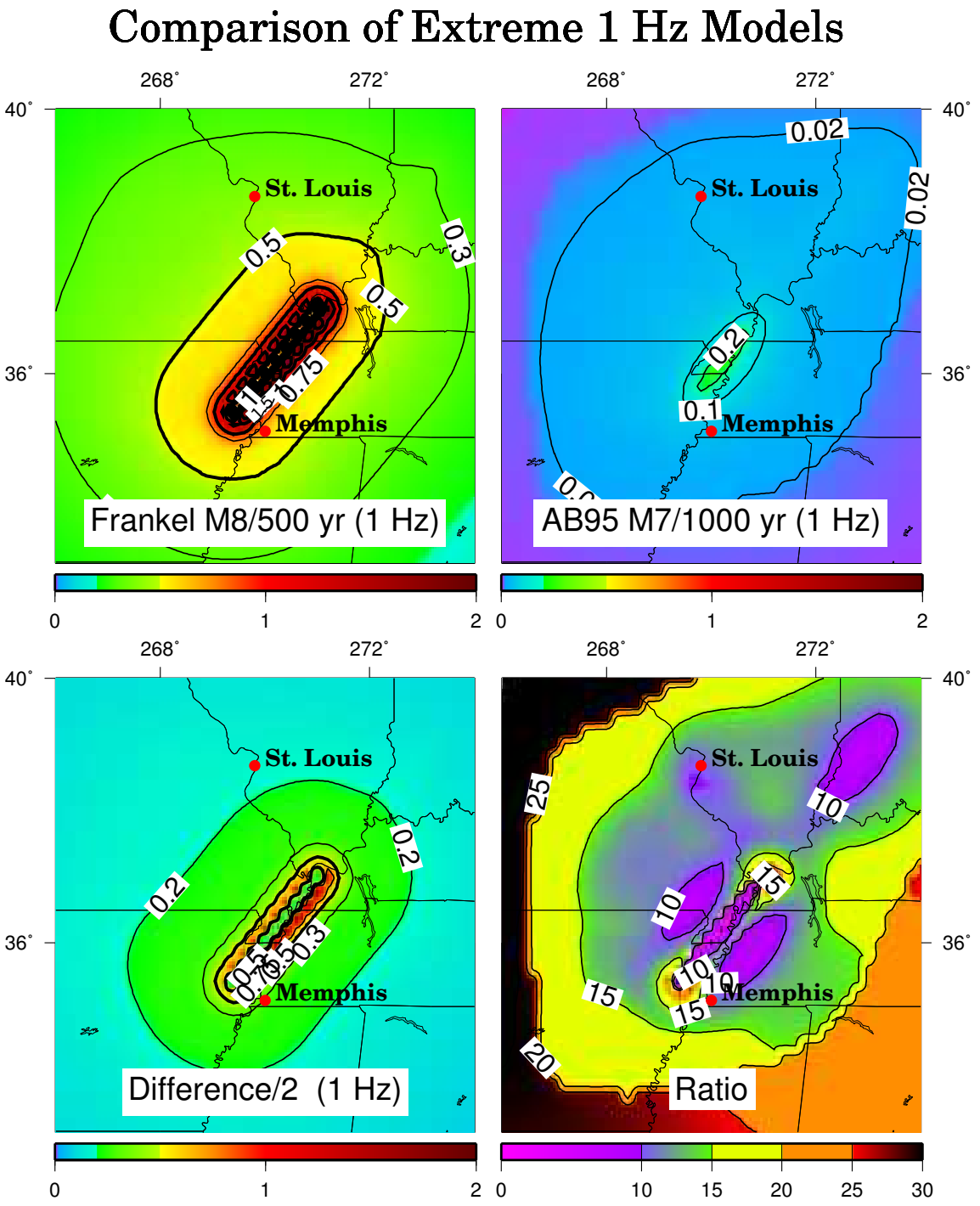

Figure 4.15: Illustration of the variability between extremal models at predicted 1Hz ground acceleration. The extremal models are Frankel/**M** 8/500 yr (top right) and AB95/**M** 7/1000 yr (top left). Lower left is the variation in models as shown by half the difference between them. Lower right illustrates the ratio of the extremal models.

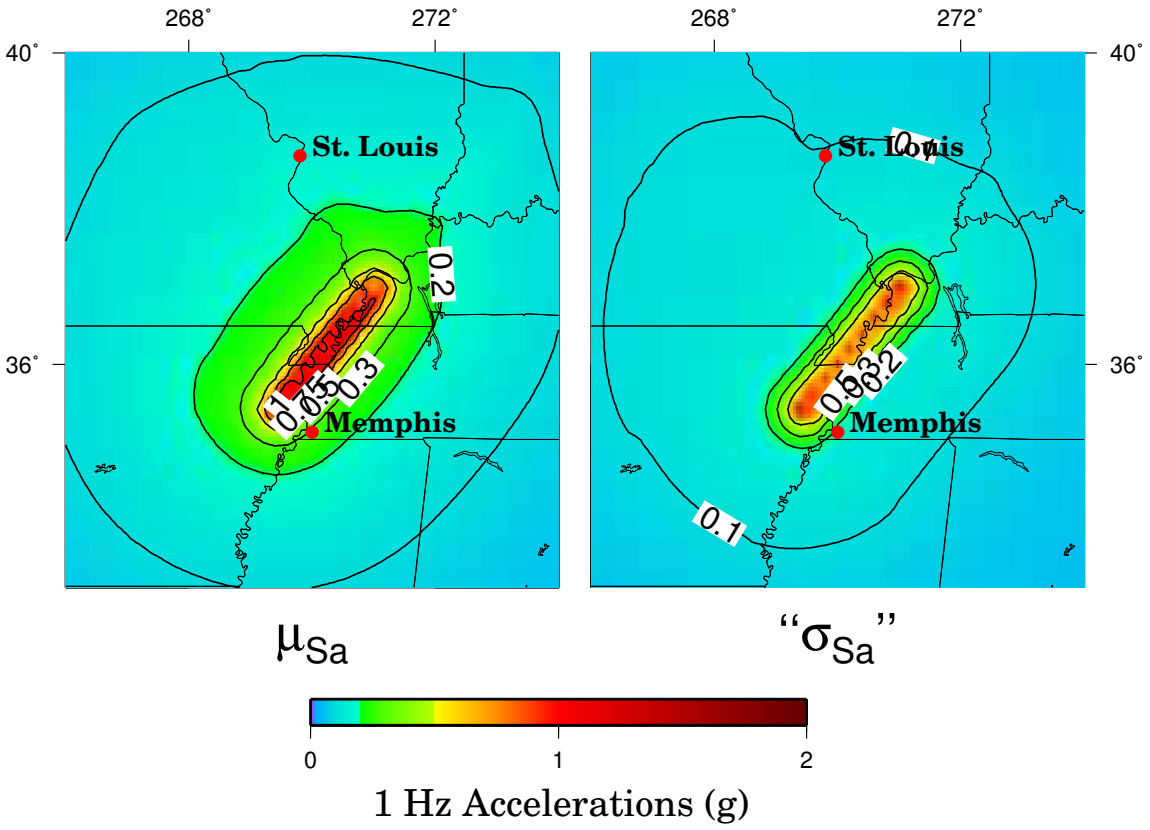

Figure 4.16: The mean predicted peak ground accelerations and uncertainties, given the 12 possible combinations of maps discussed (varying T_r, M_{max}, and ground shaking model) for 2% probability in 50 years is illustrated. The mean acceleration μ_{Sa} map (left) shows moderate accelerations at St. Louis and Memphis (0.15 and 0.28g) and have a considerable uncertainties ("1σ_{Sa}" errors are 0.10 and 0.18g).

	1Hz GROUND ACCELERATIONS (g)					
CITY	St. Louis			Memphis		
lon.,lat.	90.2°W,38.7°N			90°W,35.1°N		
	Frankel	AB95	Toro	Frankel	AB95	Toro
M8/1000yr	0.28	0.08	0.15	0.42	0.22	0.35
M7/1000yr	0.18	0.04	0.08	0.20	0.05	0.12
M8/500yr	0.38	0.11	0.20	0.63	0.35	0.54
M7/500yr	0.21	0.05	0.11	0.26	0.08	0.17
μ_{Sa}	0.15 ± 0.10			0.28 ± 0.18		

Table 4.3: Predicted 1 Hz accelerations (g), including mean, μ_{Sa}, for major cities (St. Louis and Memphis) near the New Madrid seismic zone (at 2% probability in 50 years) for various parameters sets. Using the parameter choices of *Frankel et al.* [1996] (M_{max} 8 and T_r 1000 yr with equally weighted Toro and Frankel models) yields 0.22 and 0.39 g in St. Louis and Memphis.

ing would result from a situation where M_{max} 7 event recurring every 1000 years assuming the AB95 ground shaking relation (Figure 4.13 [mid-right]). As I have done for PGA (see Section 4.5.1), I compared the variation (difference divided by 2) between these extreme models, and their ratio to illustrate the magnitude of variations resulting from changing simple and plausible parameters that effect the predicted accelerations (Figure 4.15). The model predicting maximum accelerations in this case is Frankel/**M**8/500 yr (same as for PGA) and the model predicting minimal acclelerations is AB95/**M**7/1000 yr. The AB95 model, with an M_{max} 7 event every 1000 years predicts accelerations considerably smaller than the other model choices (not using AB95 relationship), with 1 Hz accelerations quickly dropping below 0.1 g off the fault. Since accelerations predicted by this model are near-zero (as compared to the maximal model), the average variation from the mean between the two (Figure 4.15 [lower-left]) is essentially half the maximal model. Also, the ratio between the mod-

els is considerably larger than the ratios for PGA (at St. Louis the Max:Min 1 Hz acceleration ratio is about 10 and much greater in other places).

Since variations between 1 Hz accelerations with different parameter sets are great, it is particularly useful to examine the μ_{Sa} and "σ_{Sa}" to determine the uncertainties better by including the values at sites from the more moderate models (See Figure 4.16). The approximate uncertainties "σ_{Sa}" is found to be similar to the average value at most sites, thus allowing a wide range of 1 Hz accelerations to be plausible. This is illustrated by the similarity between the μ_{Sa} map (Figure 4.16 [left]) and the "σ_{Sa}" map (Figure 4.16 [right]) at 1 Hz. By including the effects the AB95 ground shaking relationship and a smaller M_{max} event, I obtain considerably smaller predicted 1 Hz accelerations ($0.15 \pm 0.10g$ at St. Louis and $0.28 \pm 0.18g$ at Memphis), than by averaging the Frankel and Toro relationships with an M_{max} 8 event ($0.25g$ at St. Louis and $0.49g$ at Memphis). The latter parameter combination is similar to that used in the maps generated for the U.S.G.S. Seismic Hazard Mapping Project [*Frankel et al.*, 1996]. The variability in 1 Hz accelerations from alternative parameter choices is particularly troublesome since it is at such frequencies that large structures fail during large nearby earthquakes [*G. Atkinson, personal communication*].

4.6 Predicted Hazard Given New Results

The U.S.G.S. hazard maps for 2% probability of exceedance in 50 years show predicted accelerations for M_{max} 8 earthquakes recurring every 1000 years from the New Madrid seismic zone [*Frankel et al.*, 1996]. Newer studies, however, show that M_{max} could be considerably lower, and T_r may be less.

Continuing paleoseismic studies in the New Madrid region have found that large distributions of liquefaction features, similar to those attributed to the 1811-12 series, around ∼900 A.D. and ∼1450 A.D [e.g., *Tuttle et al.*, 1999](see Section 1.2.3). Thus, a T_r ≈550 yr may be more plausible for M_{max} events.

Since my GPS results show a maximum of 2.2 mm/yr or right-lateral motion across the NMSZ, assuming earthquakes are a result of constant far-field strain (as is the case for plate-boundary tectonic events) the maximum allowable horizontal slip is 1.2 m every 550 years. Using the *Wells and Coppersmith* [1994] relation for global strike-slip events (Equation 1.2), 1.2 m of slip would be expected from a M_w 7.11±0.28 earthquake rupturing faulting a length between 50 and 100 km (Equation 1.1), considerably smaller than M_{max} 8, used in the U.S.G.S. seismic hazard maps. However, if you assume the M_{max} event ruptures the entire seismicly-defined fault (∼225 km) to a depth of 20 km, the seismic moment release, M_0 would be 1.6×10^{27} dyne cm, since

$$M_0 = \mu_h \vec{D} S, \tag{4.3}$$

where S is the surface area of the fault rupture (length × width; 225 km × 20 km), $\vec{D}$ is the slip and μ_h is the shear modulus of the source rock at depth ($\sim 3 \times 10^{11}$ dyne cm^{-2} for crustal rock [e.g., *Carmichael*, 1984]) [e.g., *Aki and Richards*, 1980]. This is equivalent to an M_w 7.3 earthquake (Equation 3.7), within error for a slip of 1.2 m [*Wells and Coppersmith*, 1994]. If the velocity gradient across the NMSZ, assuming right-lateral strike-slip motion, was at the maximum allowed by my GPS results (2.2 mm/yr at 95% confidence), a M_{max} 7.3 recurring every 550 yr is still a maximum,

since the assumption is made that all slip across the fault is taken up seismically, with no aseismic or afterslip events, which are common on many active faults world-wide [e.g., *DeMets*, 1997].

Thus, hazard maps for the NMSZ at 2% probability of exceedance in 50 years, developed using fault parameters suggested by the more recent data (M_{max}=7.3 and T_r=550 yr), yield considerably smaller accelerations at PGA (Figure 4.17 [left]) and 1Hz (Figure 4.17 [right]) than the U.S.G.S. seismic hazard maps [*Frankel et al.*, 1996]. Though these maps show my best approximation for two of the necessary parameters in constructing useful hazard maps, I am not arguing that these maps show the best predicted accelerations for the NMSZ, but I am only illustrating that implementing results from continuing research can significantly change values predicted in seimic hazard maps for the region.

4.7 Discussion

These examples illustrate how predicted ground accelerations depend on the choice of several crucial model parameters. In particular, although discussions of earthquake hazard often focus on the assumed maximum magnitude, M_{max}, the ground motion relation chosen can be just as, if not more, important. Other parameters can also affect the predicted accelerations. For example, whether the main New Madrid fault is represented as a single strike-slip fault (Figure 4.3 [left]) or as a complex fault with strike-slip segments separated by a thrust segment (Figure 4.3 [right]) has little effect away from the fault zone, but strongly affects the predicted acceleration near the fault in the Missouri Bootheel and Memphis. Other important parame-

2% Probability of Exceedance in 50 years with M 7.3 /550 years

Using AB95, Toro and Frankel for 'firm rock'

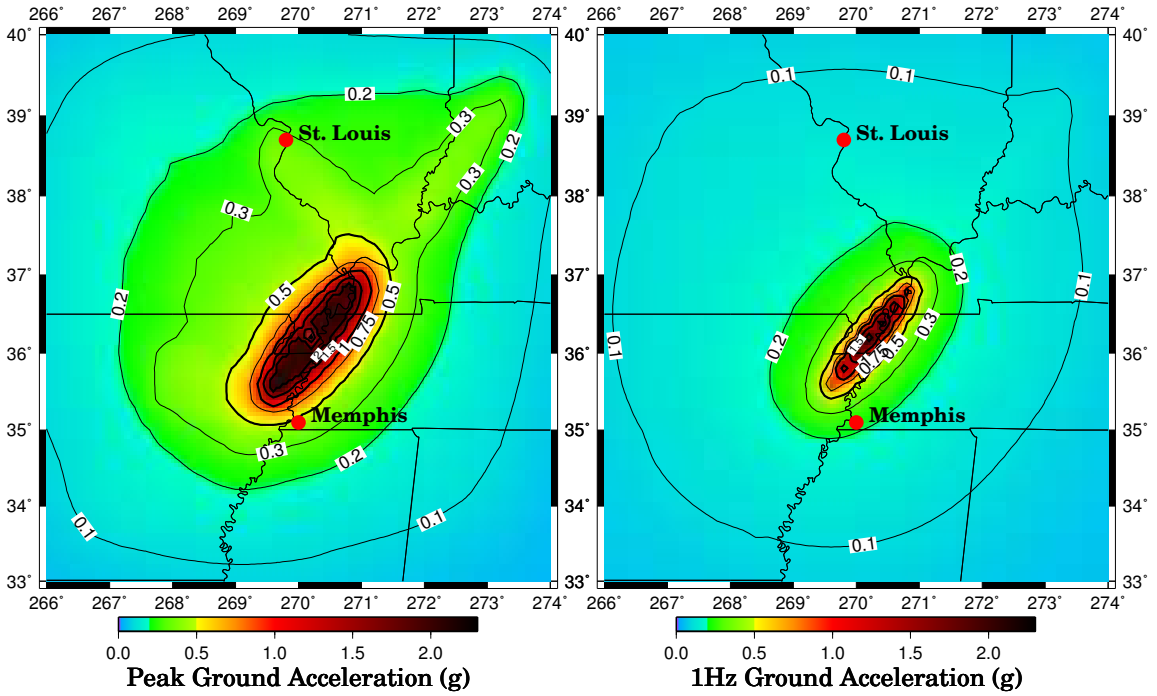

Figure 4.17: PGA (left) and 1Hz ground accelerations (right) predicted at 2% probability of exceedance in 50 years for "firm rock" site conditions. These maps are similar to those in Sections 4.5.1 and 4.5.2, but M_{max} and T_r are 7.3 and 550 years. AB95, Toro and Frankel ground shaking relations were equally weighted.

ter choices include whether one postulates both Gutenberg-Richter distribution and characteristic earthquakes (as done both here and in the *Frankel et al.* [1996] maps), and whether the probability of the occurrence of the largest earthquakes is presumed to be time-independent (as done both here and in the *Frankel et al.* [1996] maps) or time-dependent. Further refinements include uncertainty in the locations of the faults in the NMSZ, their lengths and other characteristics of fault rupture. Finally, a realistic expression of the ground accelerations requires estimation of local and regional site effects. This issue has been addressed in preliminary models by *Toro et al.* [1992] and *Toro et al.* [1994].

The example here illustrates some important features of hazard maps. Such maps are useful so long as their limitations are recognized. Certainly a plausible quantitative estimate of earthquake hazard seems likely to be more useful than none at all, although only time will tell how useful. However, it is important to bear in mind that any particular map - and the accelerations it predicts - depends crucially on the parameters chosen. Often these parameters are very poorly known, so in making any map the authors out of necessity choose model parameters they prefer and hence determined the predicted acceleration values they consider their best estimate. For example, the range of ground motion relations proposed for eastern North America reflects the absence of data for earthquakes greater than **M** 6. Given this absence of data, *Frankel et al.* [1996] explained that upon recommendations from workshop participants who "were uncomfortable" with the ground motion relation *Atkinson and Boore* [1995] derived from smaller earthquake data, instead "chose to construct" a new relation that predicted higher ground motions. Similarly, *Frankel et al.* [1996]

considered but did not use an alternative recurrence distribution based on a cumulative recurrence time of 1500 yr for events greater than **M** 7.5 which "produced substantially lower probabilistic ground motions." Thus, the *Frankel et al.* [1996] national hazard maps illustrate the way that limits in our scientific knowledge can have profound implications for the perceived hazard. The bounds on our epistemic uncertainty can be better defined by convening expert panels and elicitation processes [*SSHAC*, 1997], but the subjectivity of the results can never be eliminated because different options must still be subjectively weighted.

My point is not to criticize such choices, but to note their existence and point out that they make the estimated ground shaking correspondingly uncertain. Put another way, there is often no compelling reason to accept one hazard map as any more likely than a wide plausible range of others. Moreover, although one can examine how different parameter choices affect the predicted acceleration, it can be difficult, if not impossible, to assign meaningful formal uncertainties objectively to the parameters and hence to the predicted accelerations. The ground motion issue illustrates this challenge: suitable data would permit testing the various relations, but without data the choice is purely subjective. Due to the low seismicity of the eastern U.S., this situation may not improve for a long time.

Similarly, the uncertainty in the assumed magnitude and recurrence interval for large New Madrid earthquakes is no easier to assess objectively. Even assuming the paleoseismic data are correctly interpreted as showing two previous 1811-12 style earthquake sequences whose dates are exactly known, it is far from clear what these say about future earthquake recurrence. This issue is illustrated by data from Califor-

nia, where earthquake history is much better known. For example, the Pallett Creek paleoseismic record of large (**M** 7+) earthquakes on part of the San Andreas, probably the best record in the U.S., shows such large variability in recurrence times that the estimated probability of a similar earthquake before 2019 ranged from 7-51% [*Sieh et al.*, 1989]. More recently, the next major Parkfield earthquake, predicted in 1985 to occur between 1987 and 1993, has not yet materialized, illustrating the variability of earthquake recurrence and perhaps the limitations of the statistical approach used [*Savage*, 1993]. Even worse, the San Andreas earthquakes indicate time- variability resulting from plate motion that has obtained at the present rate for millions of years; whereas New Madrid is an intraplate system which may have "turned on" within the past 10,000 yr [*Schweig and Ellis*, 1994] and may be "shutting down" [*Newman et al.*, 1999a].

Hazard maps for New Madrid (or any other intraplate seismic zone) are not only more uncertain than for California (or any other plate boundary zone), they are more difficult to test and improve. Within a few decades, a California map can be compared to the reasonable number of moderate or large earthquakes that have occurred in California. In contrast, because even **M** 6 earthquakes in the Midwest are likely to occur on average less than once per century [*Newman et al.*, 1999a], a long time may be needed to test maps. Hence given these uncertainties, and the fact that the predicted acceleration for California has similar although smaller uncertainties, it is difficult to compare the ground shaking in California to that at New Madrid.

More generally, I recommend that discussions of hazard maps focus not on "a" map but instead on a range of maps developed by various government, academic,

and commercial groups using different assumptions. It seems likely that engineers, emergency planners, and insurance analysts would find different maps most suitable for their purposes. Such maps should explicitly present estimates of the uncertainty via graphics like those in Figures 4.11, 4.12 and 4.15, 4.16 or in *Cramer et al.* [1996], and the variability between different maps would provide another indicator of the uncertainty. Similarly, I encourage discussion of alternative models in the open literature; some of these issues have been discussed in proprietary technical reports not easily available to the general scientific community [e.g., *EPRI*, 1986].

In short, changing the assumed maximum magnitude, recurrence time and ground motion relation varies the predicted peak ground acceleration by a factor of two or more. At 1 Hz spectral frequency these parameter choices can have extreme effects on the predicted ground accelerations. Because the crucial parameters are unlikely to be known soon, any particular map - and the hazard it predicts - depends greatly on subjective choices of parameters. It is difficult to objectively assign meaningful uncertainties to the many parameters and hence the predicted hazard. The variability or uncertainty in hazard has both aleatory (inherent to nature) and epistemic (due to lack of knowledge) components. I thus recommend considering a range of maps for various parameters, which explicitly note and illustrate their uncertainties, and that these uncertainties be recognized and discussed when using hazard maps. Such an approach would be like that used in meteorology, where various groups forecasts are routinely and publicly compared.

References

Abrahamson, N., and K. Shedlock, Overview [Special issue on recent ground motion attenuation models], *Seismol. Res. Lett.*, *68*, 9–23, 1997.

Aki, K., and P. G. Richards, *Quantitative Seismology: Theory and Methods*, W. H. Freeman, San Francisco, CA, 1980.

Ambraseys, N., Engineering seismology: earthquake engineering and structural dynamics, *J. Int'l. Assoc. Earthquake Engrg.*, *17*, 1–105, 1988.

Anderson, J. G., Seismic strain rates in the central and eastern United States, *Bull. Seismol. Soc. Am.*, *76*, 273–290, 1986.

Atkinson, G., Source spectra for earthquakes in eastern North America, *Bull. Seismol. Soc. Am.*, *83*, 1778–1798, 1993a.

Atkinson, G., Notes on ground motion parameters for eastern North America: Duration and HV ratio, *Bull. Seismol. Soc. Am.*, *83*, 587–596, 1993b.

Atkinson, G., and D. Boore, Some comparisons between recent ground motion relations, *Seismol. Res. Lett.*, *61*, 24–37, 1997.

Atkinson, G., and R. Mereu, The shape of ground motion attenuation curves in southeastern Canada, *Bull. Seismol. Soc. Am.*, *82*, 2014–2031, 1992.

Atkinson, G., and P. Somerville, Calibration of time history simulation methods, *Bull. Seismol. Soc. Am.*, *84*, 400–414, 1994.

Atkinson, G. M., and D. M. Boore, Ground-motion relations for eastern North America, *Bull. Seismol. Soc. Am.*, *85*, 17–30, 1995.

Bennett, R. A., J. L. Davis, and B. P. Wernicke, Present-day pattern of Cordilleran deformation in the western United States, *Geology*, *27*, 371–374, 1999.

Bernreuter, D. L., J. B. Savy, R. W. Mensing, J. C. Chen, and B. C. Davis, *Seismic hazard characterization of the eastern United States: Lawrence Livermore National Laboratory*, 2 volumes, UCID-20421, 1985.

Blewitt, G., Advances in Global Positioning System technology for geodynamic investigations: 1978-1992, in *Geodynamics Series: Contributions of Space Geodesy to Geodynamics: Technology*, edited by D. E. Smith and D. L. Turcotte, vol. 25, pp. 195–213, AGU, Washington D. C., 1993.

Boatwright, J., Regional propagation characteristics and source parameters of earthquakes in eastern North America, *Bull. Seismol. Soc. Am.*, *84*, 1–15, 1994.

Boatwright, J., and G. Choy, Acceleration source spectra anticipated for large earthquakes in northeastern North America, *Bull. Seismol. Soc. Am.*, *82*, 660–682, 1992.

Boore, D., Stochastic simulation of high-frequency ground motions based on seismological models of the radiated spectra, *Bull. Seismol. Soc. Am.*, *73*, 1865–1894, 1983.

Boore, D., and G. Atkinson, Source spectra for the 1988 Saguenay, Quebec earthquakes, *Bull. Seismol. Soc. Am.*, *82*, 683–719, 1992.

Boore, D., W. Joyner, and L. Wennerberg, Fitting the stochastic omega-squared source model to observed response spectra in western North America: trade-offs between stress drop and kappa, *Bull. Seismol. Soc. Am.*, *82*, 1956–1963, 1992.

Braile, L., W. J. Hinze, and G. R. Keller, New Madrid seismicity, gravity anomalies, and interpreted ancient rift structures, *Seismol. Res. Lett.*, *68*, 599–610, 1997.

Braile, L. W., W. J. Hinze, R. G. Keller, E. G. Lidiak, and J. L. Sexton, Tectonic development of the New Madrid rift complex, Mississippi embayment, North America, *Tectonophysics*, *131*, 1–21, 1986.

Brune, J., Tectonic stress and the spectra of seismic shear waves from earthquakes, *J. Geophys. Res.*, *75*, 4997–5009, 1970.

Carmichael, R. S. e., *CRC handbook of physical properties of rocks (monograph)*, vol. 3, Univ. Iowa, Dep. Geol., Iowa City, IA, 1984.

Chiu, J. M., A. C. Johnston, and Y. T. Yang, Imaging the active faults of the central New Madrid seismic zone using PANDA array data, *Seismol. Res. Lett.*, *63*, 375–394, 1992.

Cornell, C. A., Engineering seismic risk analysis, *Bull. Seismol. Soc. Am.*, *58*, 1583–1606, 1968.

Cramer, C. H., M. D. Peterson, and M. S. Reichle, A Monte Carlo approach in estimating uncertainty for a seismic hazard assessment of Los Angeles, Ventura, and Orange Counties, California, *Bull. Seismol. Soc. Am.*, *86*, 1681–1691, 1996.

Crone, A., *Sample description and stratigraphic correlation of the New Madrid Test Well-1-X, New Madrid County, Missouri: U.S. Geol. Surv. Open-File Report 81-426*, U.S. Government Printing Office, 1981.

Darwin, C., *The Voyage of the Beagle (1975 reissue)*, J. M. Dent, London, 1845.

Davison, *Great Earthquakes*, Thomas Murby, London, 1936.

DeMets, C., Afterslip no longer an afterthought, *Nature*, *386*, 549, 1997.

DeMets, C., R. G. Gordon, D. F. Argus, and S. Stein, Current plate motions, *Geophys. J. Int.*, *101*, 425–478, 1990.

DeMets, C., P. E. Jansuma, G. S. Mattioli, T. H. Dixon, F. Farina, R. Bilham, E. Calais, and P. Mann, GPS geodetic constraints on Caribbean-North America Plate motion, *Geophys. Res. Lett.*, *27*, 437–440, 2000.

Dixon, T. H., An introduction to the Global Positioning System and some geological applications, *Rev. Geophys.*, *29*, 249–276, 1991.

Dixon, T. H., A. Mao, and S. Stein, How rigid is the stable interior of the North American Plate?, *Geophys. Res. Lett.*, *23*, 3035–3038, 1996.

Dixon, T. H., A. Mao, M. Bursik, M. Heflin, J. Langbein, R. Stein, and F. Webb, Continuous monitoring of surface deformation at Long Valley Caldera, California, with GPS, *J. Geophys. Res.*, *102*, 12,017–12,034, 1997.

Ekström, G., and A. M. Dziewonski, Evidence of bias in estimations of earthquake size, *Nature*, *332*, 319–323, 1988.

EPRI, *Seismic hazard methodology for the central and eastern U.S.*, 10 volumes, EPRI NP-4726, 1986, [Electric Power Research Institute (EPRI)].

Ervin, C., and L. McGinnis, Reelfoot rift: reactivated precursor to the Mississippi embayment, *Geol. Soc. Am. Bull.*, *86*, 1287–1295, 1975.

Frankel, A., Mapping seismic hazard in the central and eastern United States, *Seismol. Res. Lett.*, *66*, 8–21, 1995.

Frankel, A., C. Mueller, T. Barnhard, D. Perkins, E. Leyendecker, N. Dickman, S. Hanson, and M. Hopper, *National Seismic Hazard Maps Documentation: U.S. Geol. Surv. Open-File Report 96-532*, U.S. Government Printing Office, 1996.

Fuller, M. L., The New Madrid earthquake, *Bulletin*, US Geol. Surv., 1912.

Geller, R. J., Scaling relations for earthquake source parameters and magnitudes, *Bull. Seismol. Soc. Am.*, *66*, 1501–1523, 1976.

Gomberg, J., Tectonic deformation in the New Madrid seismic zone: Inferences from boundary element modeling, *Seismol. Res. Lett.*, *63*, 407–424, 1992.

Gomberg, J., and M. Ellis, Topography and tectonics of the central New Madrid seismic zone: Results of numerical experiments using a three-dimensional boundary element program, *J. Geophys. Res.*, *99*, 20,299–20,310, 1994.

Grana, J. P., and R. M. Richardson, Tectonic stress within the New Madrid seismic zone, *J. Geophys. Res.*, *101*, 5445–5458, 1996.

Gripp, A. E., and R. G. Gordon, Current plate velocities relative to the hotspots incorporating the NUVEL-1 global plate motion model, *Geophys. Res. Lett.*, *17*, 1109–1112, 1990.

Grollimund, B., and M. D. Zoback, Did deglaciation trigger intraplate seismicity in the New Madrid seismic zone?, *Geology*, 2000, [Submitted].

Guccione, M. J., R. B. VanArsdale, and L. H. Hehr, Evidence for late-Holocene tectonic deformation in the New Madrid seismic zone, Big Lake, northeastern Arkansas, *Geol. Soc. Am. Abstr. with Programs*, *25*, A460–1, 1993, [Abstract].

Gutenberg, B., and C. F. Richter, Frequency of earthquakes in California, *Bull. Seismol. Soc. Am.*, *185-188*, 34, 1944.

Gutenberg, B., and C. F. Richter, *Seismicity of the Earth*, 2nd ed., Princeton University Press, Princeton, New Jersey, 1954.

Hager, B., R. W. King, and M. H. Murray, Measurement of crustal deformation using the Global Positioning System, *Annu. Rev Earth Planet. Sci.*, *19*, 351–382, 1991.

Hanks, T., and R. McGuire, The character of high-frequency strong ground motion, *Bull. Seismol. Soc. Am.*, *71*, 2071–2095, 1981.

Hanks, T. C., High-frequency spectral characteristics of earthquakes and the representation of high-frequency strong ground motion, *Trans. Am. Geophys. Union (EOS)*, *59*, 325, 1978, [Abstract].

Hanks, T. C., The corner frequency shift, earthquake source models, and Q, *Bull. Seismol. Soc. Am.*, *71*, 597–612, 1981.

Hanks, T. C., and C. A. Cornell, Probabilistic seismic hazard analysis: a beginner's guide, in 5^{th} *Symposium on Current Issues Related to Nuclear Power Plant Structures, Equipment, and Piping*, 1994.

Hanks, T. C., and A. C. Johnston, Common features of the excitation and propagation of strong ground motion for North American earthquakes, *Bull. Seismol. Soc. Am.*, *82,1*, 1–23, 1992.

Hanks, T. C., and H. Kanamori, A moment magnitude scale, *J. Geophys. Res.*, *84*, 2348–2350, 1979.

Harmsen, S., D. Perkins, and A. Frankel, Deaggregation of probabilistic ground motions in the eastern United States, *Bull. Seismol. Soc. Am.*, *89*, 1–13, 1999.

Herrmann, R. B., Surface wave focal mechanisms for eastern North America earthquakes with tectonic implications, *J. Geophys. Res.*, *84*, 3543–3551, 1979.

Herrmann, R. B., and J. A. Canas, Focal mechanism studies in the New Madrid seismic zone, *Bull. Seismol. Soc. Am.*, *68*, 1095–1102, 1978.

Herrmann, R. B., S. H. Cheng, and O. W. Nuttli, Archeoseismlolgy applied to the New Madrid earthquakes of 1811 to 1812, *Bull. Seismol. Soc. Am.*, *68*, 1751–1759, 1978.

Himes, L., W. Stauder, and R. B. Herrmann, Indication of active faults in the New Madrid seismic zone from precise location of hypocenters, *Seismol. Res. Lett.*, *59*, 123–131, 1988.

Horton, S., Simulation of strong ground motion in eastern North America, in *Proceedings. 5th U.S. National Conference on Earthquake Engineering, III*, pp. 251–260, 1994.

Hough, S., J. G. Armbruster, L. Seeber, and J. F. Hough, On the Modified Mercalli Intensities and magnitudes of the 1811/1812 New Madrid, central United States, earthquakes, *J. Geophys. Res.*, 2000.

Ishimoto, M., and K. Iida, Observations sur les seisms enregistre par le microseismograph construite dernierment (I), *Bull. Earthquake Res. Inst. Univ. Tokyo*, *17*, 434–478, 1939.

Izenberg, N., R. E. Arvidson, R. A. Brackett, S. S. Saatchi, G. R. Osborn, and J. Dohrenwend, Erosional and depositional patterns associated with the 1993 Missouri River floods inferred from SIR-C and TOPSAR radar data, *J. Geophys. Res.*, *101*, 23,149–23,167, 1996.

Jibson, R. W., and D. K. Keefer, *Landslides triggered by earthquakes in the central Mississippi Valley, Tennessee and Kentucky: U.S. Geol. Surv. Prof. Pap. 1336-C.*, U.S. Government Printing Office, 1988.

Johnston, A. C., Seismic moment assessment of earthquakes in stable continental regions - II. New Madrid 1811-1812, Charleston 1886 and Lisbon 1755, *Geophys. J. Int.*, *126*, 314–344, 1996.

Johnston, A. C., and S. J. Nava, Recurrence rates and probability estimates for the New Madrid seismic zone, *J. Geophys. Res.*, *90*, 6737–6753, 1985.

Johnston, A. C., and E. S. Schweig, The enigma of the New Madrid earthquakes of 1811-1812, *Annu. Rev Earth Planet. Sci.*, *24*, 339–384, 1996.

Kelson, K. I., G. D. Simpson, R. B. VanArsdale, C. C. Haraden, and W. R. Lettis, Multiple late Holocene earthquakes along the Reelfoot fault, central New Madrid seismic zone, *J. Geophys. Res.*, *101*, 6151–6170, 1996.

Kenner, S., and P. Segall, A model for intraplate earthquake generation: Application to the New Madrid seismic zone, U.S.A., *Trans. Am. Geophys. Union (EOS)*, *81*, S310, 2000, [Abstract].

Kerkela, S., M. H. Murray, L. Liu, M. D. Zoback, and P. Segall, Strain accumulation in the New Madrid seismic zone from GPS data, 1993-1997, *Trans. Am. Geophys. Union (EOS)*, *79*, F201, 1998, [Abstract].

Lander, J. F., Seismological notes–November and December, 1968, *Bull. Seismol. Soc. Am.*, *59*, 1429–1432, 1969.

Langenheim, V. E., and T. G. Hildenbrand, Commerce geophysical lieament–Its source, geometry, and relation to the Reelfoot rift and New Madrid seismic zone, *Geol. Soc. Am. Bull.*, *109*, 580–595, 1997.

Li, Y., E. S. Schweig, M. P. Tuttle, and M. A. Ellis, Evidence for large prehistoric earthquakes in the northern New Madrid seismic zone, central United States, *Seismol. Res. Lett.*, *69*, 270–276, 1998.

Lichten, S., Y. Bar-Sever, W. Bertiger, M. Heflin, K. Hurst, R. Muellerschoen, S.-C. Wu, T. L. Yunck, and J. Zumberge, Gipsy-Oasis II: A high precision GPS data processing system and general satellite orbit analysis tool, *Tech. rep.*, Jet Propulsion Laboratory, Pasadena, CA, 1995.

Lichten, S. M., Estimation and filtering for high precision GPS applications, *Manuscripta Geodetica*, *15*, 159–176, 1990.

Lichten, S. M., and J. Border, Strategies for high precision Global Positioning System orbit determination, *J. Geophys. Res.*, *92*, 12,751–12,762, 1987.

Liu, L., M. D. Zoback, and P. Segall, Rapid intraplate strain accumulation in the New Madrid seismic zone, *Science*, *257*, 1666–1669, 1992.

Liu, Z., Earthquake modeling and active faulting in the New Madrid seismic zone, Ph.D. thesis, Saint Louis University, 1997.

Lomnitz, C., Comment on "Temporal and magnitude dependence in earthquake recurrence models" by C. A. Cornell and S. R. Winterstein, *Bull. Seismol. Soc. Am.*, *79*, 1989.

Mann, O., W. Howe, and F. H. Kellogg, Regional earthquake risk study, *Tech. rep.*, Dep. Housing and Urban Dev., Washington D. C., 1974.

Mao, A., Geophysical application of the Global Positioning System, Ph.D. thesis, University of Miami, 1998.

Mao, A., C. Harrison, and T. Dixon, Noise in GPS time series, *J. Geophys. Res.*, *104*, 2797–2816, 1999.

McGuire, R. K., Probabilistic seismic hazard analysis and design earthquakes: closing the loop, *Bull. Seismol. Soc. Am.*, *85*, 1275–1284, 1995.

McNoleg, O., The integration of GIS, remote sensing, expert systems and adaptive co-kriging for environmental habitat modeling of the highland haggis using object-oriented, fuzzy-logic and neural-network techniques, *Computers & Geosciences*, *22*, 585–588, 1996.

Metzger, A. G., 'New' historical earthquakes in the New Madrid seismic zone, *Seismol. Res. Lett.*, *67*, 47, 1996, [Abstract].

Morris, C. (Ed.), *Academic Press, Dictionary of Science and Technology*, Academic Press, San Diego, CA, 1992.

Mueller, K. J., J. Champion, M. Guccione, and K. Kelson, Fault slip rates and age of the modern New Madrid seismic zone, *Science*, *286*, 1135–1138, 1999.

Newman, A., S. Stein, J. Weber, J. Engeln, A. Mao, and T. Dixon, Slow deformation and lower seismic hazard at the New Madrid seismic zone, *Science*, *284*, 619–621, 1999a.

Newman, A., S. Stein, J. Weber, J. Engeln, A. Mao, and T. Dixon, New results justify discussion of alternative models, *Trans. Am. Geophys. Union (EOS)*, *80*, 197, 1999b.

Newman, A., J. Schneider, S. Stein, and A. Mendez, Uncertainties in seismic hazard maps for the New Madrid seismic zone, *Seismol. Res. Lett.*, *???*, ???, 2000, [Submitted].

Nuttli, O., Magnitude-recurrence relation for central Mississippi Valley earthquakes, *Bull. Seismol. Soc. Am.*, *64*, 1189–1207, 1974.

Nuttli, O. W., The Mississippi Valley earthquakes of 1811 and 1812: Intensities, ground motion, and magnitudes, *Bull. Seismol. Soc. Am.*, *63*, 227–248, 1973.

Nuttli, O. W., Average seismic source-parameter relations for mid-plate earthquakes, *Bull. Seismol. Soc. Am.*, *73*, 519–535, 1983.

Nuttli, O. W., and R. B. Herrmann, Ground motion of Mississippi Valley earthquakes, *Journal of Technical Topics in Civil Engineering*, *110*, 54–69, 1984.

Nuttlie, O. W., and K. G. Brill, *Earthquake source zones in the central United States determined from historical seismicity, An approach to seismic zonation for sitting nuclear electric power generation facilities in the eastern United States*, U.S. Nuclear Regulatory Commission NUREG/CR-1577, 1981.

Obermeier, S., *The New Madrid earthquakes: an engineering-geologic interpretation of relict liquefaction features: U.S. Geol. Surv. Prof. Pap. 1336-B.*, U.S. Government Printing Office, 1989.

Obermeier, S., J. Martin, A. Frankel, T. L. Youd, P. Munson, C. A. Munson, and E. C. Pond, *Liquefaction evidence for one or more strong Holocene earthquakes in the Wabash Valley of southern Indiana and Illinois: U.S. Geol. Surv. Prof. Pap. 1336-C.*, vol. 1536, U.S. Government Printing Office, 1993.

Obermeier, S. F., and E. C. Pond, Issues in using liquefaction features for paleoseismic analysis, *Seismol. Res. Lett.*, *70*, 34–58, 1999.

Odum, J., W. J. Stephenson, K. M. Shedlock, and T. L. Pratt, Near-surface structural model for deformation associated with the February 7, 1812, New Madrid earthquake, *Geol. Soc. Am. Bull.*, *110*, 149–162, 1998.

Okal, E. A., A theoretical discussion of time-domain magnitudes: the Prague formula for M_s and the mantle magnitude M_m, *J. Geophys. Res.*, *94*, 4194–4204, 1989.

Okal, E. A., and B. Romanowicz, On the variation of b-values with earthquake size, *Phys. Earth Planet. Inter.*, *87*, 55–76, 1994.

Ou, G., and R. Herrmann, A statistical model for peak ground motion from local to regional distances, *Bull. Seismol. Soc. Am.*, *80*, 1397–1417, 1990.

Penick Jr., J. L., *The New Madrid Earthquakes*, University of Missouri Press, Columbia, MO, 1981.

Petersen, M. D., C. H. Cramer, W. A. Bryant, M. S. Reichle, and T. R. Toppozada, Preliminary seismic hazard assessment for Los Angeles, Ventura, and Orange Counties, California, affected by the 17 January 1994 Northridge earthquake, *Bull. Seismol. Soc. Am.*, *86*, S247–S261, 1996.

Pond, E. C., Seismic parameters for the central United States based on paleoliquefaction evidence in the Wabash Valley, Ph.D. thesis, Virginia Polytechnic Institute, Blacksburg, Virginia, 1996.

Pond, E. C., and J. R. Martin, Estimated magnitudes and accelerations associated with prehistoric earthquakes in the Wabash Valley region of the central United States, *Seismol. Res. Lett.*, *68*, 611–623, 1997.

Pujol, J., A. Johnston, J. Chiu, and Y. Yang, Refinement of thrust faulting models for the central New Madrid seismic zone, *Engineering Geology*, *46*, 281–298, 1997.

Reiter, L., *Earthquake Hazard Analysis*, Columbia, New York, NY, 1990.

Richter, C. F., *Elementary Seismology*, Freeman, San Francisco, CA, 1958.

Rundle, J. B., Derivation of the complete Gutenberg-Richter magnitude-frequency relation using principle of scale invariance, *J. Geophys. Res.*, *94*, 12,337–12,342, 1989.

Rydelek, P. A., and F. F. Pollitz, Fossil strain from the 1811-1812 New Madrid earthquakes, *Geophys. Res. Lett.*, *21*, 2303–2306, 1994.

Saucier, R. T., Geoarcheological evidence of strong prehistoric earthquakes in the New Madrid (Missouri) seismic zone, *Geology*, *19*, 296–298, 1991.

Savage, J. C., The Parkfield prediction fallacy, *Bull. Seismol. Soc. Am.*, *83*, 1–6, 1993.

Savage, J. C., and R. O. Burford, Geodetic determination of relative plate motion in central California, *J. Geophys. Res.*, *78*, 832–845, 1973.

Schwartz, D. P., S. Hecker, D. Ponti, A. Bayasgalan, W. R. Lund, H. Stenner, and D. Enkbaatar, Paleoseismic reconnaissance along the 1905 Bulnay, Mongolia surface rupture, *Seismol. Res. Lett.*, *70*, 235, 1999, [Abstract].

Schweig, E. S., and M. A. Ellis, Reconciling short recurrence intervals with minor deformation in the New Madrid seismic zone, *Science*, *264*, 1308–1311, 1994.

Schweig, E. S., J. Gomberg, and M. Tuttle, Caution urged in revising earthquake hazard estimates at the New Madrid seismic zone, *Trans. Am. Geophys. Union (EOS)*, *80*, 1999.

Sexton, J., L. W. Braile, W. J. Hinze, and M. J. Campbell, Seismic reflection profiling studies of a buried Precambrian rift beneath the Wabash Valley fault zone, *Geophysics*, *51*, 640–660, 1986.

Sieh, K., M. Stuiver, and D. Brillinger, A more precise chronology of earthquakes produced by the San Andreas fault in southern California, *J. Geophys. Res.*, *94*, 603–624, 1989.

Sillard, P., Z. Altamimi, and C. Boucher, The ITRF96 realization and its associated velocity field, *Geophys. Res. Lett.*, *25*, 3223–3226, 1998.

Silva, W., and R. B. Darragh, Engineering characterization of strong ground motion recorded at rock sites, *Tech. rep.*, EPRI, 1995.

Sloss, L. L., Tectonic evolution of the craton in Phanerozoic time, in *Decade of North American Geology: The Geology of North America*, edited by L. L. Sloss, vol. D-2 of *Sedimentary Cover-North American Craton*, pp. 25–52, Geological Society of America, Boulder, CO, 1988.

Snay, R. A., Horizontal deformation in New York and Connecticut: examining contradictory results from the geodetic evidence, *J. Geophys. Res.*, *91*, 12,695–12,702, 1986.

Snay, R. A., J. F. Ni, and H. C. Neugebauer, Geodetically derived strain across the northern New Madrid seismic zone, in *Investigations of the New Madrid Seismic Zone*, vol. 1538-F, USGS Professional Paper, 1994.

SSHAC, *Recommendations for probabilistic seismic hazard analysis: guidance on uncertainty and use of experts*, U.S. Nuclear Regulatory Commission: NUREG/CR-6372, 1997, [Senior Seismic Hazard Analysis Committee (SSHAC)].

Stahle, D. W., R. B. VanArsdale, and M. K. Cleveland, Tectonic signal in bald-cypress trees at Reelfoot Lake, Tennessee, *Seismol. Res. Lett.*, *63*, 439–448, 1992.

Stauder, W., *Central Mississippi Valley Earthquake Bulletin*, vol. 1-36, Saint Louis University, Saint Louis, MO, 1974-1983.

Stein, S., Space geodesy and plate motions, in *Space Geodesy and Geodynamics, Geodynamics Ser. vol. 23*, pp. 5–20, AGU, 1993.

Stirling, M. W., S. G. Wesnousky, and K. Shimazaki, Fault trace complexity, cumulative slip, and the shape of the magnitude-frequency distribution for strike-slip faults, a global survey, *Geophys. J. Int.*, *124*, 883–868, 1996.

Street, R., A compilation of accounts describing the Mississippi Valley earthquakes of 1811-1812, *Tech. rep.*, Department of Geology, University of Kentucky, Lexington, 1980.

Street, R., A contribution to the documentation of the 1811-1812 Mississippi Valley earthquake sequence, *Earthq. Notes*, *53(2)*, 39–52, 1982.

Street, R., *The historical seismicity of the central United States: 1811-1928: U.S. Geol. Surv. Final Report: Contract 14-08-0001-21251*, U.S. Government Printing Office, 1984.

Street, R., and O. W. Nuttli, The central Mississippi Valley earthquakes of 1811-1812, in *Symposium on 'The New Madrid Seismic Zone': U.S. Geol. Surv. Open-File Report 84-770*, pp. 33–63, U.S. Government Printing Office, 1984.

Street, R. L., R. B. Herrmann, and O. W. Nuttli, Earthquake mechanics in the central United States, *Science*, *184*, 1285–1287, 1974.

Stuart, W. D., T. G. Hildebrand, and R. W. Simpson, Stressing of the New Madrid seismic zone by a lower crust detachment fault, *J. Geophys. Res.*, *102*, 27,623–27,633, 1997.

Toro, G., et al., Ground motion estimates for building codes in the central United States: Final report to United States Geological Survey, *Tech. rep.*, Risk Engineering Inc., Boulder, CO, 1994.

Toro, G. R., W. J. Silva, R. K. McGuire, and R. B. Herrmann, Probabilistic seismic hazard mapping of the Mississippi Embayment, *Seismol. Res. Lett.*, *63*, 449–476, 1992.

Toro, G. R., N. A. Abrahamson, and J. F. Schneider, Model of strong ground motions from earthquakes in central and eastern North America: Best estimates and uncertainties, *Seismol. Res. Lett.*, *68*, 41–57, 1997.

Triep, E. G., and L. R. Sykes, Frequency of occurrence of moderate to great earthquakes in intracontinental regions: implications for changes in stress, earthquake prediction, and hazard assessments, *J. Geophys. Res.*, *102*, 9923–9948, 1997.

Tuttle, M. P., and E. S. Schweig, Archeological and pedological evidence for large prehistoric earthquakes in the New Madrid seismic zone, central U.S., *Geology*, *23*, 253–256, 1995.

Tuttle, M. P., R. H. Lafferty III, M. J. Guccione, E. S. Schweig, N. Lopinot, R. F. Cande, K. Dyer-Williams, and M. Haynes, Use of archeology to date liquefaction features and seismic events in the New Madrid seismic zone, central United States, *Geoarcheology*, *11*, 451–480, 1996.

Tuttle, M. P., R. H. Lafferty III, and E. S. Schweig, *Dating of liquefaction features in New Madrid seismic zone and implication for earthquake hazard*, U.S. Nuclear Regulatory Commission NUREG/CR-0017, 1998.

Tuttle, M. P., J. Collier, L. W. Wolf, and R. H. Lafferty III, New evidence for a large earthquake in the New Madrid seismic zone between A.D. 1400 and 1670, *Geology*, *27*, 771–774, 1999.

Tuttle, M. T., Prehistoric earthquakes and their implications for earthquake potential of the New Madrid seismic zone, central United States, Ph.D. thesis, Univ. of Maryland, 1999.

VanArsdale, R. B., K. I. Kelson, and C. H. Lumsden, Northern extension of the Tennessee Reelfoot scarp into Kentucky and Missouri, *Seismol. Res. Lett.*, *66*, 57–62, 1995.

Webb, F. H., and J. F. Zumberge, *An introduction to GIPSY/OASIS - II precision software for the analysis of data from the Global Positioning System*, Jet Propulsion Laboratory, Pasadena, CA, 1993.

Weber, J., New Madrid seismic zone deformation from repeat Global Positioning System (GPS) data from surveys, Ph.D. thesis, Northwestern University, 1995.

Weber, J., S. Stein, and J. Engeln, Estimation of strain accumulation in the New Madrid seismic zone from repeat Global Positioning System surveys, *Tectonics*, *17*, 250–266, 1998.

Weertman, J., and J. R. Weertman, *Elementary Dislocation Theory*, Macmillan, New York, 1964.

Wells, D. L., and K. J. Coppersmith, New empirical relationships among magnitude, rupture length, rupture width, and surface displacement, *Bull. Seismol. Soc. Am.*, *84*, 974–1002, 1994.

Wesnousky, S. G., and L. M. Leffler, The repeat time of the 1811 and 1812 New Madrid earthquakes: A geological perspective, *Bull. Seismol. Soc. Am.*, *82*, 1756–1785, 1992.

Wessel, P., and W. Smith, New version of Generic Mapping Tools, *Trans. Am. Geophys. Union (EOS)*, *16*, 329, 1995.

Wessel, P., and W. Smith, New, improved version of Generic Mapping Tools released, *Trans. Am. Geophys. Union (EOS)*, *79*, 579, 1998.

Wheeler, R., Earthquakes and the cratonward limit of Iapetan faulting in eastern North America, *Geology*, *23*, 105–108, 1995.

Wheeler, R., Boundary separating the seismically active Reelfoot Rift from the sparsely seismic Rough Creek Graben, Kentucky and Illinois, *Seismol. Res. Lett.*, *68*, 586–598, 1997.

Wong, I. G., and S. S. Olig, Seismic hazards in the Basin and Range Province: Perspectives from probabilistic analyses, in *Western States Seismic Policy Council Proceedings, Basin and Range Province Seismic Hazards Summit*, edited by W. R. Lund, vol. 98-2, pp. 110–127, Utah Geological Survey Misc Pub., 1998.

Wu, P., and P. Johnston, Can deglaciation trigger earthquakes in N. America?, *Geophys. Res. Lett.*, *27*, 1323–1326, 2000.

Youngs, R. R., F. H. Swan, M. S. Power, D. Schwartz, and R. K. Green, Probabilistic analysis of earthquake ground shaking hazard along the Wasatch Front, Utah, in *Assessment of Regional Earthquake Hazards and Risk along the Wasatch Front, Utah: U.S. Geological Survey Open-File Report 87-585*, edited by P. L. Gori and W. W. Hays, vol. 2, pp. M1–M110, U.S. Government Printing Office, 1997.

Zoback, M. L., and M. D. Zoback, State of stress and intraplate earthquakes in the U.S., *Science*, *213*, 96–104, 1981.

Appendix A

Daily Positions of 1991 Campaign Sites in the NMSZ

Here I give the daily geographic coordinates for the 23 sites that were used in the 1991 Global Positioning System (GPS) campaign. These sites were analyzed in 1998 using JPL's GIPSY and set in ITRF96 reference frame.

Table A.1: Daily positions for 1991 GPS campaign sites used in the New Madrid study. The horizontal errors σ_{yy} and σ_{xx}, were scaled up by 1.99 and 1.85 to better approximate formal errors.

Station	Date	Latitude (°) Longitude (°) Elevation (m)	σ_{yy} σ_{xx} σ_{zz}	$corr_{yx}$ $corr_{xz}$	$corr_{yz}$
FTLW	91NOV06	37.694538567 -92.165619856 318.6179	0.023 0.046 0.021	0.153 -0.349	-0.301
GP26	91NOV06	36.011683430 -86.364074828 148.1614	0.024 0.050 0.021	0.163 -0.398	-0.256

continued on next page

Table A.1: *continued from previous page*

Station	Date	Latitude (°) Longitude (°) Elevation (m)	σ_{yy} σ_{xx} σ_{zz}	$corr_{yx}$ $corr_{xz}$	$corr_{yz}$
PJSP	91NOV06	35.117787799	0.023	0.143	-0.252
		-92.936411592	0.048	-0.346	
		249.0498	0.022		
CRSP	91NOV07	36.045737690	0.056	-0.199	0.196
		-90.666713400	0.140	-0.242	
		77.5924	0.050		
CRVL	91NOV07	36.174939205	0.032	0.329	-0.220
		-89.673916987	0.076	-0.445	
		51.7375	0.029		
EDVL	91NOV07	36.915210216	0.034	0.353	-0.224
		-87.789442308	0.078	-0.460	
		105.8719	0.029		
FARM	91NOV07	37.822052314	0.034	0.375	-0.211
		-90.460249828	0.074	-0.465	
		257.3342	0.029		
FREM	91NOV07	36.949091633	0.034	0.420	-0.302
		-91.096702051	0.077	-0.505	
		160.3472	0.031		
FTLW	91NOV07	37.694539160	0.030	0.416	-0.251
		-92.165620468	0.066	-0.394	
		318.9386	0.027		
GP17	91NOV07	36.283598488	0.033	0.322	-0.183
		-89.204242091	0.077	-0.428	
		65.2596	0.030		
GP26	91NOV07	36.011683259	0.031	0.414	-0.233
		-86.364074667	0.072	-0.418	
		148.1545	0.027		
GP47	91NOV07	35.589931343	0.036	0.442	-0.370
		-89.585533641	0.085	-0.526	
		53.7603	0.034		
GP56	91NOV07	35.231508611	0.035	0.458	-0.324
		-88.189457906	0.086	-0.544	
		95.2607	0.033		
KENN	91NOV07	36.232086873	0.131	-0.707	0.596
		-90.035074221	0.393	-0.555	

continued on next page

Table A.1: *continued from previous page*

Station	Date	Latitude (°) Longitude (°) Elevation (m)	σ_{yy} σ_{xx} σ_{zz}	$corr_{yx}$ $corr_{xz}$	$corr_{yz}$
		49.1105	0.093		
MANI	91NOV07	35.891667711	0.032	0.323	-0.224
		-90.154877177	0.077	-0.449	
		43.9951	0.030		
MAYP	91NOV07	36.765256961	0.035	0.294	-0.148
		-88.584871636	0.079	-0.464	
		128.9521	0.030		
MKND	91NOV07	37.549725146	0.034	0.360	-0.205
		-89.224871970	0.075	-0.465	
		177.6928	0.029		
MLDN	91NOV07	36.607169042	0.032	0.348	-0.228
		-89.988516151	0.075	-0.452	
		59.8966	0.029		
ORAN	91NOV07	37.092596134	0.042	0.154	0.093
		-89.615110684	0.087	-0.530	
		105.0318	0.037		
OSCE	91NOV07	35.696155401	0.033	0.370	-0.254
		-90.009609682	0.078	-0.459	
		41.5233	0.030		
OXFD	91NOV07	34.354674432	0.034	0.446	-0.308
		-89.507489627	0.085	-0.527	
		106.2779	0.034		
PJSP	91NOV07	35.117787678	0.030	0.379	-0.225
		-92.936411399	0.069	-0.380	
		249.0563	0.028		
RLSP	91NOV07	36.472412525	0.034	0.354	-0.268
		-89.345581808	0.078	-0.464	
		57.9296	0.032		
SIKE	91NOV07	36.892125267	0.033	0.357	-0.218
		-89.565200614	0.075	-0.445	
		65.4991	0.029		
SRCY	91NOV07	35.277790610	0.034	0.418	-0.286
		-91.663923908	0.081	-0.498	
		61.5976	0.034		
VCSP	91NOV07	35.162164060	0.033	0.398	-0.241

continued on next page

Table A.1: *continued from previous page*

Station	Date	Latitude (°) Longitude (°) Elevation (m)	σ_{yy} σ_{xx} σ_{zz}	$corr_{yx}$ $corr_{xz}$	$corr_{yz}$
		-90.714964821	0.078	-0.460	
		57.1316	0.031		
VILL	91NOV07	35.942684891	0.081	-0.424	0.646
		-89.831558141	0.208	-0.429	
		47.5219	0.061		
CRSP	91NOV08	36.045736619	0.031	0.170	-0.135
		-90.666715331	0.068	-0.360	
		77.4085	0.028		
CRVL	91NOV08	36.174940062	0.035	0.212	-0.230
		-89.673918152	0.074	-0.390	
		51.6091	0.034		
EDVL	91NOV08	36.915211000	0.031	0.160	-0.112
		-87.789443567	0.068	-0.316	
		105.7804	0.027		
FARM	91NOV08	37.822053039	0.031	0.188	-0.130
		-90.460251205	0.065	-0.324	
		257.2475	0.026		
FREM	91NOV08	36.949092391	0.031	0.176	-0.140
		-91.096703702	0.066	-0.341	
		160.2446	0.027		
FTLW	91NOV08	37.694539894	0.030	0.191	-0.155
		-92.165621681	0.061	-0.310	
		318.8153	0.028		
GP17	91NOV08	36.283599331	0.031	0.154	-0.115
		-89.204242786	0.067	-0.293	
		65.1173	0.027		
GP26	91NOV08	36.011683958	0.030	0.165	-0.098
		-86.364076145	0.065	-0.347	
		148.0283	0.026		
GP47	91NOV08	35.589932314	0.031	0.147	-0.123
		-89.585535123	0.068	-0.332	
		53.6210	0.028		
GP56	91NOV08	35.231509416	0.031	0.170	-0.096
		-88.189459325	0.069	-0.339	
		95.1208	0.027		

continued on next page

Table A.1: *continued from previous page*

Station	Date	Latitude (°) Longitude (°) Elevation (m)	σ_{yy} σ_{xx} σ_{zz}	$corr_{yx}$ $corr_{xz}$	$corr_{yz}$
KENN	91NOV08	36.232084877 -90.035073274 48.7081	0.031 0.068 0.027	0.165 -0.333	-0.132
MANI	91NOV08	35.891668490 -90.154878806 43.8706	0.031 0.067 0.027	0.162 -0.315	-0.122
MAYP	91NOV08	36.765257614 -88.584873092 128.8277	0.031 0.068 0.027	0.167 -0.323	-0.131
MKND	91NOV08	37.549725738 -89.224873456 177.6370	0.031 0.067 0.027	0.182 -0.338	-0.138
MLDN	91NOV08	36.607169706 -89.988517527 59.7812	0.031 0.067 0.027	0.167 -0.328	-0.137
ORAN	91NOV08	37.092596828 -89.615111784 104.9163	0.032 0.066 0.027	0.163 -0.320	-0.116
OSCE	91NOV08	35.696156124 -90.009611038 41.3980	0.031 0.067 0.027	0.159 -0.316	-0.122
OXFD	91NOV08	34.354675273 -89.507491000 106.1260	0.031 0.069 0.028	0.154 -0.350	-0.106
PJSP	91NOV08	35.117788487 -92.936412504 248.8973	0.030 0.062 0.027	0.168 -0.324	-0.117
RLSP	91NOV08	36.472413176 -89.345583089 57.7964	0.031 0.068 0.027	0.162 -0.326	-0.129
SIKE	91NOV08	36.892126015 -89.565202162 65.3827	0.031 0.067 0.027	0.162 -0.332	-0.131
SRCY	91NOV08	35.277791620 -91.663925233	0.031 0.067	0.144 -0.277	-0.090

continued on next page

Table A.1: *continued from previous page*

Station	Date	Latitude (°) Longitude (°) Elevation (m)	σ_{yy} σ_{xx} σ_{zz}	$corr_{yx}$ $corr_{xz}$	$corr_{yz}$
		61.4484	0.028		
VCSP	91NOV08	35.162164826	0.032	0.190	-0.073
		-90.714966589	0.070	-0.371	
		57.0227	0.029		
VILL	91NOV08	35.942688356	0.031	0.156	-0.128
		-89.831559287	0.067	-0.320	
		47.8065	0.027		
CRSP	91NOV09	36.045735837	0.039	-0.013	-0.113
		-90.666714791	0.068	-0.298	
		77.4952	0.030		
CRVL	91NOV09	36.174939196	0.039	-0.014	-0.100
		-89.673917755	0.067	-0.300	
		51.6810	0.028		
EDVL	91NOV09	36.915210170	0.039	-0.004	-0.105
		-87.789443320	0.067	-0.308	
		105.8601	0.028		
FARM	91NOV09	37.822052674	0.039	-0.010	-0.103
		-90.460251345	0.065	-0.296	
		257.3104	0.028		
FREM	91NOV09	36.949091722	0.039	-0.015	-0.115
		-91.096703476	0.066	-0.307	
		160.3251	0.029		
FTLW	91NOV09	37.694540765	0.045	-0.001	-0.181
		-92.165614475	0.080	-0.067	
		318.7508	0.052		
GP17	91NOV09	36.283598335	0.039	-0.011	-0.092
		-89.204242317	0.067	-0.284	
		65.2407	0.029		
GP26	91NOV09	36.011682956	0.039	-0.033	-0.075
		-86.364075354	0.066	-0.290	
		148.0904	0.029		
GP47	91NOV09	35.589931151	0.039	-0.013	-0.103
		-89.585534927	0.068	-0.323	
		53.7218	0.029		
GP56	91NOV09	35.231508346	0.039	-0.003	-0.095

continued on next page

Table A.1: *continued from previous page*

Station	Date	Latitude (°) Longitude (°) Elevation (m)	σ_{yy} σ_{xx} σ_{zz}	$corr_{yx}$ $corr_{xz}$	$corr_{yz}$
		-88.189459103 95.2241	0.069 0.029	-0.333	
KENN	91NOV09	36.232084118 -90.035072851 48.7791	0.039 0.067 0.029	-0.014 -0.308	-0.104
MANI	91NOV09	35.891667586 -90.154878421 43.9448	0.039 0.067 0.028	-0.018 -0.294	-0.098
MAYP	91NOV09	36.765256770 -88.584872894 128.9284	0.039 0.067 0.029	-0.015 -0.308	-0.106
MKND	91NOV09	37.549725023 -89.224872743 177.7393	0.039 0.066 0.028	-0.003 -0.317	-0.110
MLDN	91NOV09	36.607169044 -89.988517371 59.8432	0.039 0.066 0.028	-0.014 -0.306	-0.107
ORAN	91NOV09	37.092596055 -89.615111531 105.0305	0.039 0.066 0.029	-0.018 -0.276	-0.110
OSCE	91NOV09	35.696155224 -90.009610612 41.4564	0.039 0.067 0.029	-0.015 -0.306	-0.101
OXFD	91NOV09	34.354674103 -89.507490384 106.2092	0.039 0.070 0.029	-0.014 -0.319	-0.089
PJSP	91NOV09	35.117787488 -92.936411917 248.9724	0.038 0.064 0.031	-0.070 -0.243	-0.075
RLSP	91NOV09	36.472412190 -89.345582549 57.9097	0.039 0.067 0.029	-0.009 -0.313	-0.095
SIKE	91NOV09	36.892125223 -89.565201666 65.5105	0.039 0.066 0.029	-0.013 -0.316	-0.108

continued on next page

Table A.1: *continued from previous page*

Station	Date	Latitude (°) Longitude (°) Elevation (m)	σ_{yy} σ_{xx} σ_{zz}	$corr_{yx}$ $corr_{xz}$	$corr_{yz}$
SRCY	91NOV09	35.277790571 -91.663924730 61.5270	0.039 0.067 0.029	-0.035 -0.269	-0.090
VCSP	91NOV09	35.162163937 -90.714965883 57.0852	0.039 0.068 0.029	-0.013 -0.317	-0.097
VILL	91NOV09	35.942687411 -89.831558758 47.9101	0.040 0.079 0.035	-0.096 0.020	-0.173
CRSP	91NOV10	36.045736316 -90.666713842 77.4450	0.050 0.093 0.044	0.216 -0.361	-0.194
CRVL	91NOV10	36.174939343 -89.673916529 51.6627	0.048 0.091 0.042	0.224 -0.358	-0.179
EDVL	91NOV10	36.915210615 -87.789442198 105.8342	0.048 0.092 0.041	0.227 -0.361	-0.196
FARM	91NOV10	37.822052630 -90.460250076 257.2785	0.048 0.087 0.040	0.230 -0.359	-0.198
FREM	91NOV10	36.949092009 -91.096702341 160.3156	0.047 0.088 0.041	0.216 -0.347	-0.196
FTLW	91NOV10	37.694539407 -92.165620762 318.8678	0.046 0.083 0.039	0.223 -0.338	-0.199
GP17	91NOV10	36.283598850 -89.204241269 65.2419	0.048 0.090 0.041	0.205 -0.326	-0.175
GP26	91NOV10	36.011683474 -86.364074728 148.0633	0.047 0.089 0.041	0.224 -0.356	-0.190
GP47	91NOV10	35.589931590 -89.585533585	0.048 0.092	0.211 -0.360	-0.186

continued on next page

Table A.1: *continued from previous page*

Station	Date	Latitude (°) Longitude (°) Elevation (m)	σ_{yy} σ_{xx} σ_{zz}	$corr_{yx}$ $corr_{xz}$	$corr_{yz}$
		53.6915	0.042		
GP56	91NOV10	35.231508869	0.048	0.222	-0.193
		-88.189457775	0.095	-0.375	
		95.1774	0.043		
KENN	91NOV10	36.232084491	0.048	0.220	-0.190
		-90.035071909	0.090	-0.348	
		48.7748	0.041		
MANI	91NOV10	35.891667965	0.047	0.217	-0.186
		-90.154877385	0.090	-0.353	
		43.9521	0.041		
MAYP	91NOV10	36.765257230	0.048	0.223	-0.190
		-88.584871429	0.091	-0.357	
		128.8986	0.041		
MKND	91NOV10	37.549725349	0.048	0.237	-0.197
		-89.224871798	0.089	-0.372	
		177.6853	0.041		
MLDN	91NOV10	36.607169299	0.048	0.221	-0.195
		-89.988516242	0.089	-0.353	
		59.8497	0.041		
ORAN	91NOV10	37.092596285	0.048	0.206	-0.168
		-89.615110280	0.090	-0.350	
		105.0086	0.041		
OSCE	91NOV10	35.696155746	0.048	0.214	-0.186
		-90.009610129	0.091	-0.340	
		41.4436	0.041		
OXFD	91NOV10	34.354674668	0.048	0.195	-0.162
		-89.507489697	0.095	-0.343	
		106.1902	0.043		
PJSP	91NOV10	35.117787985	0.046	0.199	-0.166
		-92.936411457	0.086	-0.327	
		248.9579	0.041		
RLSP	91NOV10	36.472412762	0.048	0.212	-0.193
		-89.345581752	0.092	-0.336	
		57.8841	0.041		
SIKE	91NOV10	36.892125634	0.048	0.214	-0.197

continued on next page

Table A.1: *continued from previous page*

Station	Date	Latitude (°) Longitude (°) Elevation (m)	σ_{yy} σ_{xx} σ_{zz}	$corr_{yx}$ $corr_{xz}$	$corr_{yz}$
		-89.565200544	0.091	-0.348	
		65.4524	0.042		
SRCY	91NOV10	35.277791023	0.048	0.201	-0.175
		-91.663923544	0.092	-0.327	
		61.5176	0.042		
VCSP	91NOV10	35.162164341	0.048	0.214	-0.175
		-90.714965121	0.092	-0.343	
		57.0825	0.042		
VILL	91NOV10	35.942687934	0.048	0.217	-0.190
		-89.831557974	0.091	-0.346	
		47.8690	0.041		
CRSP	91NOV11	36.045737351	0.077	0.295	-0.398
		-90.666716870	0.157	-0.430	
		77.9840	0.061		
CRVL	91NOV11	36.174940323	0.078	0.295	-0.402
		-89.673920139	0.157	-0.420	
		52.1336	0.062		
EDVL	91NOV11	36.915210315	0.080	0.264	-0.429
		-87.789445961	0.163	-0.356	
		106.0764	0.065		
FARM	91NOV11	37.822051686	0.078	0.318	-0.409
		-90.460253572	0.154	-0.409	
		257.4197	0.059		
FREM	91NOV11	36.949092154	0.077	0.303	-0.408
		-91.096705412	0.154	-0.416	
		160.6459	0.061		
FTLW	91NOV11	37.694540799	0.077	0.343	-0.393
		-92.165620094	0.142	-0.472	
		319.5538	0.059		
GP17	91NOV11	36.283599392	0.079	0.260	-0.415
		-89.204245334	0.161	-0.339	
		65.6370	0.065		
GP26	91NOV11	36.011683429	0.080	0.327	-0.414
		-86.364077257	0.156	-0.481	
		148.7613	0.063		

continued on next page

Table A.1: *continued from previous page*

Station	Date	Latitude (°) Longitude (°) Elevation (m)	σ_{yy} σ_{xx} σ_{zz}	$corr_{yx}$ $corr_{xz}$	$corr_{yz}$
GP47	91NOV11	35.589933089 -89.585537452 54.2473	0.078 0.161 0.064	0.269 -0.394	-0.404
GP56	91NOV11	35.231510535 -88.189460822 95.7380	0.079 0.169 0.065	0.242 -0.400	-0.392
KENN	91NOV11	36.232085125 -90.035074927 49.2537	0.078 0.156 0.061	0.298 -0.426	-0.402
MANI	91NOV11	35.891669180 -90.154880379 44.4600	0.077 0.157 0.062	0.292 -0.427	-0.399
MAYP	91NOV11	36.765257273 -88.584875583 129.1401	0.079 0.159 0.062	0.285 -0.403	-0.416
MKND	91NOV11	37.549724534 -89.224875992 177.8435	0.079 0.157 0.060	0.309 -0.409	-0.411
MLDN	91NOV11	36.607169793 -89.988519556 60.2499	0.078 0.157 0.061	0.301 -0.429	-0.405
ORAN	91NOV11	37.092595979 -89.615112826 105.3404	0.079 0.158 0.064	0.276 -0.322	-0.418
OSCE	91NOV11	35.696157126 -90.009612309 42.0410	0.077 0.160 0.062	0.287 -0.414	-0.394
OXFD	91NOV11	34.354677068 -89.507493751 107.0078	0.131 0.335 0.206	-0.572 0.732	-0.801
PJSP	91NOV11	35.117790077 -92.936408154 249.8473	0.075 0.145 0.061	0.336 -0.482	-0.378
RLSP	91NOV11	36.472413093 -89.345584589	0.078 0.158	0.297 -0.429	-0.407

continued on next page

Table A.1: *continued from previous page*

Station	Date	Latitude (°) Longitude (°) Elevation (m)	σ_{yy} σ_{xx} σ_{zz}	$corr_{yx}$ $corr_{xz}$	$corr_{yz}$
		58.3402	0.061		
SIKE	91NOV11	36.892125706	0.078	0.297	-0.412
		-89.565204551	0.157	-0.418	
		65.7251	0.061		
SRCY	91NOV11	35.277793430	0.076	0.289	-0.373
		-91.663926926	0.156	-0.401	
		62.2051	0.062		
VCSP	91NOV11	35.162166466	0.077	0.279	-0.388
		-90.714968260	0.159	-0.421	
		57.7106	0.063		
VILL	91NOV11	35.942689041	0.078	0.294	-0.397
		-89.831561114	0.158	-0.426	
		48.3834	0.061		

Appendix B

Daily Positions of 1993 Campaign Sites in the NMSZ

Here I give the daily geographic coordinates for the 23 sites that were used in the 1993 Global Positioning System (GPS) campaigns. The sites were analyzed in 1998 using JPL's GIPSY and set in ITRF96 reference frame.

Table B.1: Daily positions for 1993 GPS campaign sites used in the New Madrid study.

Station	Date	Latitude (°) Longitude (°) Elevation (m)	σ_{yy} σ_{xx} σ_{zz}	$corr_{yx}$ $corr_{xz}$	$corr_{yz}$
CRSP	93OCT10	36.045735552	0.012	0.126	0.102
		-90.666714293	0.035	-0.177	
		77.4508	0.042		
CRVL	93OCT10	36.174939005	0.005	0.082	0.111
		-89.673917084	0.019	-0.383	
		51.6407	0.032		
EDVL	93OCT10	36.915210097	0.005	0.042	0.168
		-87.789442673	0.018	-0.270	

continued on next page

Table B.1: *continued from previous page*

Station	Date	Latitude (°) Longitude (°) Elevation (m)	σ_{yy} σ_{xx} σ_{zz}	$corr_{yx}$ $corr_{xz}$	$corr_{yz}$
		105.7768	0.030		
FARM	93OCT10	37.822052250	0.005	0.144	0.087
		-90.460250368	0.019	-0.397	
		257.2218	0.032		
FREM	93OCT10	36.949091433	0.003	0.086	-0.091
		-91.096702477	0.008	-0.075	
		160.2455	0.020		
FTLW	93OCT10	37.694538878	0.002	0.042	-0.088
		-92.165621086	0.005	-0.062	
		318.8799	0.013		
GP17	93OCT10	36.283598440	0.005	0.064	0.136
		-89.204242010	0.019	-0.366	
		65.1238	0.031		
GP26	93OCT10	36.011682945	0.004	-0.069	0.199
		-86.364075192	0.019	-0.359	
		148.1012	0.029		
GP47	93OCT10	35.589931078	0.004	0.295	-0.119
		-89.585534231	0.010	-0.315	
		53.6646	0.023		
GP56	93OCT10	35.231508440	0.005	-0.002	0.170
		-88.189458438	0.019	-0.313	
		95.1588	0.031		
KENN	93OCT10	36.232083912	0.004	0.301	-0.102
		-90.035072057	0.010	-0.290	
		48.7352	0.022		
MAYP	93OCT10	36.765256744	0.002	-0.024	-0.077
		-88.584871838	0.005	-0.071	
		128.8449	0.013		
MKND	93OCT10	37.549724889	0.005	0.103	0.142
		-89.224872406	0.019	-0.254	
		177.6323	0.031		
MLDN	93OCT10	36.607168824	0.008	0.410	-0.400
		-89.988516345	0.013	-0.515	
		59.7781	0.028		
ORAN	93OCT10	37.092595889	0.005	0.077	0.027

continued on next page

Table B.1: *continued from previous page*

Station	Date	Latitude (°) Longitude (°) Elevation (m)	σ_{yy} σ_{xx} σ_{zz}	$corr_{yx}$ $corr_{xz}$	$corr_{yz}$
		-89.615110877	0.022	-0.510	
		104.9358	0.038		
OSCE	93OCT10	35.696155089	0.006	-0.037	0.085
		-90.009610132	0.028	-0.660	
		41.4224	0.047		
OXFD	93OCT10	34.354674152	0.005	0.008	0.169
		-89.507490326	0.018	-0.361	
		106.1782	0.031		
PJSP	93OCT10	35.117787311	0.006	0.339	-0.284
		-92.936411850	0.015	-0.565	
		249.0123	0.034		
RLSP	93OCT10	36.472412216	0.005	0.061	0.064
		-89.345582135	0.021	-0.510	
		57.8173	0.036		
SIKE	93OCT10	36.892125047	0.010	0.057	-0.039
		-89.565200847	0.024	-0.136	
		65.4052	0.031		
SYRM	93OCT10	35.277712391	0.010	0.704	-0.566
		-91.663995388	0.019	-0.591	
		61.1737	0.038		
VCSP	93OCT10	35.162163804	0.012	0.079	0.039
		-90.714965498	0.049	-0.701	
		57.0496	0.068		
VILL	93OCT10	35.942687362	0.005	0.034	0.092
		-89.831558284	0.020	-0.438	
		47.8317	0.035		
CRSP	93OCT11	36.045735548	0.004	0.268	-0.043
		-90.666714105	0.011	-0.367	
		77.4344	0.026		
CRVL	93OCT11	36.174938891	0.016	0.026	-0.020
		-89.673917037	0.035	-0.089	
		51.6350	0.056		
EDVL	93OCT11	36.915210047	0.003	0.035	-0.045
		-87.789442593	0.008	-0.108	
		105.7684	0.021		

continued on next page

Table B.1: *continued from previous page*

Station	Date	Latitude (°) Longitude (°) Elevation (m)	σ_{yy} σ_{xx} σ_{zz}	$corr_{yx}$ $corr_{xz}$	$corr_{yz}$
FARM	93OCT11	37.822052172	0.003	-0.010	-0.047
		-90.460250219	0.008	-0.079	
		257.2302	0.021		
FREM	93OCT11	36.949091407	0.002	-0.024	-0.074
		-91.096702385	0.005	-0.048	
		160.2487	0.013		
FTLW	93OCT11	37.694538848	0.002	-0.116	-0.091
		-92.165621086	0.005	-0.033	
		318.8841	0.013		
GP17	93OCT11	36.283598364	0.003	0.018	-0.036
		-89.204241958	0.007	-0.078	
		65.1314	0.021		
GP26	93OCT11	36.011682909	0.003	-0.077	-0.044
		-86.364075053	0.007	-0.044	
		148.1043	0.020		
GP47	93OCT11	35.589931071	0.002	-0.010	-0.073
		-89.585534178	0.005	-0.074	
		53.6708	0.013		
GP56	93OCT11	35.231508351	0.003	-0.140	-0.060
		-88.189458559	0.009	-0.011	
		95.1163	0.022		
KENN	93OCT11	36.232083881	0.002	0.020	-0.061
		-90.035071999	0.005	-0.081	
		48.7441	0.013		
MANI	93OCT11	35.891667417	0.003	0.212	-0.104
		-90.154877557	0.007	-0.164	
		43.9149	0.019		
MAYP	93OCT11	36.765256711	0.002	-0.034	-0.086
		-88.584871800	0.005	-0.057	
		128.8544	0.013		
MKND	93OCT11	37.549724812	0.003	-0.096	-0.067
		-89.224872271	0.009	-0.040	
		177.6390	0.021		
MLDN	93OCT11	36.607168769	0.002	0.014	-0.066
		-89.988516371	0.005	-0.066	

continued on next page

Table B.1: *continued from previous page*

Station	Date	Latitude (°) Longitude (°) Elevation (m)	σ_{yy} σ_{xx} σ_{zz}	$corr_{yx}$ $corr_{xz}$	$corr_{yz}$
		59.7890	0.013		
ORAN	93OCT11	37.092595814	0.003	0.067	-0.062
		-89.615110823	0.008	-0.091	
		104.9453	0.021		
OSCE	93OCT11	35.696155074	0.004	-0.034	0.025
		-90.009610009	0.012	-0.125	
		41.4217	0.023		
OXFD	93OCT11	34.354674095	0.003	-0.002	-0.036
		-89.507490128	0.007	-0.070	
		106.1685	0.021		
PJSP	93OCT11	35.117787226	0.003	0.188	-0.111
		-92.936411930	0.008	-0.129	
		248.9973	0.021		
RLSP	93OCT11	36.472412147	0.003	-0.031	-0.033
		-89.345582012	0.008	-0.078	
		57.8088	0.021		
SIKE	93OCT11	36.892125032	0.003	0.019	-0.035
		-89.565200843	0.008	-0.077	
		65.4082	0.020		
SYRM	93OCT11	35.277712382	0.002	-0.027	-0.040
		-91.663995409	0.005	-0.087	
		61.1941	0.013		
VCSP	93OCT11	35.162163731	0.007	0.513	-0.381
		-90.714965211	0.017	-0.480	
		57.0076	0.034		
VILL	93OCT11	35.942687308	0.003	-0.148	-0.027
		-89.831558158	0.009	-0.020	
		47.8315	0.021		
CRSP	93OCT12	36.045735606	0.003	0.033	-0.054
		-90.666714120	0.007	-0.076	
		77.4665	0.021		
CRVL	93OCT12	36.174938955	0.015	0.091	-0.289
		-89.673916888	0.032	-0.230	
		51.6667	0.057		
EDVL	93OCT12	36.915210115	0.004	0.200	-0.036

continued on next page

Table B.1: *continued from previous page*

Station	Date	Latitude (°) Longitude (°) Elevation (m)	σ_{yy} σ_{xx} σ_{zz}	$corr_{yx}$ $corr_{xz}$	$corr_{yz}$
		-87.789442503	0.009	-0.217	
		105.7813	0.022		
FARM	93OCT12	37.822052264	0.003	0.217	-0.124
		-90.460250128	0.009	-0.191	
		257.2426	0.021		
FREM	93OCT12	36.949091489	0.002	0.143	-0.058
		-91.096702452	0.005	-0.131	
		160.2537	0.013		
FTLW	93OCT12	37.694538931	0.002	0.069	-0.059
		-92.165621077	0.005	-0.092	
		318.8957	0.013		
GP17	93OCT12	36.283598441	0.003	-0.064	-0.061
		-89.204241918	0.008	-0.017	
		65.1493	0.022		
GP26	93OCT12	36.011682955	0.003	-0.005	-0.027
		-86.364074958	0.007	-0.077	
		148.1222	0.020		
GP47	93OCT12	35.589931135	0.002	0.043	-0.054
		-89.585534183	0.005	-0.086	
		53.6786	0.013		
GP56	93OCT12	35.231508701	0.008	-0.019	-0.117
		-88.189458801	0.015	0.010	
		95.1323	0.031		
KENN	93OCT12	36.232083966	0.002	0.041	-0.043
		-90.035072024	0.005	-0.096	
		48.7484	0.013		
MANI	93OCT12	35.891667496	0.002	0.013	-0.050
		-90.154877537	0.005	-0.086	
		43.9260	0.013		
MAYP	93OCT12	36.765256793	0.002	0.023	-0.086
		-88.584871821	0.005	-0.082	
		128.8546	0.013		
MKND	93OCT12	37.549724910	0.003	0.045	-0.057
		-89.224872203	0.008	-0.090	
		177.6545	0.020		

continued on next page

Table B.1: *continued from previous page*

Station	Date	Latitude (°) Longitude (°) Elevation (m)	σ_{yy} σ_{xx} σ_{zz}	$corr_{yx}$ $corr_{xz}$	$corr_{yz}$
MLDN	93OCT12	36.607168835	0.002	0.056	-0.039
		-89.988516394	0.005	-0.008	
		59.7936	0.013		
ORAN	93OCT12	37.092595899	0.003	0.050	-0.056
		-89.615110688	0.008	-0.100	
		104.9504	0.020		
OSCE	93OCT12	35.696155104	0.005	0.215	-0.232
		-90.009609909	0.010	-0.161	
		41.4439	0.022		
OXFD	93OCT12	34.354674148	0.003	0.002	-0.060
		-89.507490094	0.007	-0.072	
		106.1980	0.020		
PJSP	93OCT12	35.117787323	0.018	0.057	-0.267
		-92.936412211	0.039	0.073	
		248.9685	0.087		
RLSP	93OCT12	36.472412224	0.004	0.215	-0.030
		-89.345581899	0.009	-0.210	
		57.8247	0.022		
SIKE	93OCT12	36.892125131	0.004	0.123	-0.175
		-89.565200715	0.009	-0.185	
		65.4087	0.022		
SYRM	93OCT12	35.277712458	0.002	0.196	-0.042
		-91.663995445	0.006	-0.161	
		61.1917	0.013		
VCSP	93OCT12	35.162163836	0.004	0.302	-0.090
		-90.714965119	0.012	-0.352	
		57.0273	0.027		
VILL	93OCT12	35.942687351	0.003	0.042	-0.042
		-89.831558082	0.007	-0.081	
		47.8472	0.020		
CRSP	93OCT13	36.045735678	0.003	0.047	-0.039
		-90.666714325	0.007	-0.100	
		77.4147	0.020		
EDVL	93OCT13	36.915210142	0.003	-0.057	-0.036
		-87.789442579	0.010	-0.058	

continued on next page

Table B.1: *continued from previous page*

Station	Date	Latitude (°) Longitude (°) Elevation (m)	σ_{yy} σ_{xx} σ_{zz}	$corr_{yx}$ $corr_{xz}$	$corr_{yz}$
		105.7640	0.021		
FARM	93OCT13	37.822052264	0.003	0.043	-0.055
		-90.460250243	0.007	-0.098	
		257.2241	0.020		
FREM	93OCT13	36.949091490	0.002	0.122	-0.047
		-91.096702372	0.005	-0.059	
		160.2432	0.013		
FTLW	93OCT13	37.694538900	0.002	0.065	-0.049
		-92.165621079	0.005	-0.099	
		318.8849	0.013		
GP17	93OCT13	36.283598443	0.003	0.027	-0.051
		-89.204242046	0.007	-0.096	
		65.1280	0.020		
GP26	93OCT13	36.011682928	0.002	0.009	-0.058
		-86.364074976	0.005	-0.070	
		148.1228	0.013		
GP47	93OCT13	35.589931096	0.002	0.022	-0.053
		-89.585534176	0.005	-0.073	
		53.6700	0.013		
GP56	93OCT13	35.231508429	0.004	0.161	-0.025
		-88.189458349	0.009	-0.219	
		95.1541	0.022		
KENN	93OCT13	36.232083961	0.002	0.028	-0.056
		-90.035072084	0.005	-0.084	
		48.7308	0.013		
MANI	93OCT13	35.891667482	0.002	0.054	-0.043
		-90.154877563	0.005	-0.068	
		43.9140	0.013		
MAYP	93OCT13	36.765256760	0.002	0.026	-0.073
		-88.584871816	0.005	-0.075	
		128.8528	0.013		
MKND	93OCT13	37.549724913	0.003	-0.036	-0.034
		-89.224872273	0.008	-0.071	
		177.6288	0.021		
MLDN	93OCT13	36.607168820	0.002	0.038	-0.054

continued on next page

Table B.1: *continued from previous page*

Station	Date	Latitude (°) Longitude (°) Elevation (m)	σ_{yy} σ_{xx} σ_{zz}	$corr_{yx}$ $corr_{xz}$	$corr_{yz}$
		-89.988516405	0.005	-0.083	
		59.7814	0.013		
ORAN	93OCT13	37.092595923	0.003	0.041	-0.042
		-89.615110825	0.007	-0.106	
		104.9292	0.020		
OSCE	93OCT13	35.696155068	0.004	0.032	-0.010
		-90.009609938	0.011	-0.167	
		41.3319	0.023		
OXFD	93OCT13	34.354674136	0.003	0.017	-0.050
		-89.507490161	0.007	-0.097	
		106.1710	0.020		
PJSP	93OCT13	35.117787296	0.003	-0.196	-0.140
		-92.936411782	0.006	-0.081	
		249.0037	0.016		
RLSP	93OCT13	36.472412281	0.004	0.123	-0.213
		-89.345582098	0.009	-0.104	
		57.7939	0.021		
SIKE	93OCT13	36.892125113	0.004	0.184	-0.038
		-89.565200862	0.009	-0.221	
		65.3916	0.021		
SRCY	93OCT13	35.277790444	0.004	0.404	-0.167
		-91.663924196	0.010	-0.351	
		61.4764	0.025		
VCSP	93OCT13	35.162163733	0.004	0.011	-0.017
		-90.714965254	0.009	-0.001	
		57.0248	0.022		
VILL	93OCT13	35.942687366	0.003	0.047	-0.035
		-89.831558216	0.007	-0.107	
		47.8158	0.020		
CRSP	93OCT14	36.045735607	0.003	0.066	-0.065
		-90.666713998	0.007	-0.134	
		77.4590	0.020		
EDVL	93OCT14	36.915210115	0.004	0.190	-0.031
		-87.789442379	0.009	-0.229	
		105.7708	0.022		

continued on next page

Table B.1: *continued from previous page*

Station	Date	Latitude (°) Longitude (°) Elevation (m)	σ_{yy} σ_{xx} σ_{zz}	$corr_{yx}$ $corr_{xz}$	$corr_{yz}$
FARM	93OCT14	37.822052243	0.003	0.004	-0.078
		-90.460250133	0.009	-0.093	
		257.2285	0.021		
FREM	93OCT14	36.949091470	0.002	0.047	-0.059
		-91.096702357	0.005	-0.084	
		160.2475	0.013		
FTLW	93OCT14	37.694538883	0.002	0.057	-0.067
		-92.165620951	0.005	-0.092	
		318.8871	0.013		
GP17	93OCT14	36.283598409	0.003	0.072	-0.067
		-89.204241828	0.007	-0.128	
		65.1414	0.020		
GP26	93OCT14	36.011682918	0.002	0.005	-0.055
		-86.364074971	0.005	-0.061	
		148.1124	0.013		
GP47	93OCT14	35.589931099	0.002	-0.021	-0.027
		-89.585534047	0.005	-0.088	
		53.6727	0.013		
GP56	93OCT14	35.231508468	0.005	0.234	-0.156
		-88.189458178	0.010	-0.246	
		95.1785	0.023		
KENN	93OCT14	36.232083965	0.002	0.024	-0.029
		-90.035071888	0.005	-0.092	
		48.7397	0.013		
MANI	93OCT14	35.891667474	0.002	-0.013	-0.062
		-90.154877440	0.005	-0.093	
		43.9161	0.014		
MAYP	93OCT14	36.765256791	0.002	0.077	-0.086
		-88.584871696	0.005	-0.079	
		128.8433	0.013		
MKND	93OCT14	37.549724891	0.003	0.077	-0.050
		-89.224872131	0.008	-0.117	
		177.6359	0.020		
MLDN	93OCT14	36.607168812	0.002	-0.003	-0.048
		-89.988516320	0.005	-0.096	

continued on next page

Table B.1: *continued from previous page*

Station	Date	Latitude (°) Longitude (°) Elevation (m)	σ_{yy} σ_{xx} σ_{zz}	$corr_{yx}$ $corr_{xz}$	$corr_{yz}$
		59.7833	0.013		
ORAN	93OCT14	37.092595880	0.003	0.076	-0.055
		-89.615110669	0.007	-0.127	
		104.9449	0.020		
OSCE	93OCT14	35.696155149	0.004	0.274	-0.133
		-90.009609785	0.009	-0.313	
		41.3298	0.023		
OXFD	93OCT14	34.354674143	0.003	0.032	-0.054
		-89.507490032	0.007	-0.107	
		106.1884	0.020		
PJSP	93OCT14	35.117787290	0.002	-0.021	-0.065
		-92.936411742	0.005	-0.028	
		249.0150	0.013		
RLSP	93OCT14	36.472412236	0.004	0.174	-0.179
		-89.345581823	0.009	-0.267	
		57.8256	0.022		
SIKE	93OCT14	36.892125104	0.004	0.215	-0.042
		-89.565200671	0.009	-0.240	
		65.4001	0.022		
SRCY	93OCT14	35.277790434	0.002	0.029	-0.062
		-91.663924069	0.005	-0.079	
		61.4830	0.013		
VCSP	93OCT14	35.162163816	0.004	0.287	-0.181
		-90.714965136	0.011	-0.412	
		57.0367	0.025		
VILL	93OCT14	35.942687343	0.003	0.116	-0.060
		-89.831558025	0.008	-0.143	
		47.8311	0.020		
FREM	93OCT15	36.949091481	0.003	-0.049	-0.055
		-91.096702461	0.006	0.063	
		160.2253	0.015		
FTLW	93OCT15	37.694538925	0.002	0.119	-0.055
		-92.165621061	0.006	-0.068	
		318.8565	0.013		
GP26	93OCT15	36.011682966	0.002	-0.076	-0.107

continued on next page

Table B.1: *continued from previous page*

Station	Date	Latitude (°) Longitude (°) Elevation (m)	σ_{yy} σ_{xx} σ_{zz}	$corr_{yx}$ $corr_{xz}$	$corr_{yz}$
		-86.364074971	0.006	0.090	
		148.1051	0.015		
MAYP	93OCT15	36.765256792	0.002	0.065	-0.083
		-88.584871778	0.005	-0.041	
		128.8379	0.013		
PJSP	93OCT15	35.117787325	0.002	-0.083	-0.034
		-92.936411851	0.006	0.018	
		248.9954	0.015		
SRCY	93OCT15	35.277790482	0.002	0.059	-0.046
		-91.663924161	0.006	-0.043	
		61.4552	0.013		

Appendix C

Daily Positions of 1997 Campaign Sites in the NMSZ

Here I give the daily geographic coordinates for the 23 sites that were used in the 1997 Global Positioning System (GPS) campaigns. The sites were analyzed in 1998 using JPL's GIPSY and set in ITRF96 reference frame.

Table C.1: Daily positions for 1997 GPS campaign sites used in the New Madrid study.

Station	Date	Latitude (°) Longitude (°) Elevation (m)	σ_{yy} σ_{xx} σ_{zz}	$corr_{yx}$ $corr_{xz}$	$corr_{yz}$
EDVL	97OCT05	36.915210044	0.005	0.537	-0.346
		-87.789443054	0.012	-0.369	
		105.7788	0.025		
GP26	97OCT05	36.011682858	0.004	0.471	-0.322
		-86.364075450	0.011	-0.377	
		148.1002	0.023		
GP56	97OCT05	35.231508363	0.005	0.527	-0.333
		-88.189458725	0.012	-0.374	
		95.1726	0.024		
OSCE	97OCT05	35.696155004	0.005	0.501	-0.351

continued on next page

Table C.1: *continued from previous page*

Station	Date	Latitude (°) Longitude (°) Elevation (m)	σ_{yy} σ_{xx} σ_{zz}	$corr_{yx}$ $corr_{xz}$	$corr_{yz}$
		-90.009610408	0.011	-0.346	
		41.4357	0.025		
OXFD	97OCT05	34.354674036	0.005	0.465	-0.329
		-89.507490577	0.011	-0.317	
		106.1656	0.025		
PJSP	97OCT05	35.117787154	0.005	0.436	-0.365
		-92.936412379	0.011	-0.264	
		249.0268	0.027		
SRCY	97OCT05	35.277790312	0.005	0.503	-0.378
		-91.663924690	0.011	-0.319	
		61.4778	0.025		
EDVL	97OCT06	36.915210037	0.005	0.561	-0.346
		-87.789443094	0.011	-0.318	
		105.7649	0.023		
GP26	97OCT06	36.011682906	0.005	0.535	-0.319
		-86.364075469	0.012	-0.330	
		148.0831	0.023		
GP56	97OCT06	35.231508395	0.005	0.518	-0.356
		-88.189458716	0.011	-0.307	
		95.1263	0.024		
OSCE	97OCT06	35.696154988	0.004	0.459	-0.366
		-90.009610480	0.010	-0.362	
		41.4301	0.024		
OXFD	97OCT06	34.354674054	0.005	0.400	-0.302
		-89.507490711	0.011	-0.270	
		106.1830	0.025		
PJSP	97OCT06	35.117787162	0.006	0.402	-0.302
		-92.936412436	0.014	-0.367	
		249.0167	0.030		
SRCY	97OCT06	35.277790335	0.005	0.476	-0.324
		-91.663924703	0.011	-0.280	
		61.4870	0.025		
CRSP	97OCT07	36.045735555	0.005	0.450	-0.353
		-90.666714641	0.011	-0.301	
		77.4608	0.025		

continued on next page

Table C.1: *continued from previous page*

Station	Date	Latitude (°) Longitude (°) Elevation (m)	σ_{yy} σ_{xx} σ_{zz}	$corr_{yx}$ $corr_{xz}$	$corr_{yz}$
FREM	97OCT07	36.949091308 -91.096703114 160.2829	0.005 0.011 0.024	0.496 -0.280	-0.346
GP17	97OCT07	36.283598363 -89.204242437 65.1474	0.005 0.011 0.024	0.541 -0.323	-0.301
GP47	97OCT07	35.589930926 -89.585534597 53.6607	0.007 0.014 0.029	0.472 -0.323	-0.449
MAYP	97OCT07	36.765256660 -88.584872254 128.8445	0.007 0.013 0.029	0.475 -0.331	-0.468
MKND	97OCT07	37.549724819 -89.224872752 177.6227	0.007 0.015 0.026	0.280 -0.215	-0.286
MLDN	97OCT07	36.607168711 -89.988516811 59.7783	0.007 0.017 0.033	0.607 -0.482	-0.404
VCSP	97OCT07	35.162163568 -90.714965621 57.0848	0.011 0.022 0.043	-0.072 0.233	-0.366
CRSP	97OCT08	36.045735467 -90.666714649 77.4242	0.005 0.011 0.027	0.436 -0.308	-0.387
FREM	97OCT08	36.949091291 -91.096702923 160.2374	0.005 0.010 0.024	0.462 -0.272	-0.308
GP17	97OCT08	36.283598311 -89.204242503 65.1167	0.005 0.011 0.024	0.486 -0.323	-0.344
GP47	97OCT08	35.589930883 -89.585534738 53.6596	0.005 0.010 0.023	0.483 -0.297	-0.344
MAYP	97OCT08	36.765256574 -88.584872398	0.006 0.014	0.522 -0.396	-0.305

continued on next page

Table C.1: *continued from previous page*

Station	Date	Latitude (°) Longitude (°) Elevation (m)	σ_{yy} σ_{xx} σ_{zz}	$corr_{yx}$ $corr_{xz}$	$corr_{yz}$
		128.8506	0.026		
MKND	97OCT08	37.549724757	0.005	0.451	-0.335
		-89.224872707	0.010	-0.309	
		177.6183	0.023		
MLDN	97OCT08	36.607168624	0.005	0.493	-0.349
		-89.988516947	0.010	-0.315	
		59.7720	0.024		
VCSP	97OCT08	35.162163658	0.005	0.447	-0.313
		-90.714965798	0.010	-0.253	
		57.0160	0.025		
FARM	97OCT09	37.822052224	0.006	0.602	-0.378
		-90.460250648	0.014	-0.413	
		257.1978	0.028		
FTLW	97OCT09	37.694538825	0.006	0.568	-0.376
		-92.165621789	0.014	-0.444	
		318.8969	0.028		
KENN	97OCT09	36.232083859	0.005	0.463	-0.336
		-90.035072478	0.011	-0.282	
		48.7214	0.024		
MANI	97OCT09	35.891667471	0.005	0.424	-0.340
		-90.154877979	0.011	-0.251	
		43.8895	0.025		
ORAN	97OCT09	37.092595827	0.007	0.602	-0.307
		-89.615111380	0.016	-0.458	
		104.9535	0.032		
RLSP	97OCT09	36.472412157	0.008	0.554	-0.392
		-89.345582477	0.014	-0.326	
		57.8033	0.029		
SIKE	97OCT09	36.892125067	0.005	0.515	-0.310
		-89.565200994	0.011	-0.314	
		65.3749	0.024		
VILL	97OCT09	35.942687377	0.005	0.418	-0.339
		-89.831558552	0.010	-0.297	
		47.8133	0.024		
FARM	97OCT10	37.822052135	0.005	0.434	-0.341

continued on next page

Table C.1: *continued from previous page*

Station	Date	Latitude (°) Longitude (°) Elevation (m)	σ_{yy} σ_{xx} σ_{zz}	$corr_{yx}$ $corr_{xz}$	$corr_{yz}$
		-90.460250747 257.2193	0.010 0.023	-0.277	
FTLW	97OCT10	37.694538769 -92.165621571 318.8795	0.005 0.010 0.024	0.455 -0.240	-0.330
KENN	97OCT10	36.232083841 -90.035072504 48.7029	0.005 0.010 0.024	0.412 -0.281	-0.315
MANI	97OCT10	35.891667357 -90.154877975 43.8914	0.005 0.011 0.024	0.486 -0.227	-0.349
ORAN	97OCT10	37.092595817 -89.615111456 104.9328	0.006 0.015 0.029	0.602 -0.458	-0.377
RLSP	97OCT10	36.472412165 -89.345582633 57.8076	0.005 0.010 0.023	0.416 -0.279	-0.329
SIKE	97OCT10	36.892125034 -89.565201291 65.3890	0.005 0.011 0.024	0.511 -0.281	-0.331
VILL	97OCT10	35.942687284 -89.831558624 47.8054	0.005 0.011 0.025	0.484 -0.234	-0.256